Università degli Studi di Napoli Federico II

Scuola di Dottorato in Ingegneria Industriale

Scuola Politecnica e delle Scienze di Base

Dottorato Innovativo con Caratterizzazione Industriale

Dipartimento di Ingegneria Industriale

Energy Recovery Solutions for Off-Road Vehicles: Simulation, Testing and Hydraulic Circuit Innovation for an Holistic Approach

Relatori

Ch.mo Prof. Ing. Adolfo Senatore

Ch.mo Prof. Ing. Emma Frosina

Ch.mo Prof. Ing. Pietro Marani

Ch.mo Prof. Ing. Andrea Vacca

Ing. Davide Mesturini

Candidato

Antonella Bonavolontà

matricola DR993530

XXXIV Ciclo

Table of Contents

List of Tables

List of Figures

Chapter I: **Introduction**

Today, work machines (especially excavators) continue to need huge amounts of fuel to run their operations. This aspect results not only in a great economic burden to be borne, but also in a great environmental damage.

As in all sectors, even in the work machines one, the issue of energy efficiency has become the main challenge for companies operating in this field.

Energy efficiency is not only synonymous with reducing consumption, but it is also closely linked to the reduction of pollutant emissions. All this interest is aimed at coping with the increase in fuel prices and the increasingly stringent limitations on pollutants; to achieve these objectives, in recent years a lot of innovative solutions have been born and are being born, in particular great steps have been reached thanks to the concepts of Energy Recovery and Hybridization.

In these years, the hybrid systems have been widely used with the goal to achieve higher fuel economy thanks to a better engine management, which is possible, for example, with the addition of an energy storage device. This technology has been already used for a long time for on-road vehicles, which have more stringent regulations, and since the early 2000's it has also drawn the attention of the off-road OEM's.

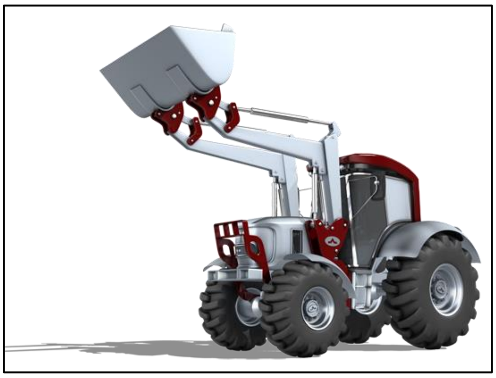

a)

b)

c)

d)

Figure 1. a) Agriculture; b) Construction and Earth moving; c) Material Handling; d) Industrial Vehicles

In particular, most of the attention regarding off-road hybrid vehicles development has been done with excavators. The periodic features of the duty cycle, the heavy load transients and large amount of recoverable energy, in fact, make excavators the ideal baseline machine for the demonstration of hybrid technology for off-road vehicles as it yields higher fuel economy improvements and a shorter payback time.

Over the last two decades several different hybrid architectures have been studied for excavators, some of them using batteries and electric motors for hybridization.

Both hydraulic and electric technologies have each their own advantages and disadvantages. For example, electric technology may comply with zero-emission regulation (i.e. machines that can only operate with the battery with the engine off), but due to the limited power density, it is, usually, more suitable for small size excavators.

On the other hand, large size excavators may benefit more from hydraulic hybrid technology that can have the advantage of a higher power density and of lower costs of the components. In common, both technologies have the challenge in reaching the market due to the low Diesel price, which increases the expected payback time of each machine. Nevertheless, increased environmental awareness has pushed governments towards more stringent regulations, which ultimately will lead to a higher demand for more fuel-efficient machines.

I.1 Objective and subject of study

The main objective of this Ph.D. thesis is to provide an optimized Flow Sharing Directional Control Valve (DCV shown in Figure 2), specifically developed for maximizing the Energy Recovery opportunities in typical mobile applications.

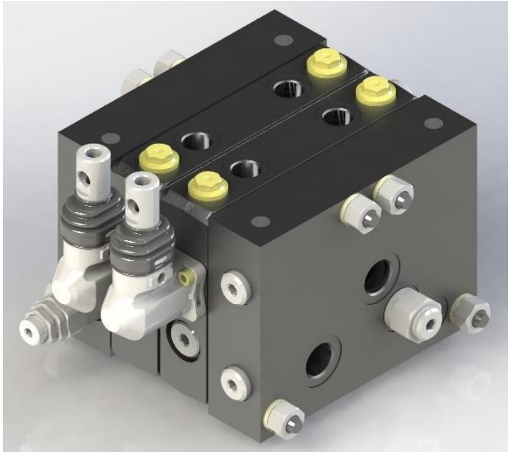

Figure 2. Walvoil Energy Recovery DCV prototype

The final goal is the application of the new Energy Recovery architecture on an Off-road machine, in particular on a 5t excavator (Bobcat 435, in Figure 3) that for a series of reasons that later will be explained is the best machine to be tested with this energy recovery layout.

Figure 3. 5 t Excavator Bobcat 435 ZHS

In Chapter II a detailed description of the new Directional Control Valve will be explained. In particular, the attention will be focused on its functioning inside the hydraulic circuit. Moreover, the advantages of this new architecture will be described.

The experimental and numerical activities will be explained respectively in Chapter III and IV. Finally, in Chapter V the most important energy analysis about this project will be shown.

It is essential to do a clarification about the Ph.D. program before going deep into the next sections. This Industrial Ph.D. belongs to a particular program, established between Confindustria and STEMS (Science and Technology Institute for Sustainable Energy and Mobility, ex CNR- IMAMOTER). They promoted an Industrial Ph.D. scholarship with the goal to develop an industrial research program in the companies and to spread the innovation in response to the technological and economic needs of industries, especially small and medium-sized ones, as well as the country's economy. Then it has robust industrial characterization to promote and create high postgraduate formation and doctoral level specialization consistently with the Italian productive system's needs. For this specific project the other two authorities, supporting the University of Naples Federico II, are the industrial company Walvoil S.p.A., the STEMS Research Center, both located in the North of Italy and the Purdue University (USA), in particular with the Maha Fluid Power Center lead by Prof. Andrea Vacca.

Moreover, all the numerical approaches and methodologies presented in this work of thesis are developed by the Fluid Power

Research Group of the industrial engineering department at the University of Naples Federico II lead by Prof. Adolfo Senatore and Prof. Emma Frosina.

I.2 State of the art

Hybrid architectures are generally classified in three main types: Series Hybrid, Parallel Hybrid and Series-Parallel Hybrid (Figure 4).

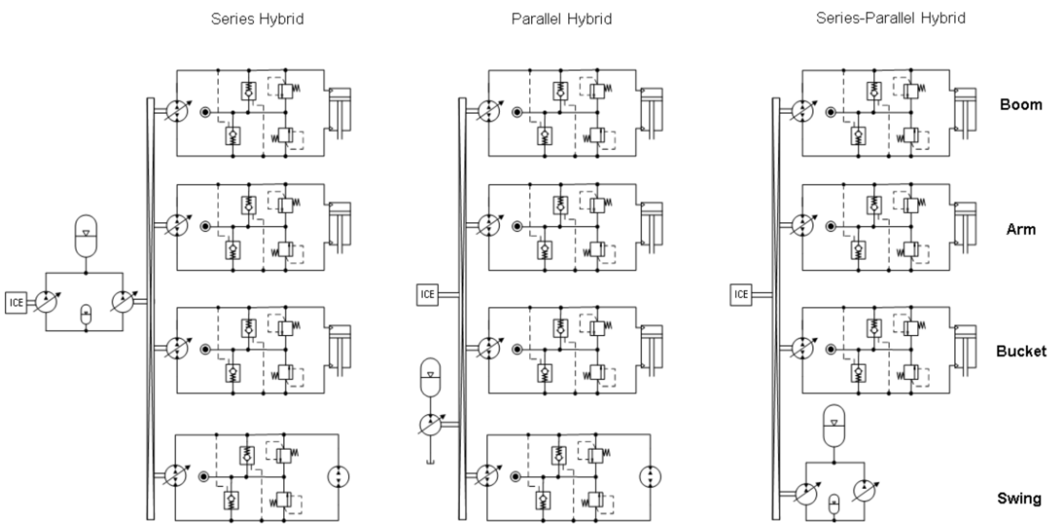

Figure 4. Schematics of excavators' hybrid architectures with displacement-controlled actuators

I.2.1 Series Hybrid

In a Series Hybrid architecture there is no mechanical connection between the Internal Combustion Engine (ICE) and the final users. In this configuration the advantage is that the engine speed can be controlled independently of the flow request of the final users, as long as enough power is available. On the other hand, the electric motor that is used to drive the output shaft needs to be sized to achieve the overall power demand of the actuators, which might be prohibitive in terms of cost and space requirements.

I.2.2 Parallel Hybrid

A different approach is to have the energy storage device in parallel. In these systems, referred to as parallel hybrids, the same unit that charges the accumulator is also used to discharge it. Although such systems can level the engine torque during load variations, the engine speed is still constrained by the flow request of all users.

I.2.3 Series-Parallel Hybrid

An intermediate approach is to have one or more actuators in a series configuration, while others are still mechanically connected to the engine in what is known as series-parallel hybrid. This architecture is especially attractive to excavators, due to easy integration of the series section with the swing motor, also allowing energy recuperation from the cabin inertia.

A comparison between all three main hybrid architectures in their electric version was carried out by Kwon et al. [1]. In their analysis, it was concluded that series-hybrid architecture is the most efficient one, because it enables better engine operation. However, their analysis was approximated in the sense that constant efficiencies were considered for all components with no regard devoted to their sizes and operating conditions. The paper also concludes that the cost of a series-hybrid solution would lead to a longer payback time when compared to a series-parallel solution. A similar comparison was carried out by Lee et al. in [2], a work made in cooperation with Hyundai. In their case, a comparison between a parallel, a standard series hybrid and a compound power-split was carried out. In their analysis, all hybrid configurations were electric, and the hydraulic system was the one of standard excavators. No comparison was made with a baseline machine; however, it was described that in comparison with the power-split, the series hybrid and the parallel hybrid showed that the proposed compound system performed better. Nevertheless, the authors concluded that the parallel system was more efficient than the series one, differently from what found by Kwon et al.

On the hydraulic hybrid side, many solutions for hybridization can be found in literature, varying from the well-known architectures previously described to simpler systems with energy-recovery devices applied to a single actuator. One example of such system is the Energy Recovery System (ERS) proposed by Bedotti et al. [3], in which the boom actuator was connected to an accumulator through a proportional valve during the lowering phase. The stored energy was re-used in the system by connecting the accumulator to the inlet of the charge pump, which was used as a hydraulic motor, assisting the engine to power the main LS pump. In the same publication, Bedotti et al. also implemented a similar system in the swing actuator. However, this system has the clear disadvantage of requiring one high-pressure accumulator and one fixed displacement motor per actuator with available recoverable energy. Additionally, in order to control the actuator's motion, a proportional valve is used, introducing metering losses, thus reducing the ability of the system to recover all the available energy.

Wang, et al. [4] proposed a series-parallel hybrid with a boom energy recovery device. In their proposal, an electric hybrid swing was placed in series with the engine, while the other actuators were kept with the original hydraulic system. To recover potential energy from the boom cylinder, a directional on/off valve was used to connect the bore chamber of the boom to a fixed displacement motor, which was used to drive an electric generator. Although more expensive, such a system avoids the throttling losses present in the system proposed by Bedotti et al. [3] once the electric generator can be used to control the lowering of the boom as long as it is maintained within its operating speed range.

A different approach was proposed by Vukovic, Sgro, and Murrenhoff [5] and later improved in [6]. In what they named the STEAM excavator; two accumulators are used to maintain three different pressure levels in the machine. Independent metering technology is used to connect the desired pressure level to the actuator chamber, with the aim of reducing throttling losses associated with the actuator regulation. Although the proposed system does not eliminate throttling losses, it is able to considerably reduce them. Additionally, the accumulator is used to provide extra flow when needed, so that the ICE speed does not need to follow the operator flow request, similarly to a series-hybrid solution. A 55% increase in efficiency during an air grading cycle was declared with this approach. A similar solution was also proposed by Heybroek and Sahlman [7]. In their case, only two pressure levels are used. To achieve a higher number of discrete forces available and reduce throttling losses in the independent metering valves, they used a novel design for the linear actuators, known as multi-chamber cylinders. In a similar way as the STEAM case, the accumulators were also used to provide extra flow and decouple engine speed from flow demand. For this system, measurements showed a fuel efficiency improvement that varied from 34 to 50%. The author's research center has investigated a Series-Parallel hybrid with displacement-controlled actuators. Hughes et al. [8] first replaced the standard load-sensing (LS) system of a mini excavator with displacement-controlled actuators (DC), which eliminate valve throttling losses and allows the system to recover potential/kinetic energy from any actuator. Just by replacing the LS system with DC the machine was able to achieve 40% improvement in fuel consumption during a truck-loading cycle as shown by Zimmerman, Busquets, and Ivantysynova in [9]. Later, Zimmerman and Ivantysynova [10] proposed a series-parallel hybrid with a secondary-controlled hybrid swing in series and the other DC actuators in parallel, like shown in Figure 4. Hippalgaonkar and Ivantysynova [11] implemented a supervisory controller based on Equivalent Fuel Consumption Management Strategy and achieved 20% improvement in fuel consumption with respect to the DC excavator in simulation. This represents a total improvement of 50% in comparison with the original LS machine, putting the Series-parallel hybrid solution among the most efficient architectures of hydraulic hybrid excavators ever studied. The controlled was further improved by Busquets and Ivantysynova [12], but no data about the machine fuel consumption with the new controller was published.

I.3 Conclusions of the preliminary study

At the beginning of this energy recovery project, a thorough literature study was carried out to understand which component of the machine was the main cause of the energy losses.

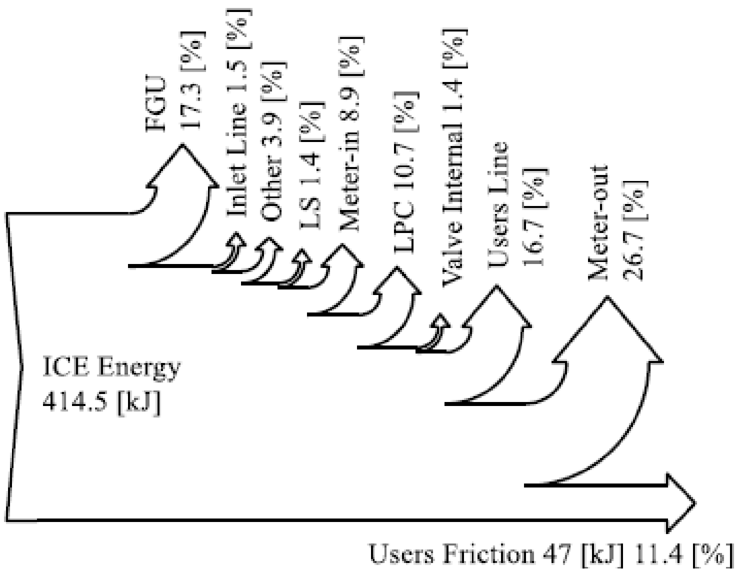

Figure 5. Sankey Diagram for a digging cycle of a 9 t excavator

The Sankey diagram in Figure 5 represents the energy balance of one excavation cycle of a middle size excavator (9 t). The machine is equipped with a 46 kW Diesel engine, the power supply unit (FGU) is composed of an axial piston pump (variable displacement) and an external gear pump, the distributor (DFCV) adopts the Flow-Sharing logic and it feeds nine users. The excavation cycle adopted is defined by the JCMAS standards, where the cycle is performed without material handling and without coming into contact with the ground. The diagram quantifies the energy losses in the system, starting from the mechanical energy coming from the internal combustion engine (ICE) up to the energy dissipated in friction in the cylinders. The energy dissipated by the FGU is 17.3%, by the DFCV 49.1%, by the friction to the cylinders 11.4%, by the pressure relief valves 3.9%, the connection line between the DPCV and the actuators 16.7% and finally 1.5% from the hydraulic connection line between the FGU and the DPCV. In particular, in the DFCV the greatest losses are given by the meter-in (8.9%), by the meter-out (26.7%) and by the LPC compensators (10.7%). Then, the Directional Control Valve (DCV) is an extremely dissipative component, causing most of the energy losses within the hydraulic system of a work machine. This thesis project, in fact, will aim precisely at analyzing the performance of a DCV with innovative architecture, to evaluate the improvements from the energy point of view.

I.3.1 Solutions for Energy Saving

In recent years, in order to improve the energy performance of the valve, thanks to the modeling and simulation of these systems, many possible solutions have been presented; two of these are listed below.

I.3.1.1 Double LS pump

This solution was created to reduce the dissipation of compensators. In a Load Sensing (LS) circuit, the compensators have the task of "breaking down" the excess pressure in the case of the pre-compensated ones, and that of acting as an "obstacle" to increase the pressure downstream of the metering area in the post-compensated. With the addition of another LS pump, the users can be divided so as to group together those with similar load levels, thus preventing the compensators of the less loaded utilities from dissipating large amounts of energy.

Cycles	Standard	Dual LS pump	Δmf
Digging	34.12 (g/cycle)	31.87 (g/cycle)	-6.59%
Grading	10.52 (g/cycle)	9.89 (g/cycle)	-6.07%
JCMAS	8.77 (l/h)	8.35 (l/h)	-4.78%

Table 1. Fuel saving with double LS pump

As shown in Table 1, with the implementation of this solution it is possible to save important quantities of fuel. The Sankey diagram for a double LS pump is shown in Figure 6.

It is observed how the dissipations given by the compensator (LPC) have dropped down by more than 80%. The downside of this solution will be a higher initial investment cost.

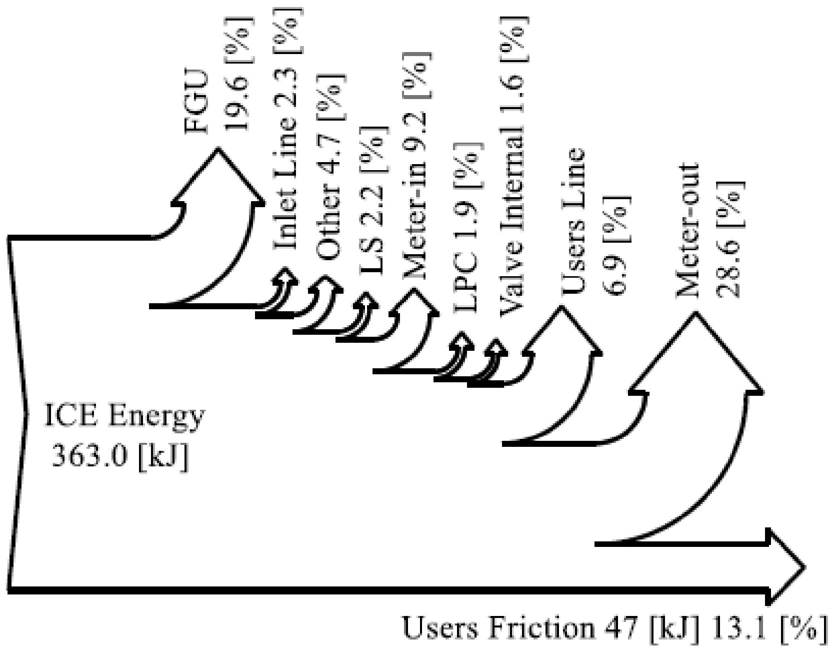

Figure 6. Sankey Diagram for a double LS pump

I.3.1.2 Pump-margin (PM) reduction

LS systems are characterized by energy losses due to lamination through the metering areas; thanks to the compensation it is thus possible to proportionally control the flow rate through the crossing area, regardless of the load. It is possible to reduce energy dissipation by reducing the value of the pump-margin, however it is not trivial to determine this value; with a reduction of the PM there is consequently a reduction of the handling speed, it is therefore necessary to find the right compromise. Taking as an example a lowering in PM of 22% (from 22 to 17 bar), an improvement in energy terms is obtained (Table 2) without significantly compromising the performance of the machine.

Cycles	Standard	PM reduction	Δm_f
Digging	34.12 (g/cycle)	32.58 (g/cycle)	-4.51%
Grading	10.52 (g/cycle)	10.07 (g/cycle)	-4.37%
JCMAS	8.77 (l/h)	8.4 (l/h)	-4.21%

Table 2. Fuel saving with pump-margin reduction

The reduction of energy dissipation deriving from the decrease of the pump-margin is associated with the lowering of energy dissipation in the meter-in and in the meter-out. This solution, unlike the double LS pump, does not involve an increase in the cost of the system, but can be easily implemented at the expense of a small reduction in the speed of movement of the actuators. The Sankey diagram of this solution is shown in Figure 7.

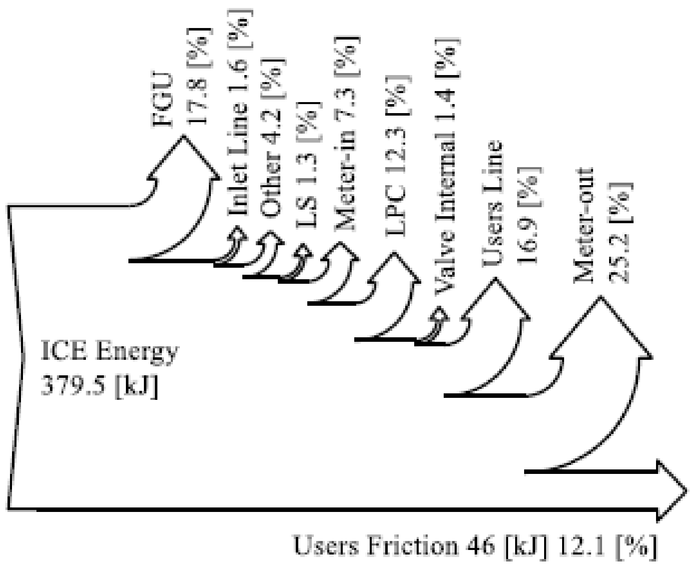

Figure 7. Sankey Diagram for the pump-margin reduction

An Energy Recovery System aims to collect this energy in presence of overrunning loads, then making it available to be reintroduced into the system or to be used in other functions. Naturally, the energy recovery involves the introduction of various complications within the circuit, making it a convenient solution only if there are large amounts of energy involved. To satisfy this condition, it is necessary that high flow rates and pressures must be present in the section on which this solution is applied. By observing the Q - Δp diagrams in Figure 8, referring to an excavation cycle on a Linde 36 t excavator [13], it is possible to verify that these conditions are present in the Boom and Swing sections.

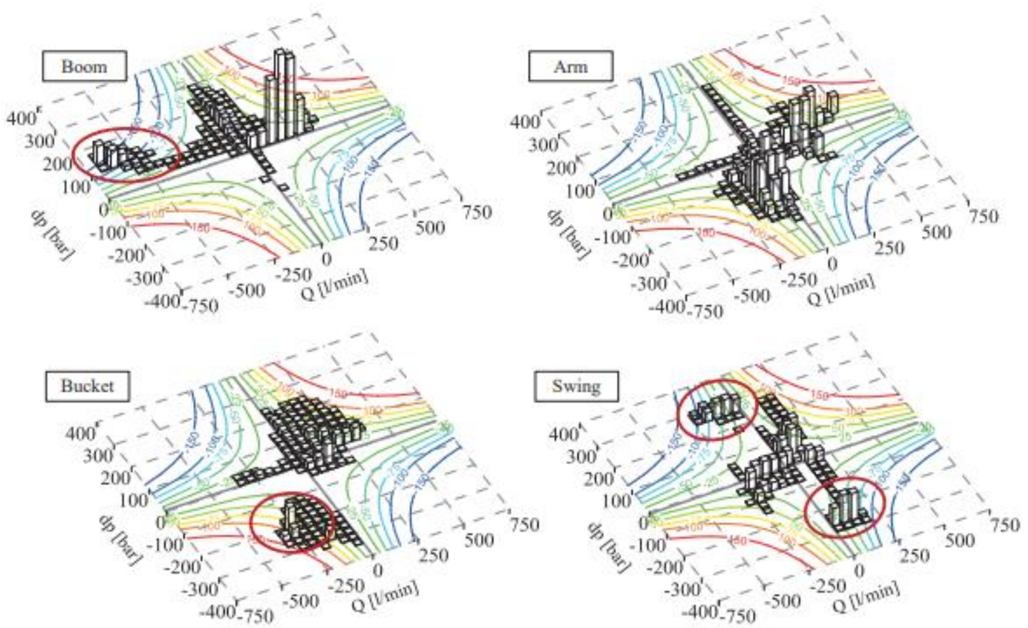

Figure 8. Diagram showing the Q-Δp histograms for all the actuators, excavator Linde 36 t

The regions with high losses are highlighted in red. These include: boom lowering in quadrant 2, bucket actuation in quadrant 3 and swing braking in quadrants 2 and 4.

Another example is the Rexroth's Power Regenerative Boom® (PRB) system [14], which on a Doosan 38 t excavator claims to be able to recover 16% of the overall energy required by the engine from boom down motion (Figure 9). The energy charged energy into an accumulator is reused after boom down motion, and the pressurized oil goes to a hydraulic motor.

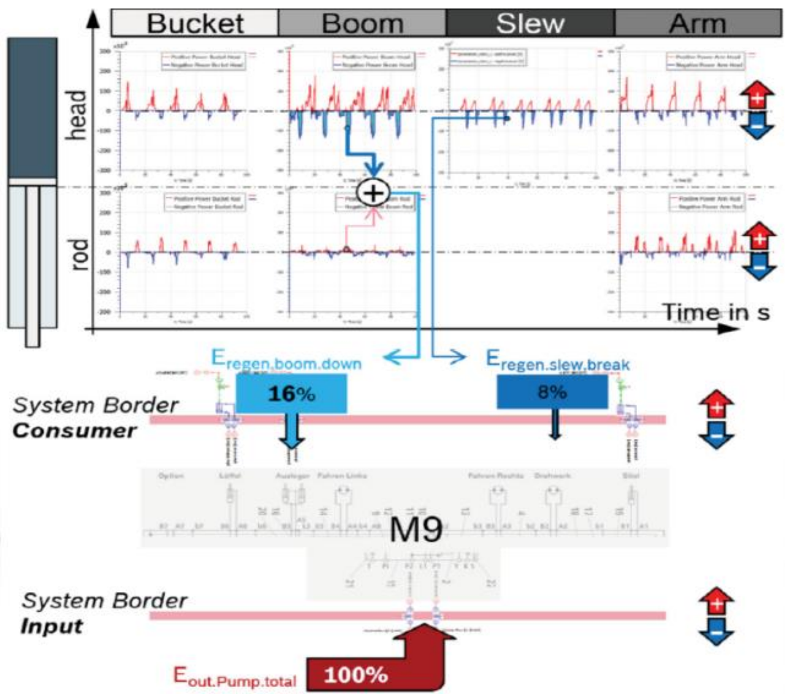

Figure 9. Rexroth Power Regenerative Boom®

I.3.2 The subject of the study

The innovation is based on the idea of a new system architecture consisting in the energy saving and recovery from sources already present on the machine with the goal of their final reuse.

Chapter II: **Energy Recovery System with the new DCV**

II.1 Introduction

In the last years, as already mentioned in Chapter I, environmental concerns and global warming about exhaustion of natural resources have stimulated the development of environmentally "friendly" vehicles.

In particular, in automobile industry, the hybridization of conventional powertrains has been actively studied as a short-term solution for the CO2 and emissions problem.

Various types of hybrid vehicles have been successfully merchandised by major automobile manufacturers and these vehicles show a significant performance improvement in fuel economy. Successful hybridization of conventional power train also stimulated the hybridization of off-road vehicles and construction vehicles. Being fuel costs generally account for a large portion of the total cost, the idea that the hybridization of these vehicles was expected to be profitable led most companies to undertake this journey.

However, the power trains of these systems have different features from those typical of other types of vehicles; for example, they usually contain hydraulic systems and auxiliary equipments.

In fact, increasing the system efficiency of hydraulically operated mobile machines has been the focus of a lot of researches in recent years. Different new architectures have been proposed in literature, all with the aim of accomplishing the following four goals:

- to reduce components efficiency losses (of the engine and pumps);
- to decrease idling losses;
- to avoid throttling losses;
- to recover potential and kinetic energy from actuators.

The difficulty in designing a system that deals with all these separate factors is that addressing anyone of them usually affects another negatively.

This complex system of tradeoffs is further complicated by the problem that in industry any new idea has to be more efficient but especially not cost considerably more than the previous architecture. In summary, the pursuit of more efficient mobile hydraulic systems can be described as an extremely challenging task with a set of even more restrictive boundary conditions. It is, therefore, no surprise that relatively few true innovations have found their way into the market.

From the energy analysis mentioned in the previous chapter, the largest percentage of energy dissipated in the form of heat is highlighted in the meter-out notch of the DCV.

Before introducing the architecture of this innovative DCV (paragraph II.2), the following sub-paragraphs will illustrate the role that directional valves play within a hydraulic circuit and the operating *Load Sensing* principle and *Flow Sharing* condition on which the new Energy Recovery system is based.

II.1.1 Directional Control Valves

The Directional Control Valves, known with the acronym DCV, are hydraulic components with the aim to control the flow rate in a Fluid Power system, to correctly ensure the connection between the different hydraulic lines.

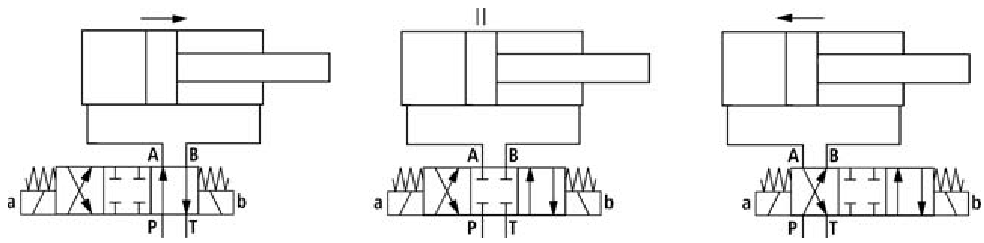

Figure 10. Actuation methods of a 4/3 Directional Control Valve **(**DCV) example 4/3

One of the most used families of directional valves is the so called "*spool*" valves, taking their name from the mobile element called spool (or cursor).

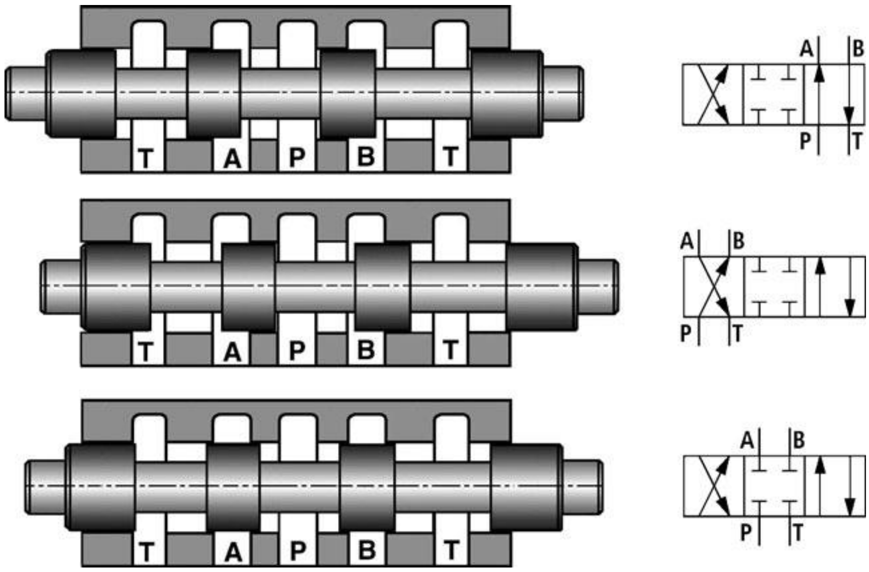

Figure 11. Spool valve 4/3

This type of valve has the advantage of being able to connect numerous ports, while maintaining the possibility of offering many control positions. A fundamental parameter of the spool valves is the "overlap": as shown in Figure 12, this parameter determines the opening or closing of a port, when the spool is in its rest position.

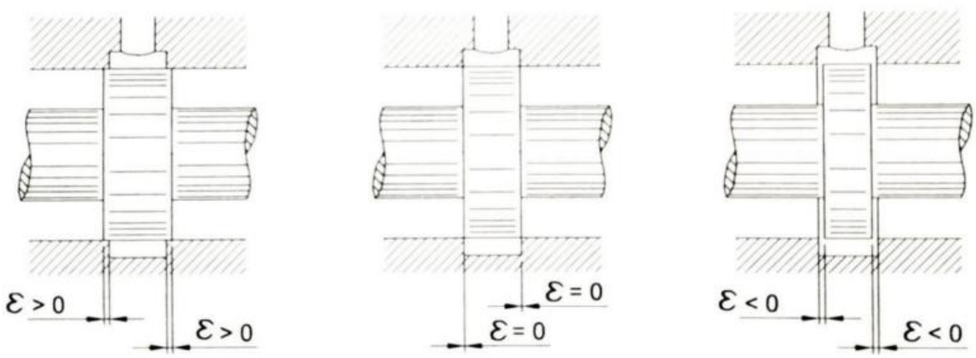

Figure 12. Overlap: from left to right, positive, zero, negative

The type of overlap affects the flow rate-displacement curve of the valve, in particular:

- positive (Figure 13): the flow rate is null for $|Y| \leq Y_0$;

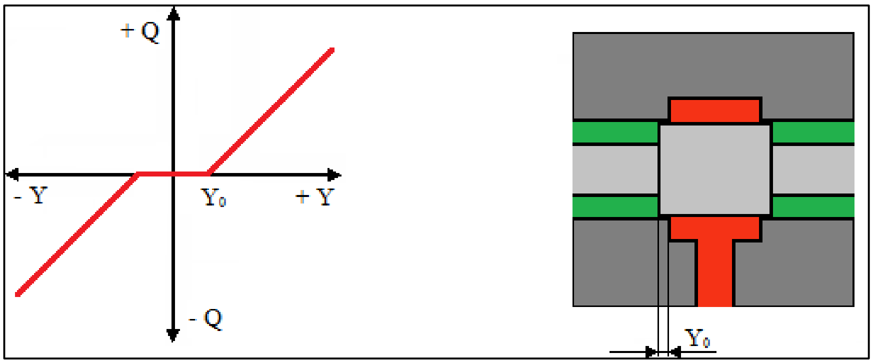

Figure 13. Positive overlap

- zero (Figure 14): the flow rate is null only for Y=0;

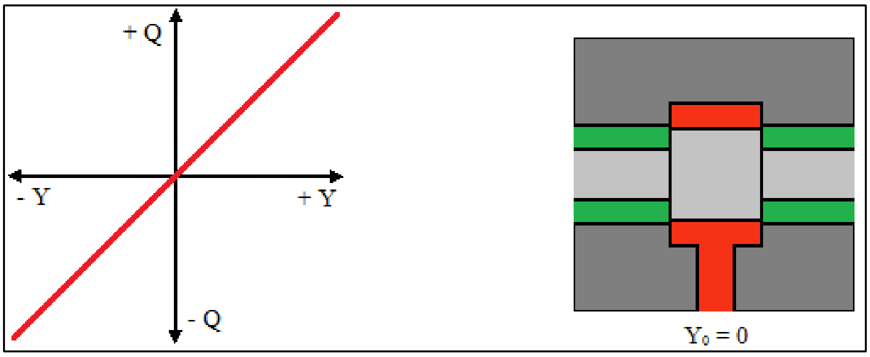

Figure 14. Zero overlap

- negative (Figure 15): the flow rate is never null.

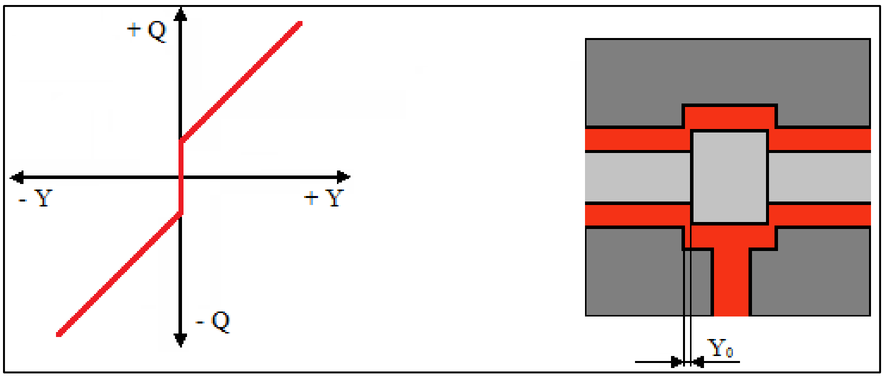

Figure 15. Negative overlap

Spool positioning can be done in different ways, some examples are shown in Table 3.

Type of control	Illustration
Hydraulic control	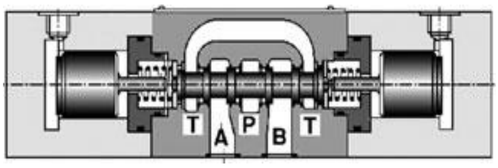
Mechanic control with manual lever	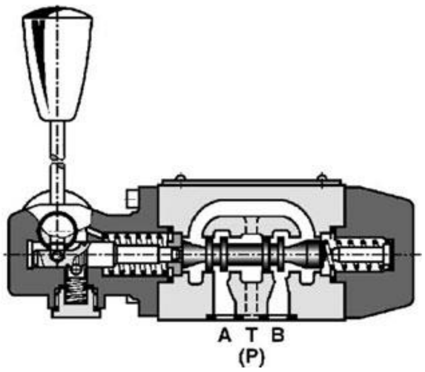
Pneumatic control	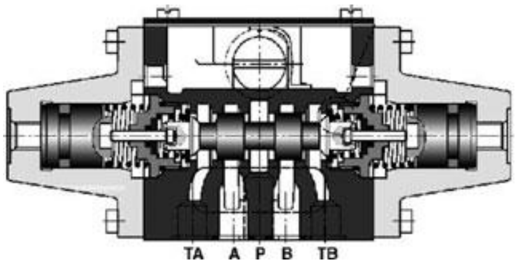
Electric control with DC solenoids	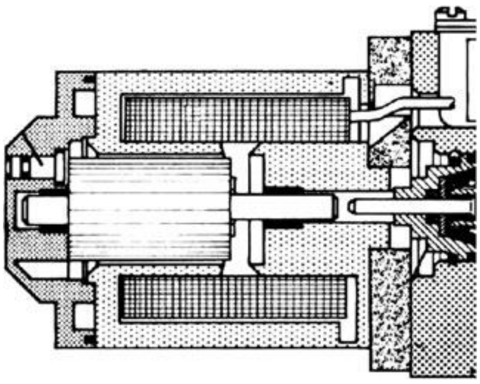

Electric control with AC solenoids	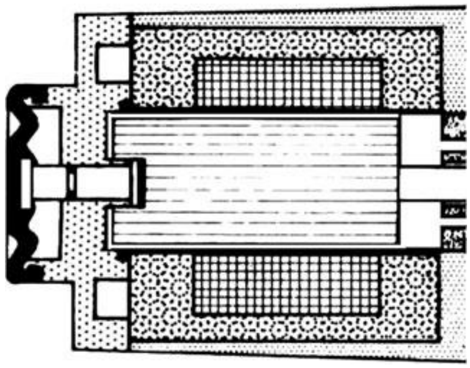

Table 3. Control systems for the spool displacement

II.1.2 The Load Sensing concept

A lot of hydraulic systems adopt Load Sensing control circuits; their peculiarity is to automatically adapt to the user's load in each instant of use. This aspect is fundamental when a power supply group (hydraulic pump) must simultaneously supply several users stressed by time-varying loads, as it must be able to satisfy the flow rate request of each user maintaining good controllability by the operator. This type of control also has a positive effect on energy consumption because the group power supply continuously adapts to the load of the main user, thus limiting the energy waste. To understand the functioning and evolution of these systems, the simple circuit in Figure 16 can be considered, consisting of a GA power supply group with variable flow and an absolute pressure limiter calibrated to the p^* value, which serves a generic utilization group (GU) by means of a continuously positioned valve controlled by a controller C.

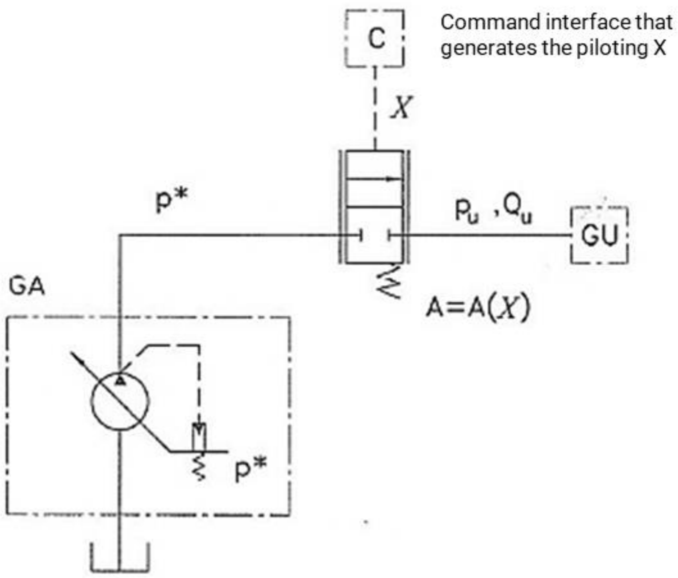

Figure 16. Velocity control dependent from p_u

Considering now the energy plan in Figure 17, the point of use of GU must respect the limit conditions of flow and pressure:

- the maximum deliverable flow rate, $\boldsymbol{Q_0}$ $[\frac{m^3}{s}]$, deliverable by the pump, given $\boldsymbol{\omega}$ $[\frac{rad}{s}]$ the pump rotational speed and $\boldsymbol{V_{max}}$ $[\frac{m^3}{rad}]$ the pump maximum displacement:

$$Q_0 = w \cdot V_{max} \tag{1}$$

- the calibration pressure $\boldsymbol{p}^*$ [Pa] of the absolute pressure limiter.

Known the values of the requested flow rate $\boldsymbol{Q_u}$ and of the pressure $\boldsymbol{p_u}$ set by GA, the useful power is obtained:

$$P_{useful} = Q_u \cdot p_u \tag{2}$$

The spent power is instead:

$$P_{spent} = Q_u \cdot p^* \tag{3}$$

Making the difference it gets the lost power:

$$P_{lost} = P_{spent} - P_{useful} = Q_u \cdot (p^* - p_u) \tag{4}$$

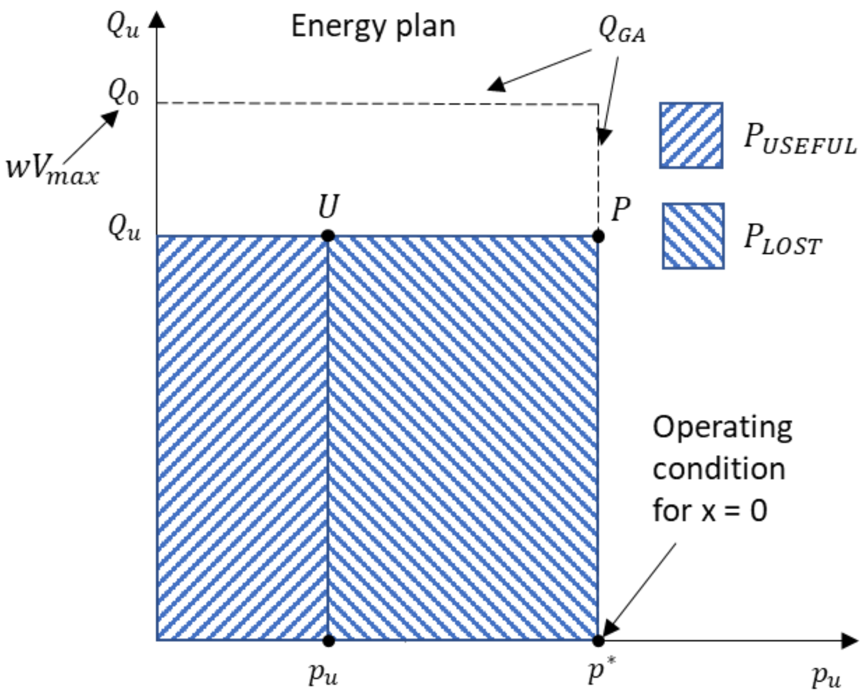

Figure 17. Energy plan

From Figure 17 it is possible to observe that the dissipated power is maximized for high flow rates and low pressures imposed by user. Moreover, the power absorbed by the pump is always the same, regardless of the imposed load, making it a system that is not sensitive to the load.

Then, there is an important problem related to energy dissipation. Moreover, there is also a problem of controllability.

In condition of turbulent flow, it will be introduced the orifice equation:

$$Q = C_d \cdot A_0 \cdot \sqrt{\frac{2 \cdot \Delta p}{\rho}} \tag{5}$$

where:

- $\boldsymbol{Q}$ is the volumetric flow rate;
- $\boldsymbol{C_d}$ is the discharge coefficient;
- $\boldsymbol{A_0}$ is the orifice cross section;
- $\Delta \boldsymbol{p}$ is the pressure difference;
- **ϱ** is the fluid density.

In the considered system, the crossing area is determined by the piloting signal **X,** which from controller **C** acts on the valve modifying its spool position; then the crossing area is $A(x)$.

Then the equation becomes:

$$Q = C_d \cdot A_{(x)} \cdot \sqrt{\frac{2 \cdot (p^* - p_u)}{\rho}} \tag{6}$$

As highlighted by the controllability plan, for the same position X of the spool, if the user pressure p_u increases the flow rate Q_u drops down; this aspect creates problems because when the actuator is lightly loaded it moves faster compared to when it is more loaded, with the same command X.

Then, the flow rate arriving to users will not be directly proportional to the crossing area, thus giving bad controllability of the system.

A simple example of system that well explains the load sensing logic and which allows to partially reduce these problems is showed in Figure 18.

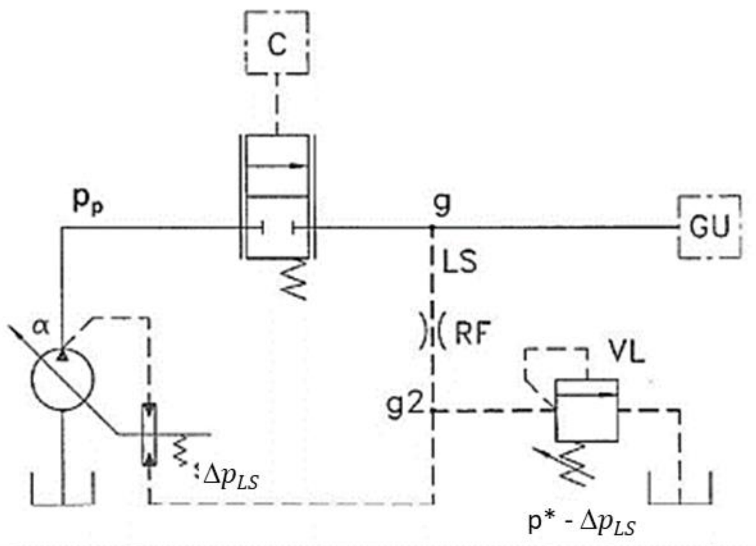

Figure 18. Load Sensing principle

In this system there is a variable displacement pump controlled by a differential pressure limiter in which, through the piloting LS line, the load pressure information is taken, increased by a constant amount Δp_{LS}, and, then, compared to the pump delivery pressure. By this configuration, a constant pressure difference can be maintained across the valve and the load controllability is ensured in all conditions.

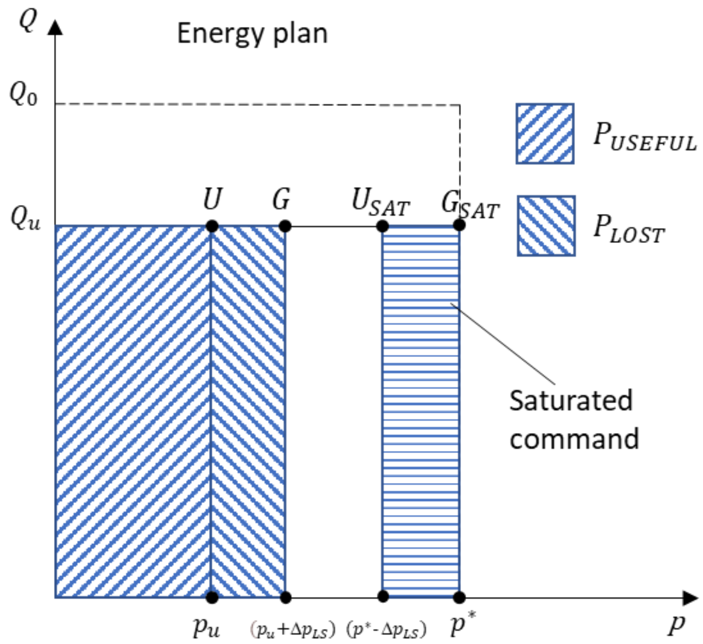

Figure 19. Energy plan with LS variable displacement pump

The differential pressure limiter ensures the following condition:

$$p_p = p_u + \Delta p_{LS} \tag{7}$$

Therefore, a constant pressure difference equal to Δp_{LS} is set to the valve controlled by the operator, this value is called "*pump margin*" or "*stand by*":

$$\Delta p = p_p - p_u = \Delta p_{LS} \tag{8}$$

Consequently, the flow rate value Q_u is independent from the pressure p_u requested from the user; recalling the equation of the orifice (Equation 5), it follows that the flow rate, and therefore the speed of the actuator, are proportional to the X command value: this means that there is only is one curve in the controllability plan. Furthermore, there is a considerable improvement in the energy plan, in fact the pump delivery pressure no longer stays at the constant value of p * but it adapts to the load conditions p_u by only adding the stand by value Δp_{LS}.

As concerns the power:

$$P_{useful} = Q_u \cdot p_u \tag{9}$$

$$P_{spent} = Q_u \cdot (p_u + \Delta p_{LS}) \tag{10}$$

$$P_{lost} = P_{spent} - P_{useful} = Q_u \cdot \Delta p_{LS} \tag{11}$$

If the two plans are compared (Figure 17 and Figure 19), it can be seen that, in the present case, the lost power P_{lost} is certainly lower.

In the previous case, the correct functioning of a LS system is verified when there is a single user; now a system with two users will be considered, as shown in Figure 20.

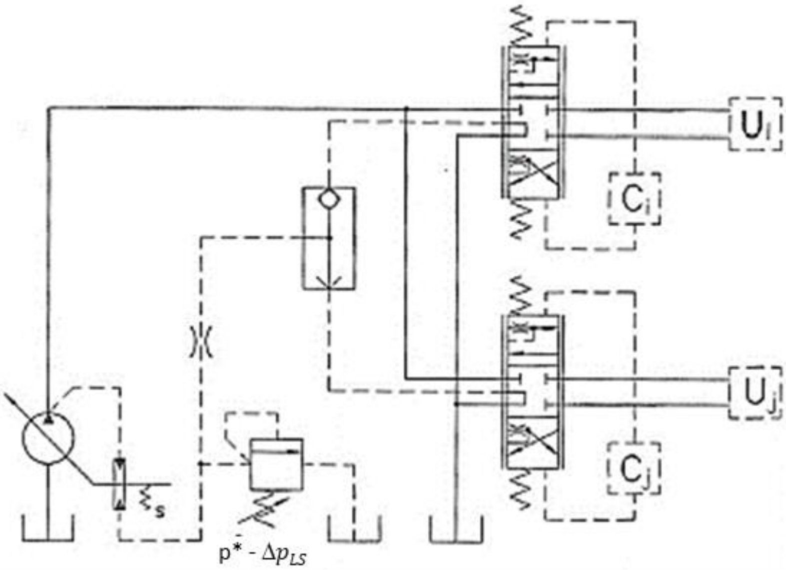

Figure 20. LS system with two generic users

In this system there is a shuttle valve with the function of sending the higher LS pressure signal between the two users, so as to be able to satisfy both users.

Assuming that both users require the same load, the global LS signal will be equal to the two local LS signals; in these conditions the Δ_p across the two metering sections will be constant and therefore controllability will also be guaranteed.

On the other hand, if it is assumed that the loads are different from each other, the LS signal arriving at the pump is that of the dominant user. Analyzing the pressures, it is easy to understand that in this case only the Δp of the dominant section is constant, while the dominated one is devoid of controllability, since the flow rate will also depend on the load of the other user, in addition to the crossing area.

In the controllability plan, we continue to have a single curve for the most loaded user, while the other is fed by a flow rate that is dependent on the load history; therefore, for the latter user fails to be controllable.

II.1.3 Pre-compensation and Post-compensation (Flow Sharing) systems

The controllability problem can be solved by introducing a local pressure compensator for each control valve capable of making all the sections work with a constant Δp through the metering areas.

The compensators can be inserted upstream or downstream of the DCV.

The pre-compensated architecture will be analyzed below, with local compensators placed upstream of the metering sections (Figure 21).

II.1.3.1 . Pre-compensation

The pre-compensators are normally open elements that throttle and dissipate the pressures in the dominated sections. Let assume $p_{L1} > p_{L2}$, the LS signal will therefore be that of section 1; the compensators are calibrated by taking the local LS signal, then the compensator of the dominated user will throttle the excess pressure until a value capable of guaranteeing stand-by across the metering area is reached. With this logic it is possible to ensure the controllability of all the users.

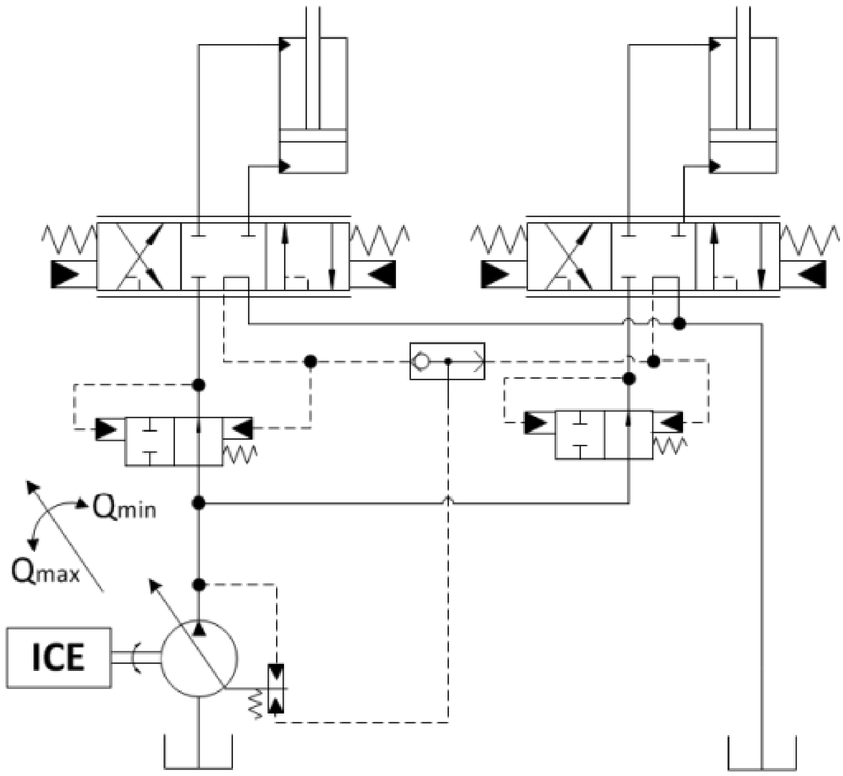

Figure 21. LS pre-compensation system

This architecture suffers in flow saturation conditions; in fact, if this condition is reached, the flow rate to the dominant user will begin to decline, failing to satisfy the request in order to generate the Δp required by the crossing area; at first this does not happen in the dominated section.

II.1.3.2 Post-compensation (Flow Sharing)

The flow rate saturation condition can be well managed through the introduction of an architecture with post-compensation, where the local compensators are placed downstream of the metering area (Figure 22). In this case, both metering areas sense upstream the pump pressure, the local compensators are normally closed elements that sense the global LS pressure. If the user is dominant, the pressure downstream of the metering area will be high enough to open the compensator and let pass the flow; the dominated user, on the other hand, will have a lower pressure downstream of the metering area and therefore the compensator will be partially or totally closed, thus increasing the pressure until stand-by is imposed in the metering area. In this solution, all the metering sections have the same downstream pressure (ensured by the compensators connected to the global p_{LS}), the same concept is valid for the upstream "felt" pressure (i.e. the delivery pressure from the pump p_p); thanks to this condition the problem of flow saturation is solved, since the sections "see" the same pressures p upstream and downstream, generating a reduction in flow proportional to the areas in all the users, so that there are no different controllability conditions in the various users. This feature is known as Flow-Sharing.

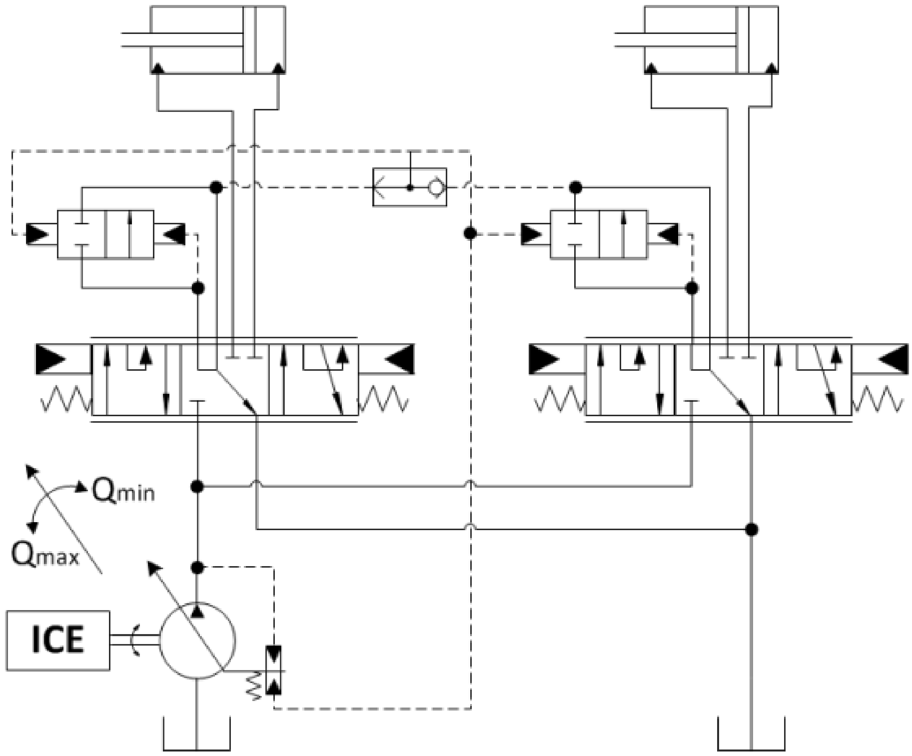

Figure 22. LS post-compensation system (Flow Sharing)

II.2 Innovative System Architecture description

The innovative system architecture (Figure 23) developed in this project is based on a centralized Flow Sharing DCV based on the well-known Load Sensing principle, capable of significant reduction in metering losses and remarkable energy recovery from both inertial loads and simultaneous operations.

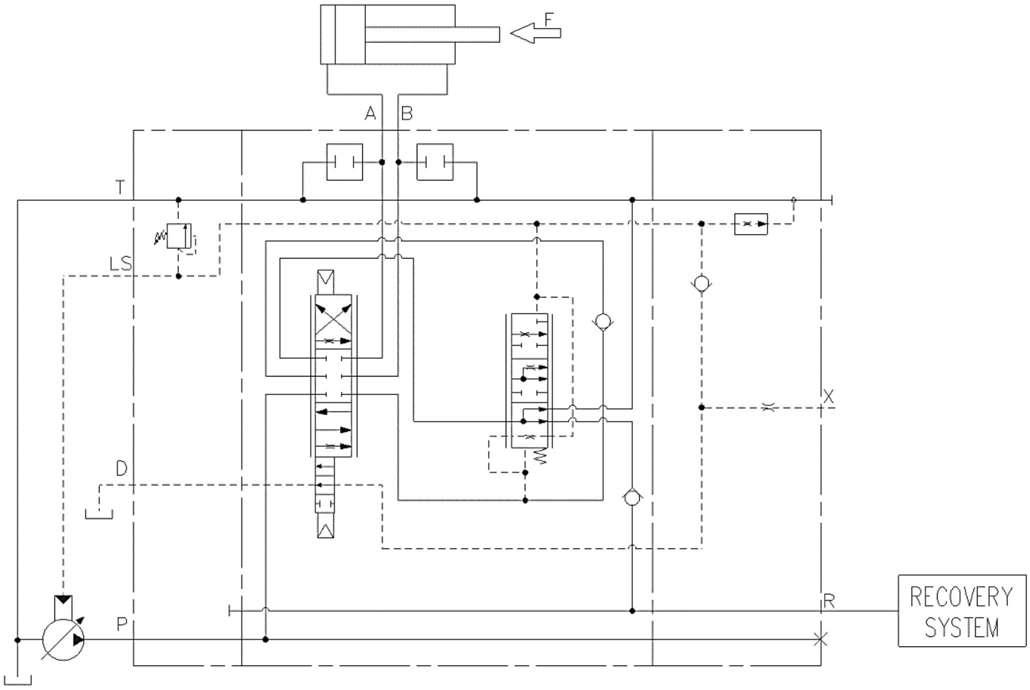

Figure 23. Hydraulic circuit of the Energy Recovery DCV

LS principle (explained in *II.1.2*) guarantees that the speed of the actuator does not depend on the load (i.e. work port pressure) but only on its spool stroke; flow sharing (explained in *II.1.3.2*) ensures that in case of pump saturation the flow given by the pump feeds all working actuators proportionally.

Each section of a flow sharing DCV has its own compensator, whose function is to keep the pressure drop across meter-in notches equal to the pump margin in all working sections, throttling the flow and therefore dissipating energy; unlike the standard valve, the compensation does not happen downstream of the meter-in (post-compensation), but on the return line from the actuators, downstream of the meter-out.

II.2.1 The main spool

The main spool of this valve, shown in Figure 24, will be analyzed in detail below.

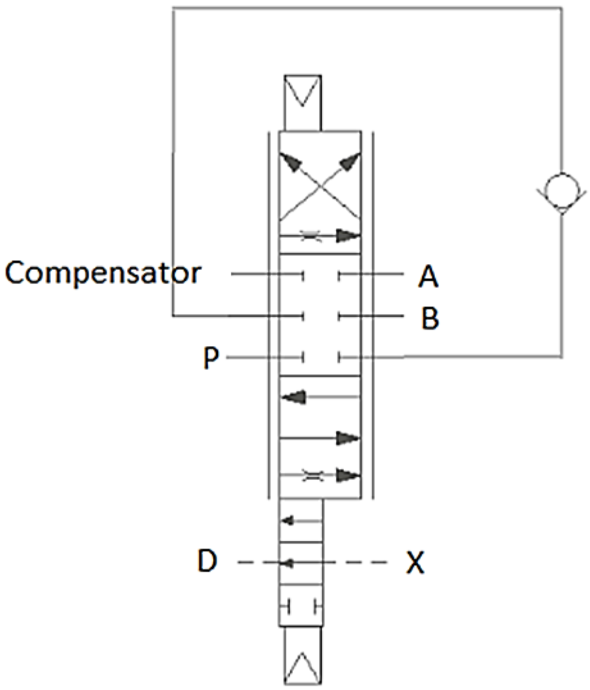

Figure 24. Main spool of the Energy Recovery DCV

The flow rate coming out from the power supply line crosses the meter-in section and through a check valve reaches the bridge; from the bridge, the flow is sent to users A or B, while the one that comes back from the user goes to the compensator. It can be observed that the meter-out section is free of throttling; in the standard Directional Control Valve the meter-out notches are fundamental for the controllability of the load, since they guarantee a counter pressure that helps to support it during an overrunning load, also making an important contribution to avoiding cavitation. However, the presence of these notches could be an obstacle when the conditions mentioned above are not present, forcing the system to "push" to discharge the flow. With the new valve, the absence of throttle on return notches leads to energy savings but at the same time causes problems in overrunning load condition when the section is the only one that is working; the solution to this problem will be described in the next paragraph.

II.2.2 The Downstream Compensator

The innovative component of this valve is the Downstream Compensator (in Figure 25) which, based on a purely mechanical design and without electronic components, controls the flow rate on the return line; this is an advantageous aspect both for controlling the speed of overrunning loads and the compensation in case of multiple functions.

The Three-Way Downstream Compensation idea, in fact, was born with the goal of realizing a single device able to make a hydraulic recovery from both the inertial loads and the local compensation.

The concept of a 3 ways compensator was already introduced by [15] and [16], but in this case the system was limited to realize internal regenerations, making impossible the energy storage from the overrunning loads and local compensations. For this reason, a downstream compensation system was realized through the introduction of a new 3 ways compensator architecture.

The "Downstream Compensator" is a local compensator spool placed directly downstream the main spool meter out notches A_{OUT} of each working section. This compensator position allows to control return flow Q_{OUT}: it is capable of maintaining a constant pressure drop p_{OUT} across the main spool discharge notches A_{OUT}. In this way the spool of the actuators is independent from the pressure load and only depends from the discharge notch opening.

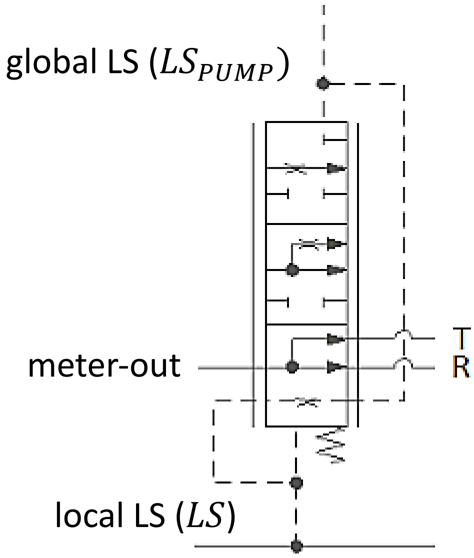

Figure 251. Compensator of the Energy Recovery DCV

The compensator pilot system consists of two pressure signals taken from the delivery line: the local pressure LS of the corresponding main spool (p_{LS}), acting on the spring side and the global LS pressure of the pump (p_{LS_PUMP}), acting on the opposite side.

The selection of the pressure signals happens through a line inside the compensator. It will be opened when there is no compensation (local LS = global LS), while it will close when there is compensation (local LS < global LS).

The pressure drop on the meter in notch is regulated by the compensator through the following equation:

$$p_{LS} \cdot A_{PIL} + F_{SPRING} \; = \; p_{LS\_PUMP} \cdot A_{PIL} \tag{12}$$

Every compensator works on the return line, aiming to copy the p_{LS_PUMP} pressure in the local p_{LS} line.

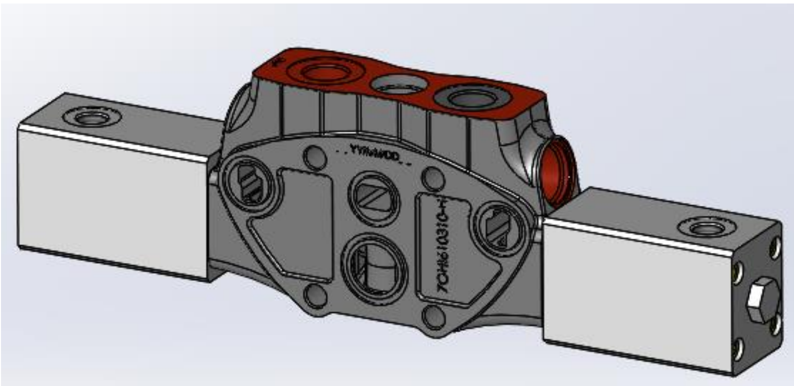

Figure 26. Walvoil prototype of the Downstream compensator

The particular embodiment of the compensator provides three ways, which allow the main spool discharge line to be connected, respectively, to the system tank T or to an energy recovery line R.

In Figure 27 the compensator section is represented.

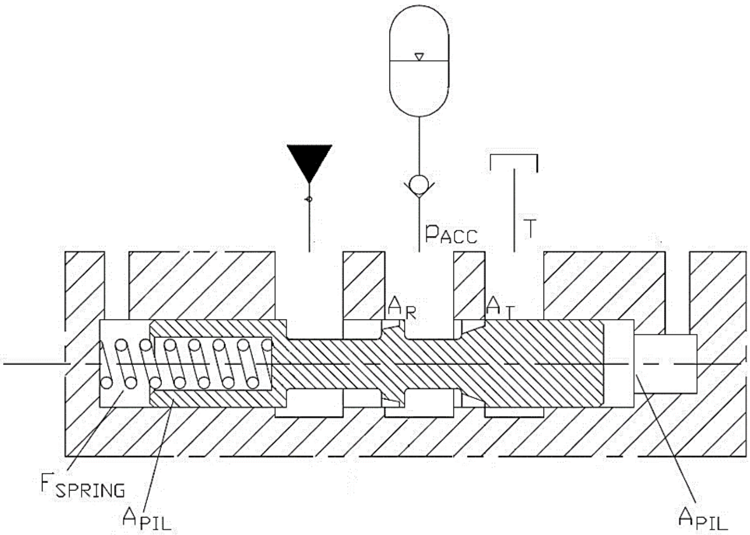

Figure 27. Downstream compensator section

In the rest position, the two notches (A_R and A_T) are normally opened. Along its stroke (x_{COMP}), it first closes the connection to the tank A_T and, afterwards, the connection to the recovery line A_R starts to throttle, so as to achieve a throttling function which preferably conveys the meter out flow towards the energy recovery line R.

The connection to the recovery line R remains open until the end of the compensator stroke, while the one to the tank line T close at about half a stroke, thus managing to recover on line R.

In case the R line cannot accept further flow, due to the accumulator pressure level (p_{ACC}), the discharge flow will be redirected to the system tank, without compromising the actuator speed.

The compensation downstream of the meter-out generates the so-called " *pressures multiplication* " phenomenon. This phenomenon leads to an increase in the pressures upstream of the compensator in the dominated sections; it is caused by the compensator itself that tries to copy the global LS pressure coming from the dominant section. This phenomenon actually makes the loads of the less loaded users equal to that of the most loaded section. To solve the problem of overrunning loads when only one section is operated (previously mentioned), an X line has been introduced for the “doping” of the LS signal. A low-pressure signal enters from this line (for example 15 bar); in presence of a single section operating in overrunning load, the global LS pressure should go to zero but the signal on the X line will keep the global LS line at a minimum value (for example 15 bar). Thanks to this system, the section (local LS tending to 0 bar) will "believe" to be dominated, causing the compensator throttling and taking the place of the outlet notches on return line of a standard DCV. This way is also the only one to throttle or close the T line in the compensator in these conditions, thus allowing recovery on the R line. In the paragraph *II.2.4.1* all the operating conditions of this architecture will be discussed.

It is important to underline that this compensator does not need additional devices or pressure signals to provide for the correct regulation of the meter out flow; its functionality is based on a completely mechanical design, without the support of any electronic control. The valve section design, previously described, is quite simple, consisting in a main spool and in a compensator spool like the most typical Load Sensing valves. It follows that the additional costs of the system only reside in the flow rate Re-Used system that will be described in the sub-paragraph II.2.6.

II.2.3 System Tuning

The Figure 28 shows the hydraulic schematic with two sections of the new proposed solution. The architecture consists of a 6-way spool and a 3-way compensator.

The new concept is derived by a typical Load Sensing directional control valve layout. The main spool selects along its stroke the LS signal from user's ports. The highest LS signal is then delivered to a conventional variable displacement Load Sensing pump that supplies flow at delivery pressure p equal to LS plus a fixed margin Δp_{LS} (*pump margin* described in sub-paragraph II.1.2). The Meter in notches area A_{IN} in the main spool define the flow Q_{IN} delivered to the user.

$$Q_{IN} \propto A_{IN} \cdot \sqrt{\Delta p_{LS}} \qquad 13$$

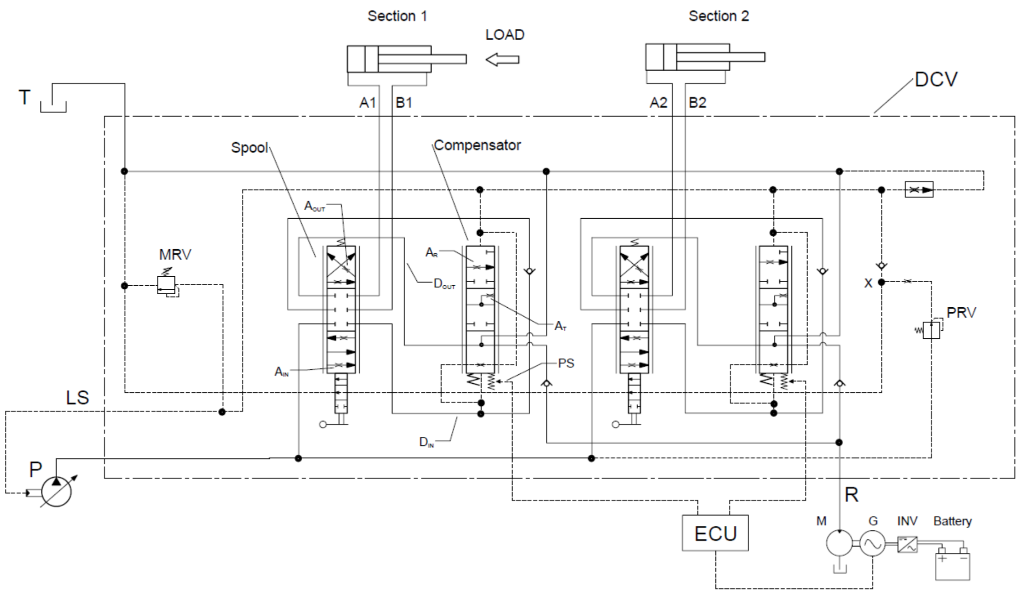

Figure 28. Hydraulic schematic with DCV and Re-Use system

Oil from pump P feeds in parallel the meter-in area A_{IN} of each spool and then the relative actuator through a check valve in channel D_{IN} downstream the meter-in; then oil returns from the actuator to the spool meter-out A_{OUT}.

The 3-way compensator located downstream the meter-out D_{OUT} sends the return flow Q_{OUT} in a preferred way through a check valve towards a regenerative line R, otherwise to tank T. A spring of negligible force keeps the local compensator in open position. The signal downstream the meter-in pushes the local compensator to open, while the load sensing signal LS acts in the closing direction.

Only when the local compensator is fully open, it sends its pressure signal into LS line; when the local compensator is throttling the flow Q_{OUT}, it copies the LS signal in D_{IN}. The result is that all meter-in areas see the same pressure drop $p_P - p_{LS}$ equal to the pump margin Δp_{LS}.

A low-pressure pilot source X (pressure multiplication phenomenon before described) can possibly feed the LS line depending on the spool position. In Figure 28, when a spool feeds the base side A, supposing the load resistant, pilot source X is dumped to tank and does not feed the LS line; if at least one spool feeds the rod side B, supposing the load overrunning, pilot source X pressurizes and feeds the LS line. Hence, in presence of overrunning loads, even when a single actuator is working and its local compensator is supposed to be fully open, the pilot source X makes the compensator throttle and thus potentially recover.

II.2.4 *Architecture operating conditions*

The principal operating modes of this architecture (referring to Figure 27) are listed below and the other working conditions will be combinations of these ones.

II.2.4.1 *Actuation of a single section with resistant load*

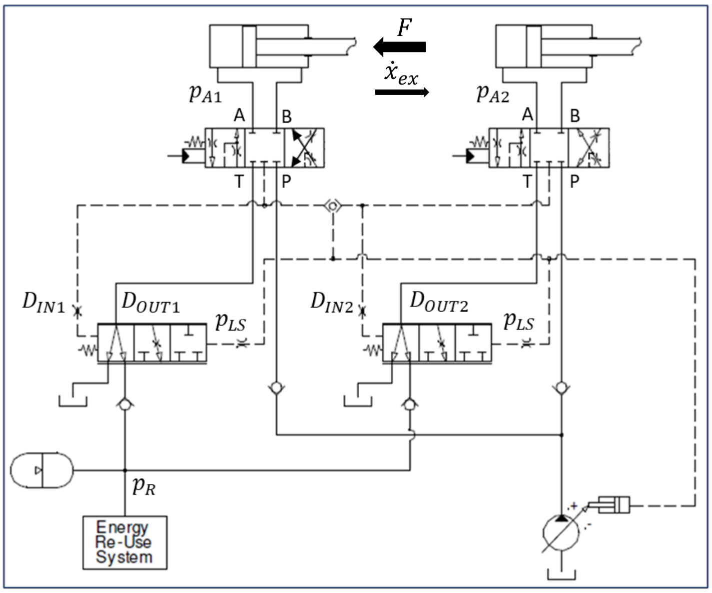

Figure 29. Single section with resistant load

Let assume that the spool in section 1 is actuated in P>A/B>T position (cylinder extension) and that the force on the actuator pushes the rod, i.e. load is resistant (Figure 29). In this condition, pressure signal downstream the meter-in D_{IN1} is equal to the load p_{A1} and opens the local compensator, therefore the line D_{OUT} downstream the meter-out is connected to tank T. The signal D_{IN1} feeds the LS line, therefore p_{LS} is equal to p_A. The pressure drop across the meter-in notches A_{IN} of the spool is equal to the pump margin Δp_{LS}, which means that the work port flow Q_A is proportional to the meter-in area A_{IN} and therefore depends on the spool stroke only (load sensing principle):

$$Q_{\mathrm{A}} \propto A_{\mathrm{IN}} \cdot \sqrt{\Delta p_{LS}} \tag{14}$$

In this condition, there is no difference compared to a traditional load sensing flow sharing valve; there are no recovery opportunities, therefore the compensator is fully open to tank, minimizing the pressure drops and operating pressure.

II.2.4.2 Simultaneous actuation of two sections: one at higher resistant load (dominant section) and the other at lower resistant load (dependent section)

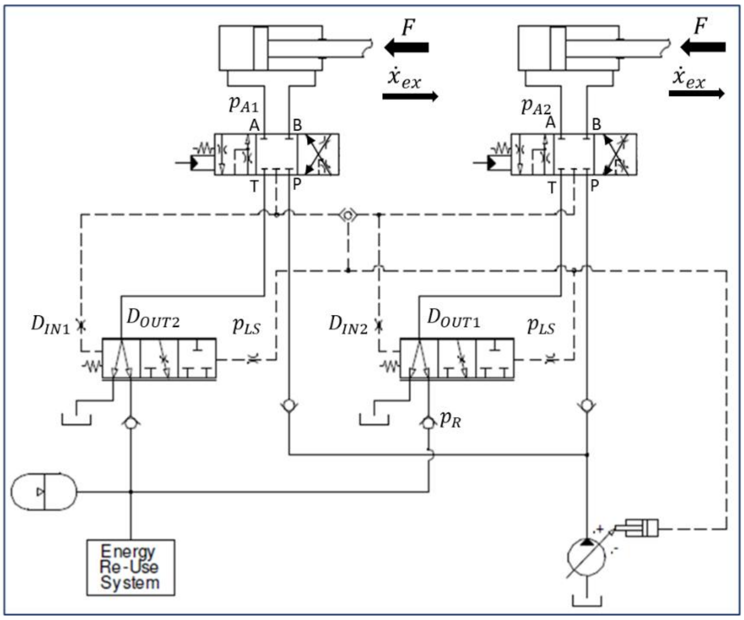

Figure 30. Simultaneous actuation of two sections (compensation conditions)

Let assume that both spools are actuated in P>A/B>T position (cylinders extension) and that the forces on both the actuators push the rods, i.e. loads are resistant (Figure 30). Let pressure at work port A1 p_{A1} be higher than pressure at work port A2 p_{A2}.

Section 1 is dominant and its compensator works exactly as described in the previous sub-paragraph: local compensator is fully open and LS pressure p_{LS} is equal to work port pressure p_{A1}.

Section 2 is dependant and its compensator copies the LS pressure p_{LS} in D_{IN2} downstream the meter-in, throttling the meter out flow Q_{OUT2}.

Pressure drop across meter-in notches is equal to pump margin Δp_{LS} in both sections, therefore equation (14) applies to both. This means that the work port flows depend on the spool stroke only (load sensing principle) and decrease proportionally in case of pump saturation (flow sharing principle).

The local compensator design is such that the connection between D_{OUT} and T closes at approximately 50% of its max stroke, while the connection between D_{OUT} and R closes at approximately 90% of its max stroke. The compensator of dependant section 2, which throttles the return flow Q_{OUT2}, feeds in a preferred way the recovery line R if pressure in D_{OUT} is higher than in R, otherwise the tank T.

Therefore, it is possible to recover energy during simultaneous movements in dependant sections, according to pressure in R: if pressure in R is lower than D_{OUT2}, recovery is possible; otherwise, it is not.

Note that during a simultaneous actuation of two sections, it is not possible to recognize the dominant section by simply looking at the work port pressures p_{A1} and p_{A2}, since they are identical in all sections. It is necessary to look at the work port pressure difference p_{A1}-p_{B1} and p_{A2}-p_{B2}.

II.2.4.3 Actuation of a single section with overrunning load

Traditional flow sharing valves often manage overrunning loads with a high backpressure generated by the meter-out notches, to prevent the cavitation of the actuator. Spool design has to consider the worst case, the highest overrunning load; therefore, when the load is low, energy dissipation occurs. In the new DCV, downstream compensator performs a variable restriction, which covers the function of the spool meter-out notches; therefore, spool meter-out area A_{OUT} can be larger, with a consequent energy saving when the load is low, respect to a traditional load sensing valve.

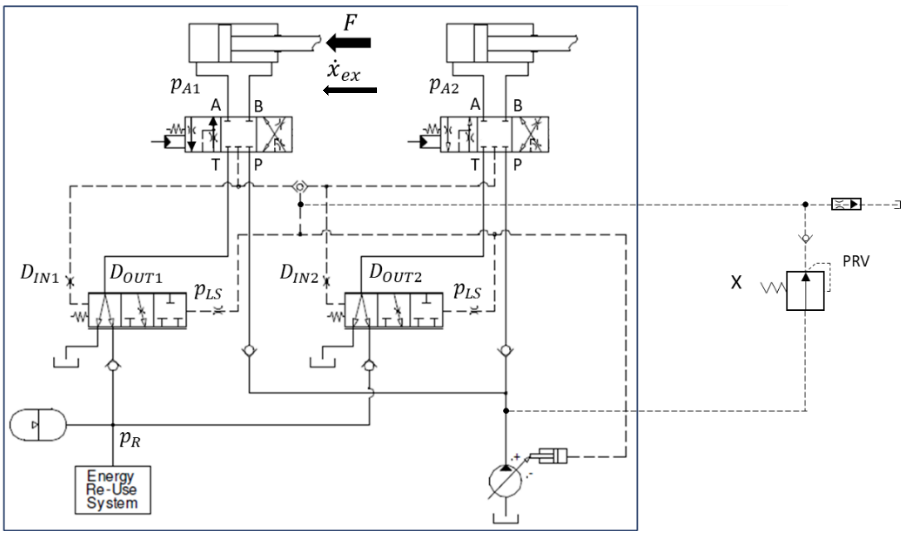

Figure 31. Actuation of a single section with overrunning load

Referring to Figure 31, let us assume that: the spool in section 1 is actuated in P>B/A>T position (cylinder retraction); the force on the actuator pushes the rod, i.e. load is overrunning; the meter-out area A_{OUT} is large. Thanks to the logic present on the spool, pilot pressure X feeds LS line, thus the local compensator works as if the section was dependant: the local compensator copies the LS pressure in D_{IN} downstream the meter-in. Pressure drop across meter-in notches is equal to pump margin Δp_{LS} (load sensing flow sharing principle). The meter-out flow Q_{OUT} goes in a preferred way into the R line, if the pressure in R is lower than in D_{OUT}; otherwise, it goes to tank T. Recovery is possible depending on the pressure in R: if the pressure in R is lower than D_{OUT} the recovery is possible.

In conclusion, the new DCV allows to save energy, having larger meter-out notches compared to a traditional flow-sharing valve, and to recover energy with overrunning loads.

II.2.5 Power diagram comparison

Figure 32 shows the power that the new DCV intends to recover during compensation or when lowering a load, compared to the power loss of a Traditional Load Sensing Flow Sharing DCV.

From hydraulic point of view, the maximum theoretical recovery corresponds to the power loss occurring in conventional LS systems due to compensation, or to the power loss due to spool meter-out with overrunning loads.

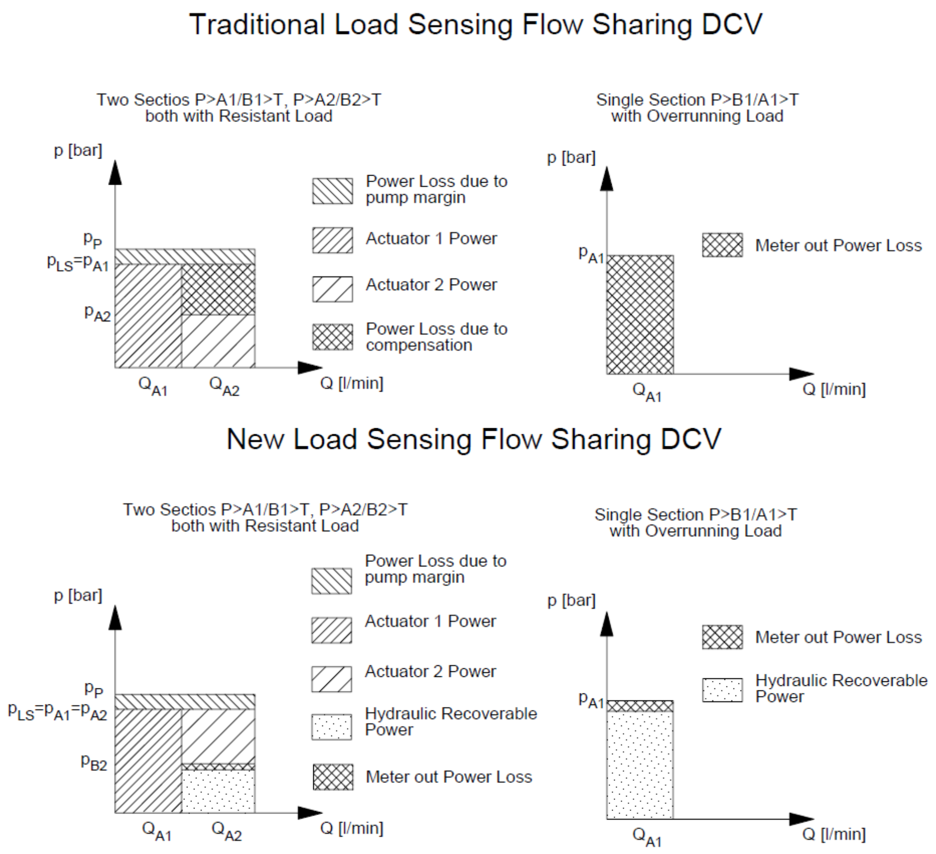

Figure 32. Power Diagram Comparison between traditional and new Load Sensing Flow Sharing DCV

It should be finally noted that as for traditional DCV, the new DCV as well allows to apply superimposed methods to reduce the pump margin power losses, such as variable stand by [17] [18] or pump positive control [19].

II.2.6 Energy Recovery Control Strategy

Once the recovered flow is available in the R line, its management depends on the choices of the equipment manufacturer.

The recovered power on the R line is directly proportional to the flow rate and to the pressure on that line:

$$P_R \approx Q_R \cdot p_R \approx C \cdot w \approx V \cdot I \tag{15}$$

From this evaluation, the following considerations can be derived:

- Q_R has no value if $p_R = 0$;
- p_R could be fixed to a certain value but it would not fully exploit the recovery opportunities;
- p_R could be defined by an accumulator but it would not fully exploit the recovery opportunities;

and then the final conclusion is:

- p_R needs to be dynamically controlled.

Summarizing, it could be possible to regenerate the recovered flow directly into the system, to store it in a hydraulic accumulator, or to transform it in electrical energy and store it in a battery.

From the experimental tests and numerical simulations run during this Ph.D. work (available in the next chapter), it was evident that this last solution provides the best opportunity to fully exploit the energy flow rate collected by the new DCV.

Particularly, an active electronic control of the backpressure p_R, allows the maximum recovery and to avoid excessive dissipation through the downstream compensators.

This pressure on the recovery line p_R can be dynamically controlled by these components in series (Figure 28): a hydraulic motor M, coupled to an AC generator G which charges a Battery thanks to an inverter INV. This recovery system layout is provided with a control logic that maximizes the efficiency.

The power on R line is recovered only if a resistant torque is generated on hydraulic motor Each local compensator sends its position by means of a position sensor PS to an Electronic Control Unit ECU, which manages the resistant torque on generator G.

This resistant torque increases the pressure on R line p_R and consequently the compensator reduces its throttling and then it opens till a position of maximum efficiency. By reading the compensation position it is possible to provide electronically the correct torque to the generator, in order to maximize the recovery.

In detail, the control strategy used in this system is described in Figure 33.

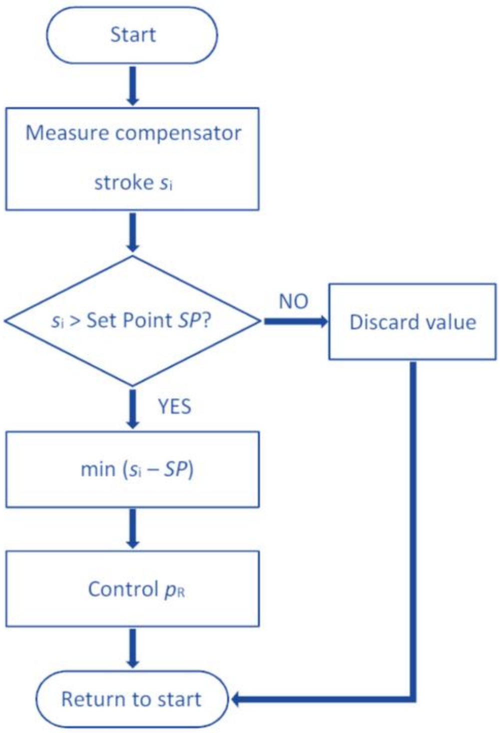

Figure 33. Control strategy

Assuming that:

- $\boldsymbol{s_i}$ is the compensator stroke (i = 1...n where n is the number of sections);
- **SP** is the optimal set point that corresponds to a position where T line is closed and R line is maximally opened (between 60% and 80% of max compensator stroke);
- $\boldsymbol{p_R}$ is the pressure on the recovery line that has to be varied.

The strategy is a closed loop actuation of p_R with the feedback of the compensator stroke s_i. A position sensor PS measures the compensator stroke that is compared to the set point SP. If the compensator stroke s_i is lower than the set point *SP*, the value does not influence the controller. Among s_i values higher than *SP*, the minimum s_i gives the error, which defines the correction to give to p_R .

This control strategy was validated through a pressure compensation test with a numerical model (illustrated in the next chapter) developed in the lumped and distributed parameters software Simcenter Amesim®.

Chapter III: **Experimental activities**

III.1 Experimental activities components

III.1.1 Bobcat 435 ZHS

For the execution of the digging cycle analyzed in this thesis work, a Bobcat 435 ZHS mini-excavator was used (Figure 34).

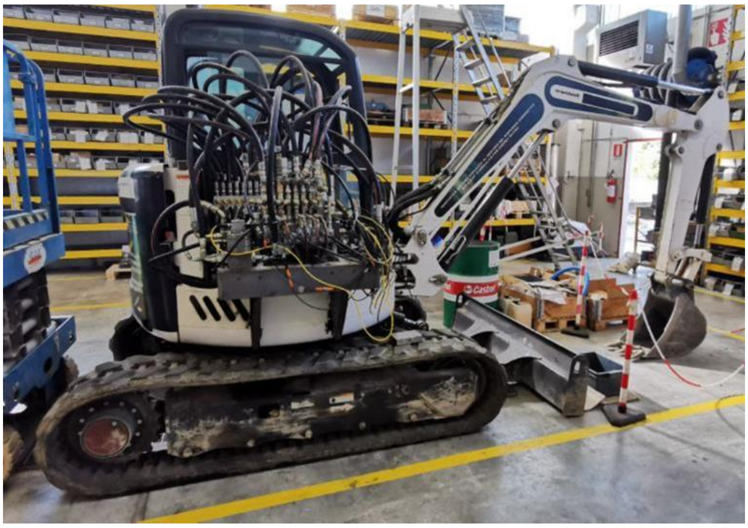

Figure 34. Bobcat 435 ZHS

The main features of this excavator are listed in Table 4.

BOBCAT 435 ZHS	
Engine Model	V2003-M-DI-TE2B
Engine Fuel	Diesel
Engine Cooling	Liquid
Engine Power	49 HP (36.5 kW)
Fuel Tank	67.4 l
Maximum Dig Depth	3.42 m
Bucket Digging Force	35105 N
Weight	4788 kg
Travel Speed - Low	4.5 km/h
Travel Speed - High	8.7 km/h
Pump Capacity	147.7 l/min
Auxiliary Std Flow	75 l/min
Hydraulic Reservoir	29.9 l
Slew Speed	9.3 rpm

Table 4. Bobcat 435 ZHS main features

This excavator is composed by four principal actuators: boom, arm, bucket and swing (Figure 35).

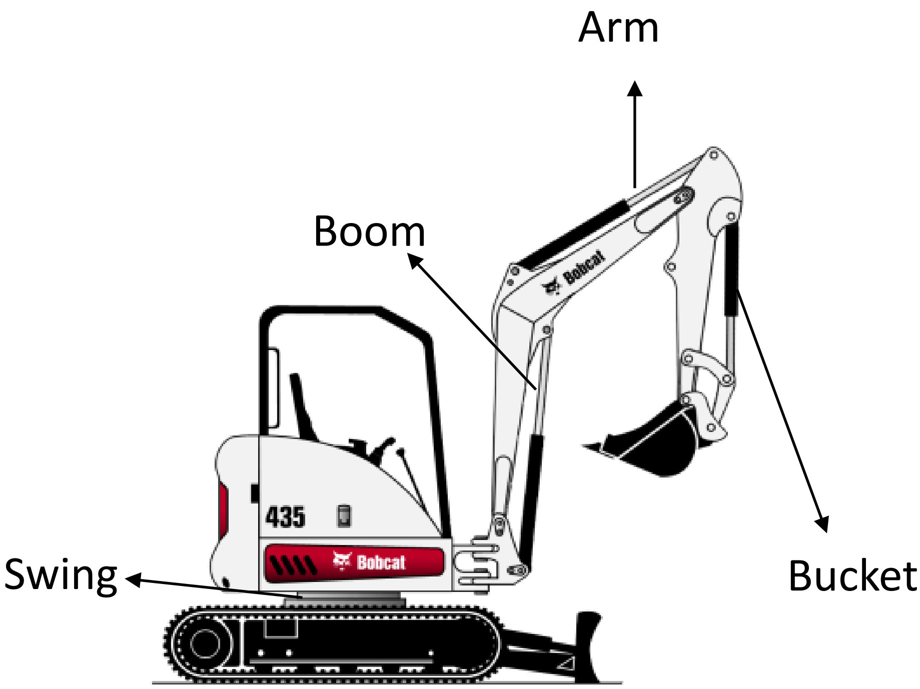

Figure 35. Bobcat 435 ZHS actuators

Figure 36. Boom actuator of the Bobcat 435 ZHS excavator

Figure 37. Arm actuator of the Bobcat 435 ZHS excavator

Figure 38. Bucket actuator of the Bobcat 435 ZHS excavator

The DCV actually mounted on this machine is a traditional Walvoil DCV as shown in Figure 39.

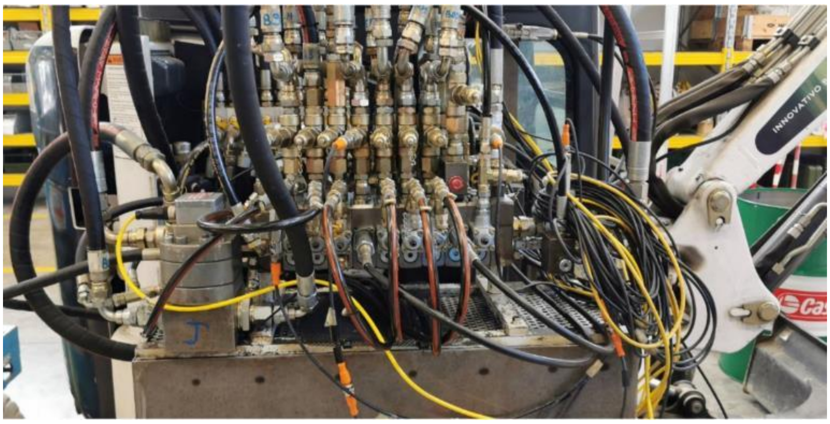

Figure 39. DPX100, DCV on the Bobcat 435 ZHS

III.1.2 Energy Recovery DCV

The new DCV was used to perform all the bench tests, in particular three different compensators were used that modify the functionality of the valve itself. The first compensator is aimed at post-compensation in meter-in, the second at post-compensation in meter-out without energy recovery and, finally, the third at post-compensation in meter-out with energy recovery.

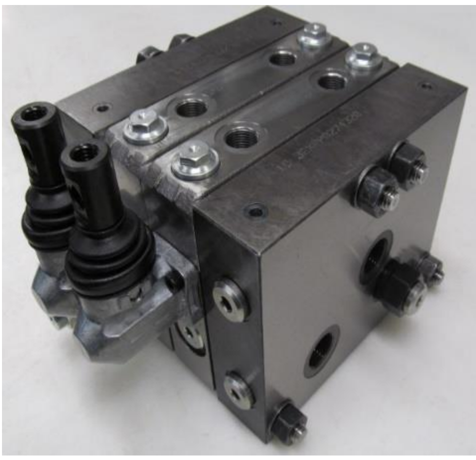

Figure 40. Final product new DCV

III.1.3 Test bench

The experimental tests carried out on the DCV were performed with the aid of a test bench located at Walvoil Test Department.

Figure 41. Test bench number 14, Walvoil Test Department

The test bench used is the number 14 of Walvoil Test Department. It is made up of two stations: 14a (left) and 14b (right). The bench is able to test the characteristics of numerous hydraulic components, such as monobloc, modular and Load Sensing DCV. The bench side 14a is supplied by a variable displacement Rexroth axial piston pump with variable displacement (element 15 in Figure 42), driven by a 55 kW electric motor. The maximum pump displacement (V_0 max) is 125 $\frac{cm^3}{rev}$ the maximum deliverable flow rate is 180 $\frac{L}{min}$ at a pressure of 170 bar. The station 14a has a maximum working pressure of 350 bar, tolerating peaks up to 400 bar; the outlet connection of the station in the hydraulic diagram is represented by P1.

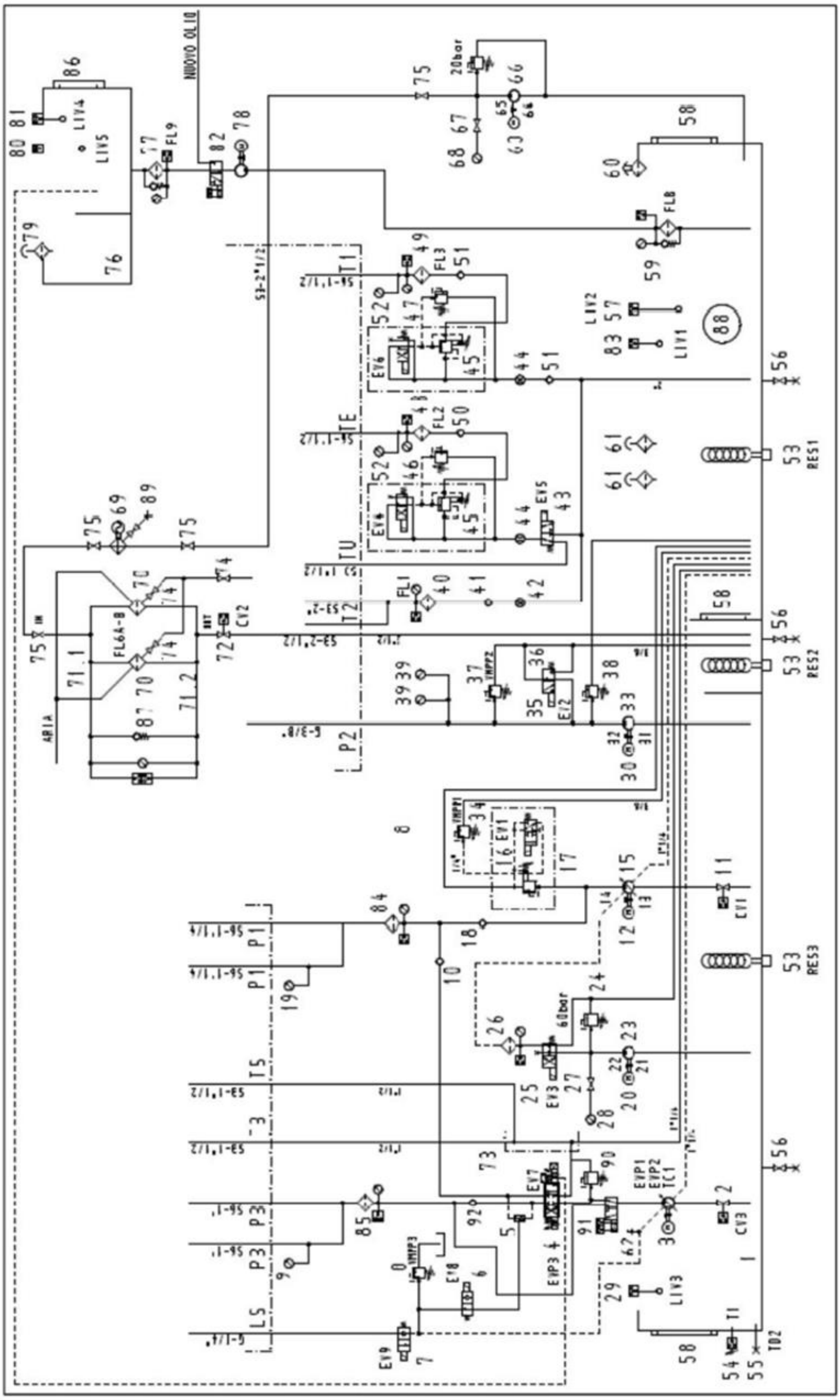

Figure 42. Hydraulic scheme of Test bench

Station 14b is also powered by a Rexroth axial piston pump with variable displacement (element 3 in the hydraulic diagram), but with a lower maximum displacement (V_0 max = 71 $\frac{cm^3}{rev}$). The electric motor that drives the pump has a power of 55 kW and the pump is capable of delivering a maximum flow rate of 106 $\frac{l}{min}$ at a pressure of 350 bar. The outlet connection is represented by P3, the maximum working pressure is 420 bar. The two pumps P1 and P3 have the possibility of working independently, allowing two separate tests to be carried out in the two stations; P1 and P3 can also work together to power station 14a ("master" station), thus achieving a flow rate of 286 $\frac{l}{min}$. In addition to the two main pumps, there is also a common pump to the two stations (P2 in the circuit diagram), in particular a Hawe submersible pump with radial pistons with fixed displacement is mounted, driven by a 4.1 kW electric motor. The maximum flow rate of this pump is 6 $\frac{l}{min}$, the maximum working pressure is 350 bar, accepting maximum peaks of 500 bar. There are three auxiliary pumps inside the test bench: element 23 for moving the plate (displacement change) of pump P1; element 66 (off-line) for the thermal regulation and filtration of the working fluid; element 78 for the recovery of oil from the collection tanks of the bench and the introduction of new oil. The information on the oil temperature (which is measured by the thermostat 54 in the tank) is made available to the user through two control panels (Figure 43), where there are two touchscreen displays through which the user can intervene to change the temperature. Outside the building where the counter is located there are air heat exchangers, inside the tank there are resistances; depending on whether the measured temperature is higher or lower than the set one, these two systems will intervene to regulate it.

Figure 43. Control panel with the test bench touchscreen display

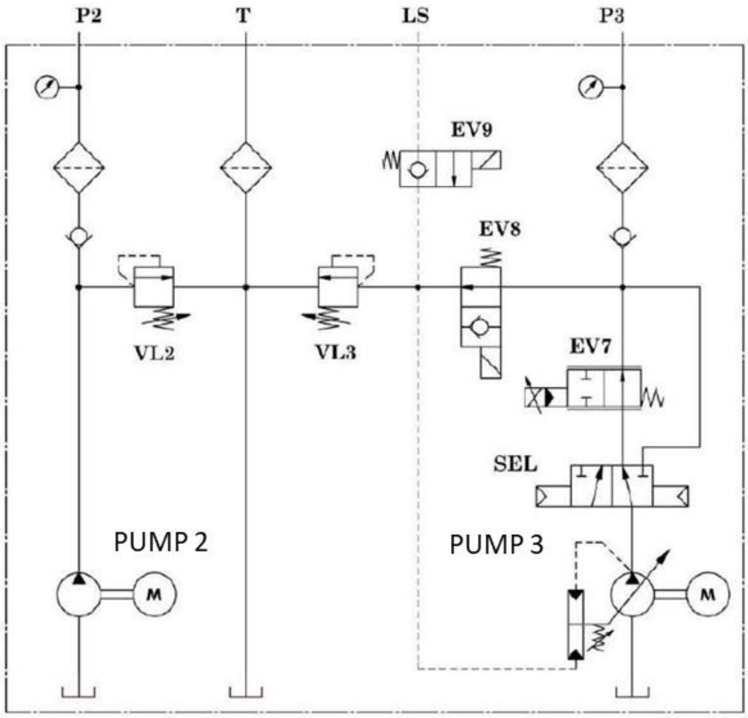

Figure 44. Simplified hydraulic diagram of station 14b

The tests were carried out on bench 14b (simplified hydraulic diagram shown in Figure 44), which control valves (EV8 - EV9) are able to operate the pump in LS mode with variable displacement or in fixed displacement mode; in this latter case the EV7 potentiometer adjusts the delivered flow rate. When the station works in LS mode with variable displacement, the SEL selector is operated so that the flow rate delivered by the pump bypasses the EV7 element, so as to eliminate the pressure losses due to this element. Another important element on the control panel is the red "mushroom" button, which has the emergency stop function.

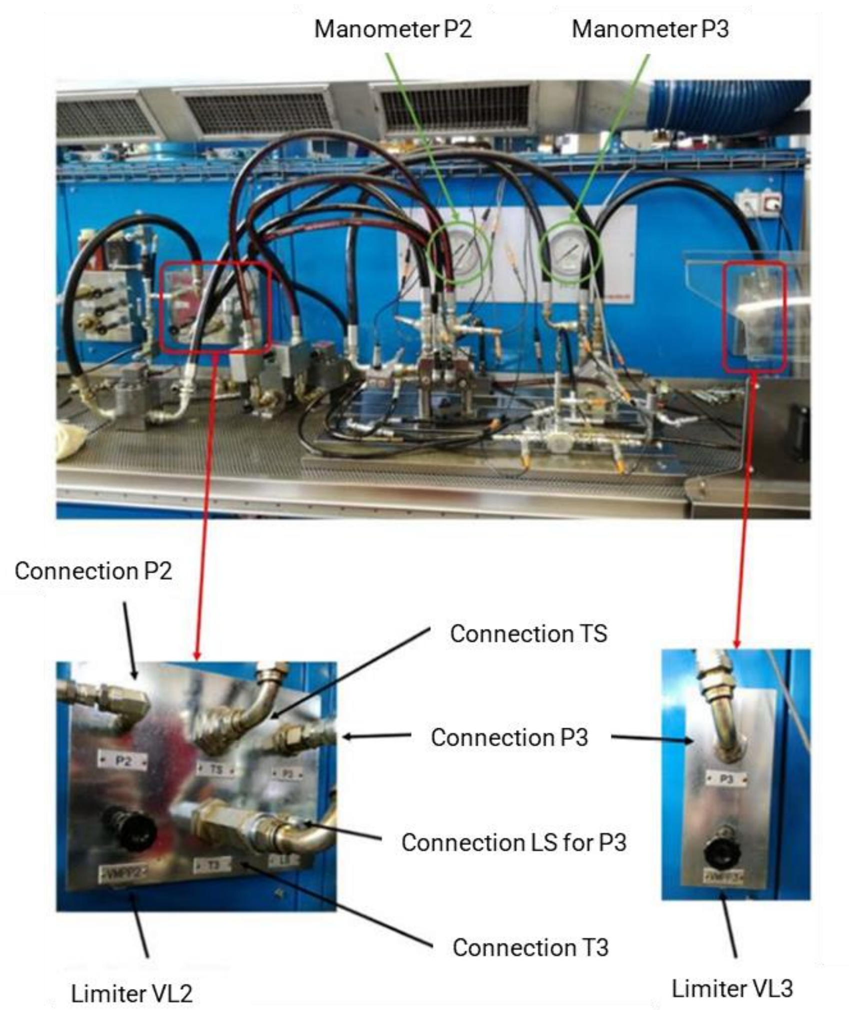

Figure 45. Station 14b

The information of the pressure values delivered by pumps P2 and P3 that supply the station is given by the manometers mounted on the bench, visible in Figure 45; the same figure also shows the different bench connections, with the two knobs for adjusting the pressure relief valves VL2 and VL3, which have the function of defining the maximum pressures that can be reached.

III.1.4 Electronic for acquisition

III.1.4.1 Rack and acquisition card

The acquisitions of flow rates, pressures and positions made during the experimental tests were possible thanks to the use of modular loggers.

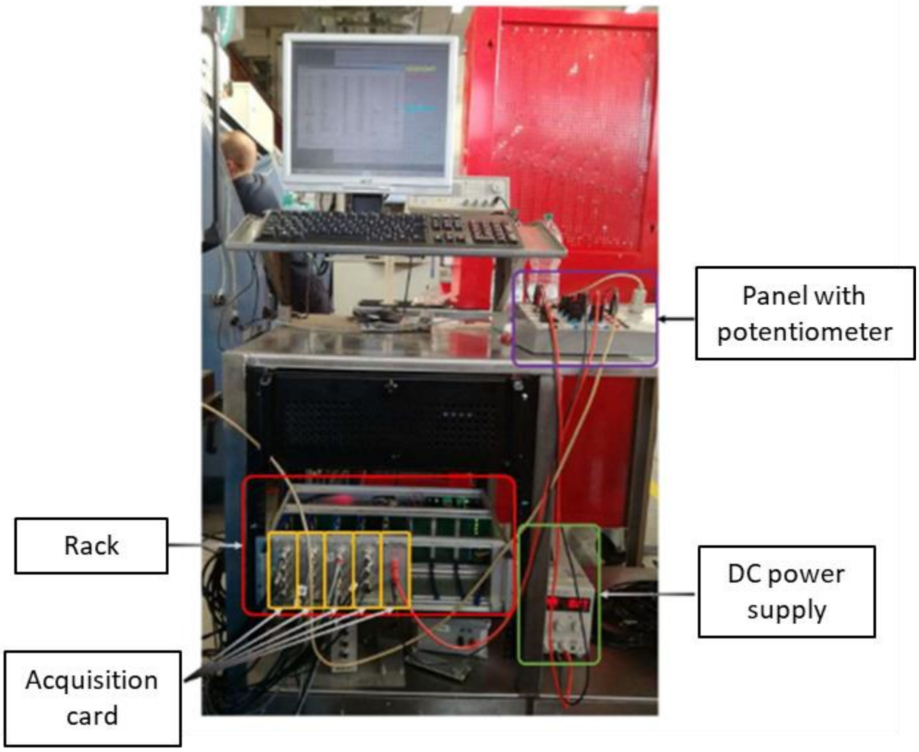

Figure 46. Acquisition system

These devices are equipped with acquisition cards inside them from which the signals come that will then be managed by the acquirers. Depending on the type of input signal, the acquisition cards can be classified into different families: frequency signal or analog signal (current or voltage).

III.1.4.2 Acquisition card: signal in frequency

The frequency acquisition cards receive in input the signals of the instruments that work in frequency, such as the flow meters and the phonic wheels.

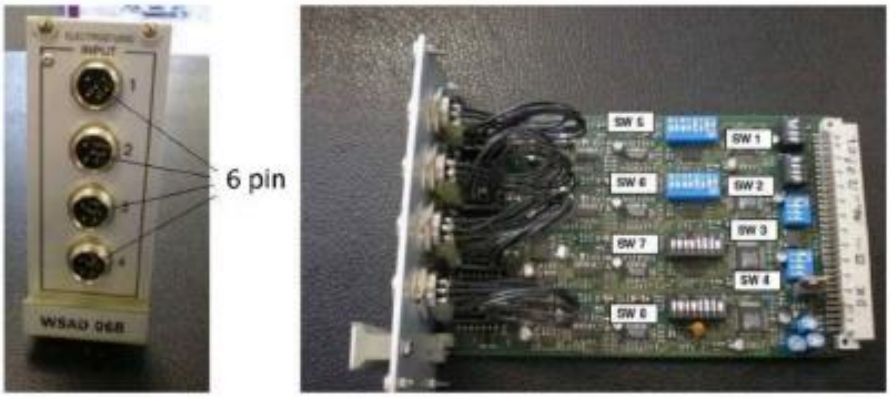

Figure 47. Frequency card acquisition

As shown in Figure 47, these cards are equipped with 6-pin microphone connectors and 8 sets of micro switches. The connectors have the task of choosing the channel of the acquired signal, while the pins are functional to setting the working frequency of the instrument.

III.1.4.3 Acquisition card: signal in current

The current acquisition cards receive current signals with values from 0 to 20 mA in input. They were used for the acquisition of signals from Trafag transducers, in the specific case of the experimental tests performed. As shown in Figure 48, these cards are equipped with 3-pin microphone connectors.

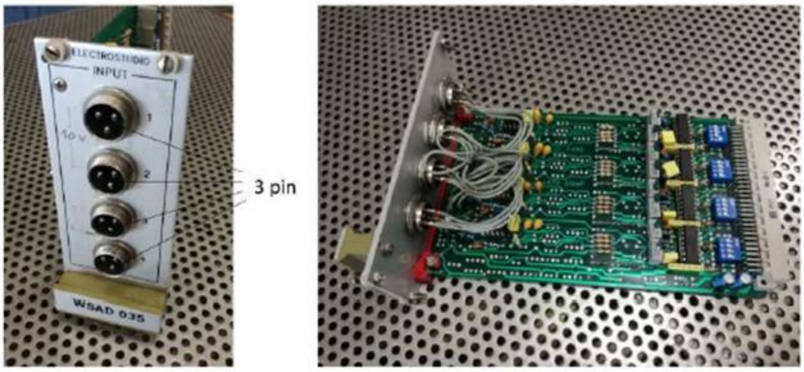

Figure 48. Current acquisition card

III.1.4.4 Mixed capture card

These cards acquisition category is characterized by the presence of different types of microphone connectors, capable of receiving current and voltage signals too, these ones are normally 4-pin and with input signal between 0 - 3 V or 0 - 10 V. They are also able to receive signals from potentiometric sensors, such as the Gefran position transducers used during the tests.

III.1.5 Transducers

III.1.5.1 Gefran PY2 displacement transducers

For the acquisition of the spool position signals, Gefran PY2 potentiometric displacement transducers were used, whose characteristics are shown in Table 5.

Gefran PY2	
Stroke	25/50 mm
Accuracy	±0.2%
Temperature range	-30 ÷ 100 °C
Connection	5 pin

Table 5. Gefran PY2 characteristics

The transducer positioning during the experimental tests is guaranteed by an articulated arm, constrained to the bench (Figure 49).

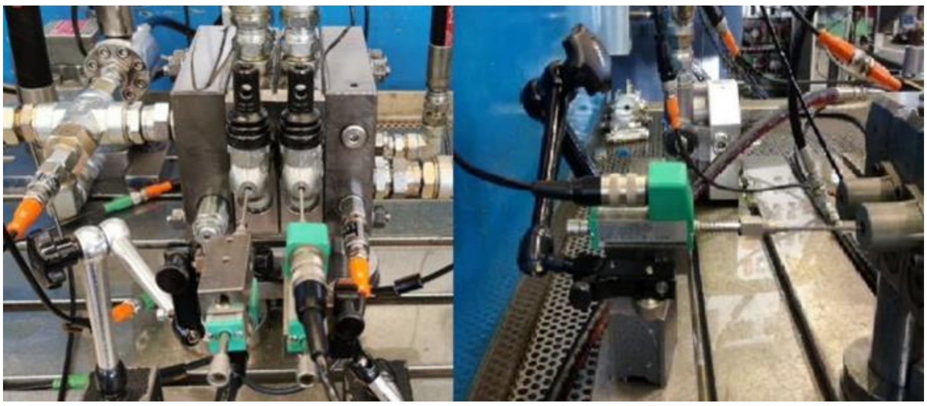

Figure 49. Gefran PY2 transducers mounted on an articulated arm

III.1.5.2 VSE – VS2 Flow rate mem

VSE - VS2 gear flow meters were used to measure the flow rates. This type of manometers works thanks to the movement of two calibrated gear wheels (Figure 50). The flow, passing inside the instrument, sets the two wheels in rotation; the rotation of the two elements is picked up by inductive pick-up sensors and whenever the passage of a tooth is picked up by the sensors, a pulse signal is generated.

Figure 50. Gears detail of VSE - VS2

Each single pulse is associated with a volume that generates it, called pulse volume V_m; it will depend on the size of the meter. The magneto-resistive *pick-up* sensors are positioned with a circular phase shift from one to the other of ¼ distance between two teeth, thanks to which it is possible to trace the direction of rotation (Figure 51). The signals are made more robust thanks to the presence of amplifiers. The frequency of the square wave signal that will be formed will be directly proportional to the instantaneous flow rate that crosses the instrument; in this case, the uncertainty is ± 0.3%.

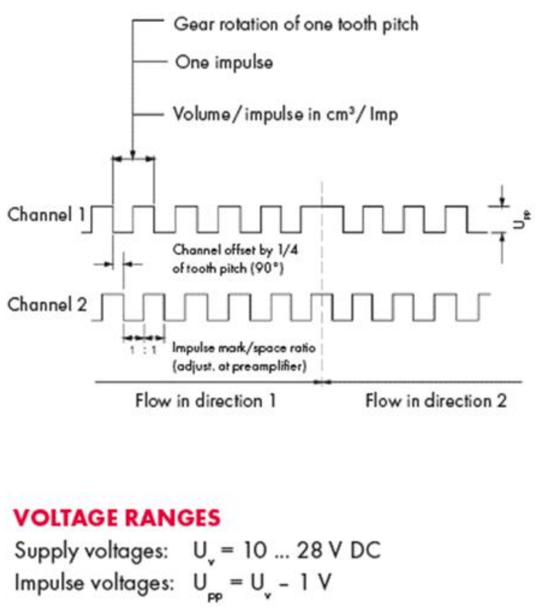

Figure 51. VSE signals flow meters

The maximum measurable flow rate is 120 $\frac{l}{min}$, the maximum acceptable pressure is 350 bar and the working temperature range is -40 ÷ 120 ° C. Figure 52 shows the characteristics of the pressure drops.

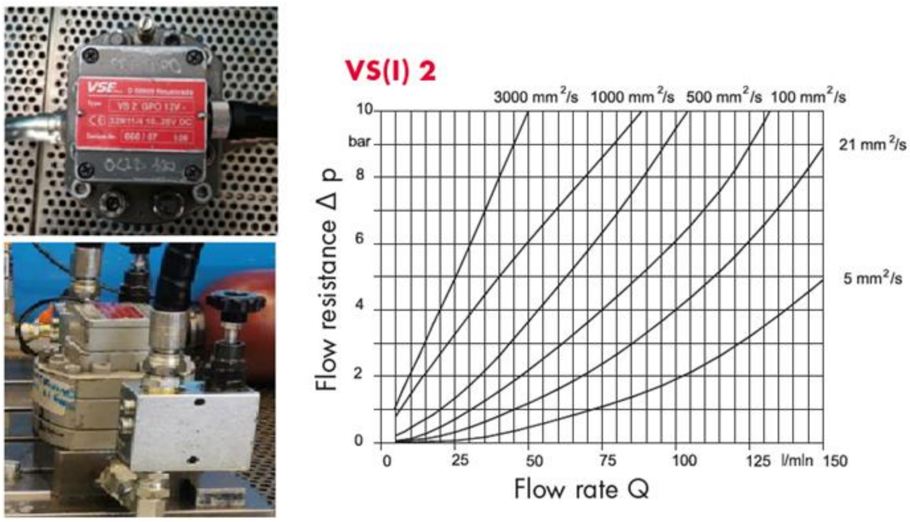

Figure 52. VSE VS2 and the pressure drops curve

III.1.5.3 Trafag NAT pressure transducers

Trafag NAT transducers (Figure 53) were used to measure the pressures, their main features are summarized in Table 6.

Figure 53. Trafag NAT pressure transducers

Trafag NAT	
Range	0 ÷ 600 bar
Accuracy	±0.3%
Output	4 ÷ 20 mA
Temperature range	-25 ÷ 85 °C
Connection	4 pin

Table 6. Trafag NAT pressure transducers main features

It is observed that the output signal (which will then go into the acquisition cards) ranges from 4 to 20 mA, while the acquisition card has a range from 0 to 20 mA; it is therefore necessary to make a correction, due to the 4 mA gap, in order to find the begin scale:

$$Begin\ scale = -4 \cdot \left(\frac{Full\ scale}{16}\right) \quad [bar] \tag{16}$$

In this way a 4 mA signal coming from the transducer will coincide with a pressure equal to 0 bar; a 20 mA will coincide with 600 bar (full scale), as shown in the graph in Figure 54.

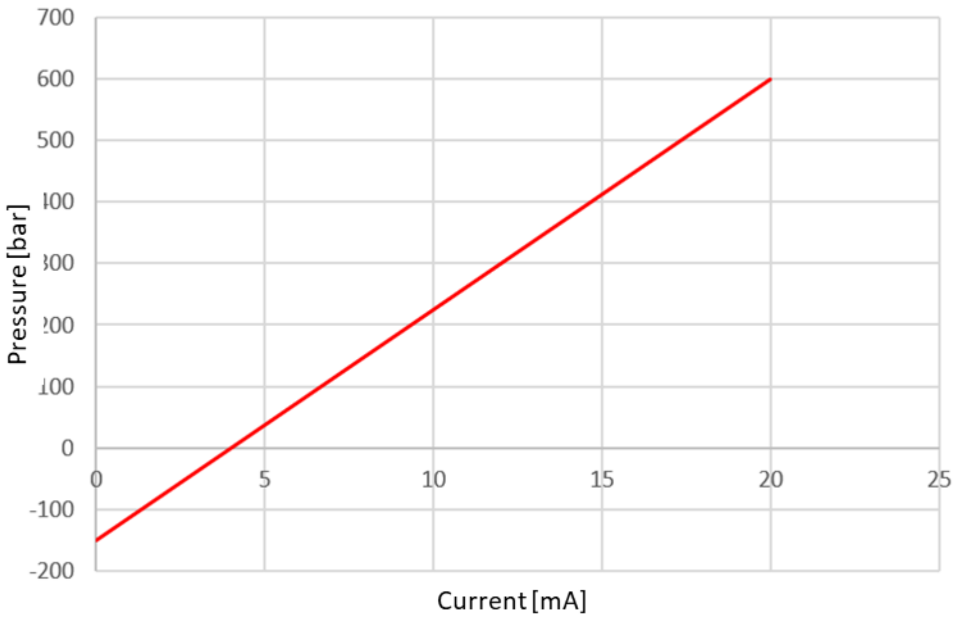

Figure 54. Trafag NAT calibration transducer curve

III.1.6 Pressure limiter valve

This element has the functionality of ensuring that the pressure value at a certain point does not exceed a certain value. The valve in question is a normally closed element, which opens when the calibration value is exceeded, sending the excess flow to the tank line. Thanks to its behavior, it is widely used as a safety valve, to safeguard the circuit from abnormal overpressures. The ISO scheme is shown in Figure 55.

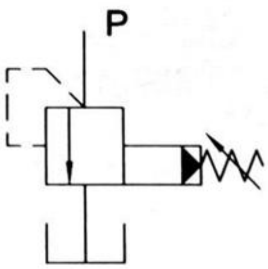

Figure 55. Pressure limiter valve ISO scheme

It is possible to understand its functioning in detail of the cartridge pressure limiter valve in Figure 56.

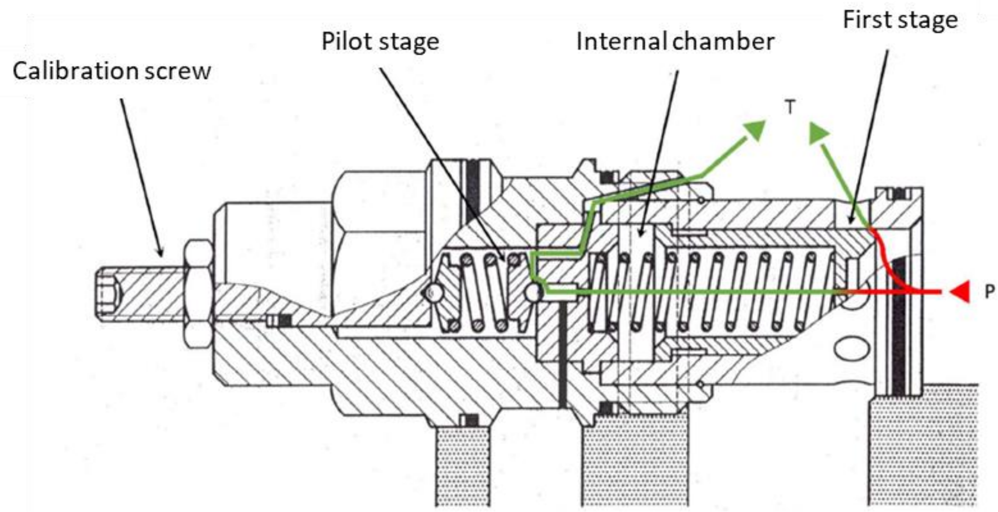

Figure 56. Cartridge piloted relief valve

Being piloted, there is a pilot stage and a main stage; if the pressure is large enough to overcome the spring preload in the pilot stage, a flow towards T will begin to establish, which in passing through the orifice of the element in the main stage, generates a pressure drop in the internal chamber. At this point, the pressure on the right will be able to move the element of the main stage to the left, thus opening the passage towards T, thus stabilizing the pressure P. A cartridge valve is also installed in the bench, shown in Figure 57, whose characteristic diagram is represented in Figure 58.

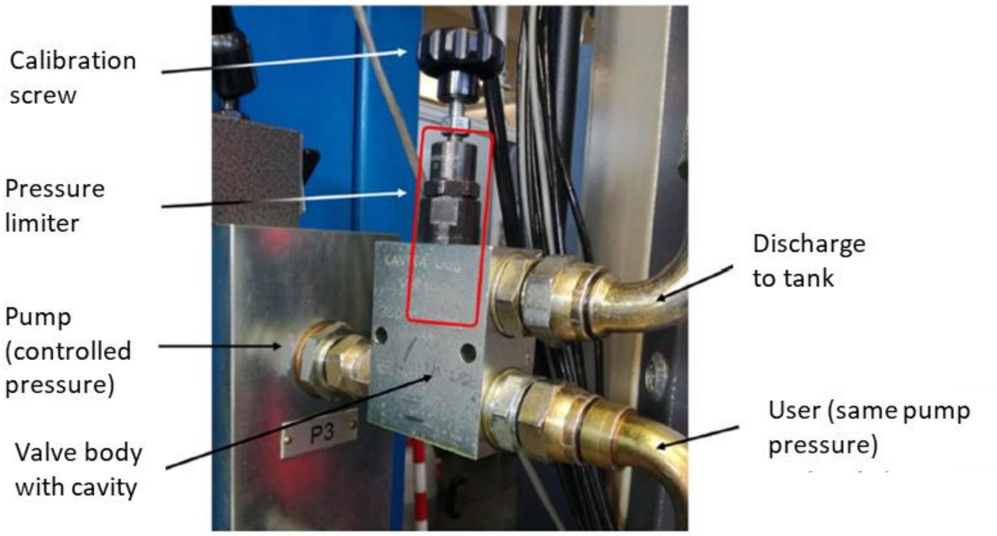

Figure 57. Cartridge pilot operated pressure relief valve mounted on the test bench

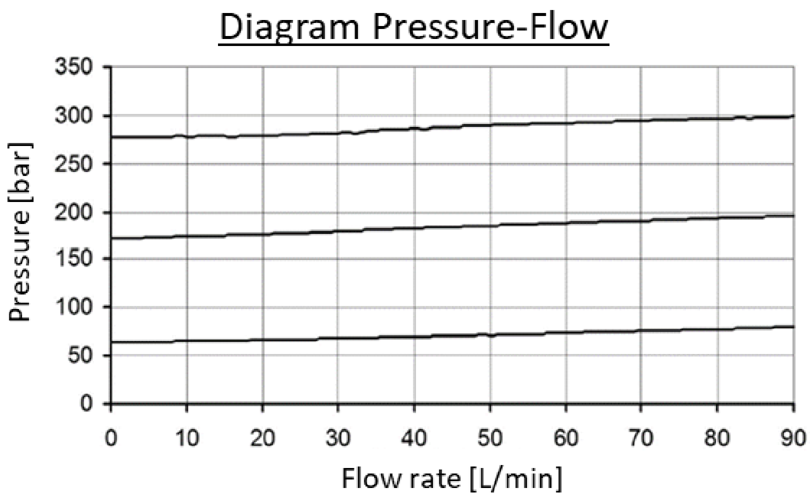

Figure 58. Characteristic diagram of the VLP mounted on the test bench

III.1.7 Digging cycle component of Bobcat 435 ZHS

As mentioned above, a traditional Walvoil DCV (DPX100 model) is installed on the Bobcat 435 ZHS excavator used for the excavation cycle (Figure 59), through which the machine users are supplied. The users that will be analyzed in this thesis will be those for the boom (first arm), the arm (depth arm), the bucket (movement of the bucket) and the swing (rotation of the turret), shown in Figure 59.

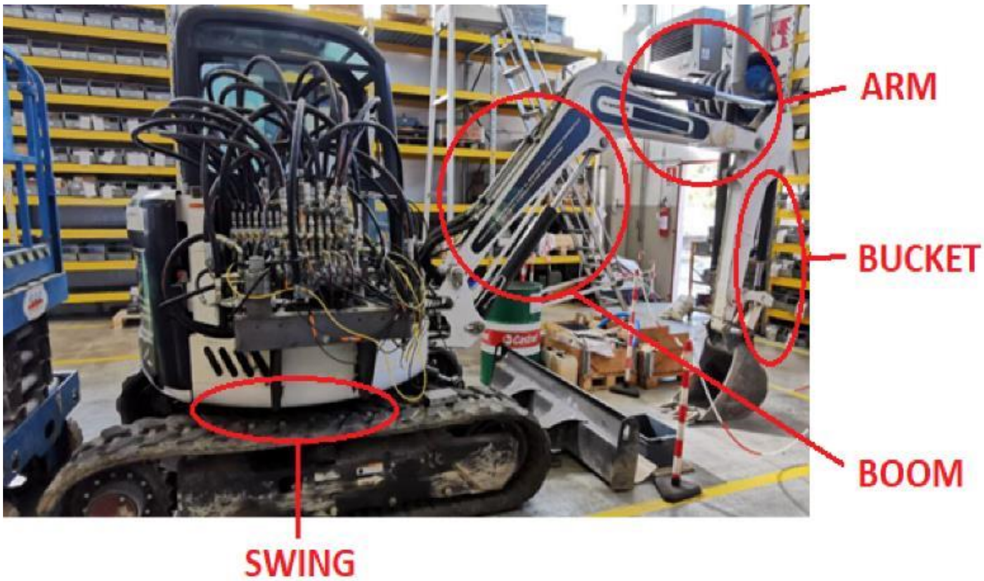

Figure 59. Boom, arm, bucket and swing actuators

The system operation and the connection between the DCV and the users are shown in the hydraulic diagram in Figure 60.

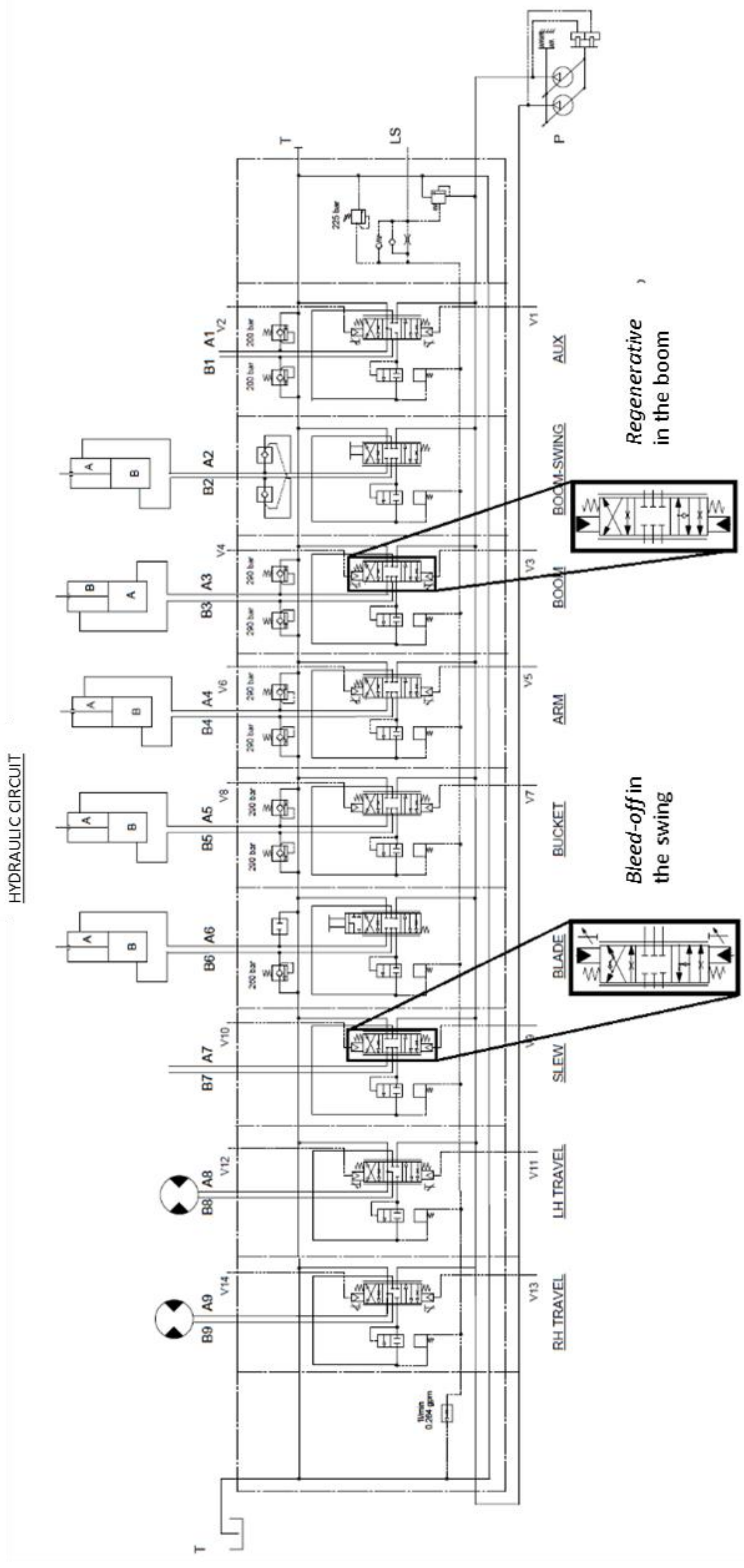

Figure 60. Bobcat 435 hydraulic circuit with DPX100

III.1.7.1 Boom

The boom cylinder dimensions and the connections with the DCV are shown in Table 7.

Cylinder - Boom	
Cylinder diameter	95.3 mm
Rod diameter	50.8 mm
Length	678.7 mm
Head side connection	User A
Rod side connection	User B

Table 7. Geometry features and hydraulic connections of the Boom

The main spool used in the boom section is depicted in Figure 61.

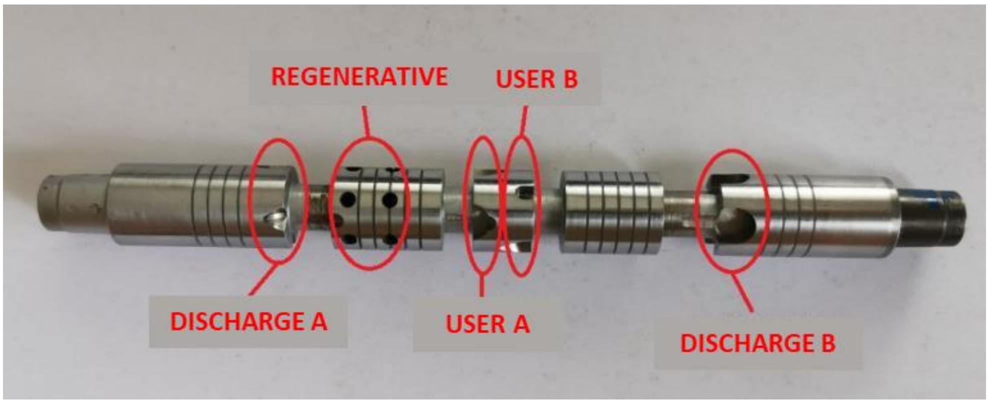

Figure 61. Boom section's main spool

The spool in question is not standard, in fact it is possible to observe the presence of a regenerative function; the holes on the spool communicate use A with the bridge when supplying use B (Figure 62).

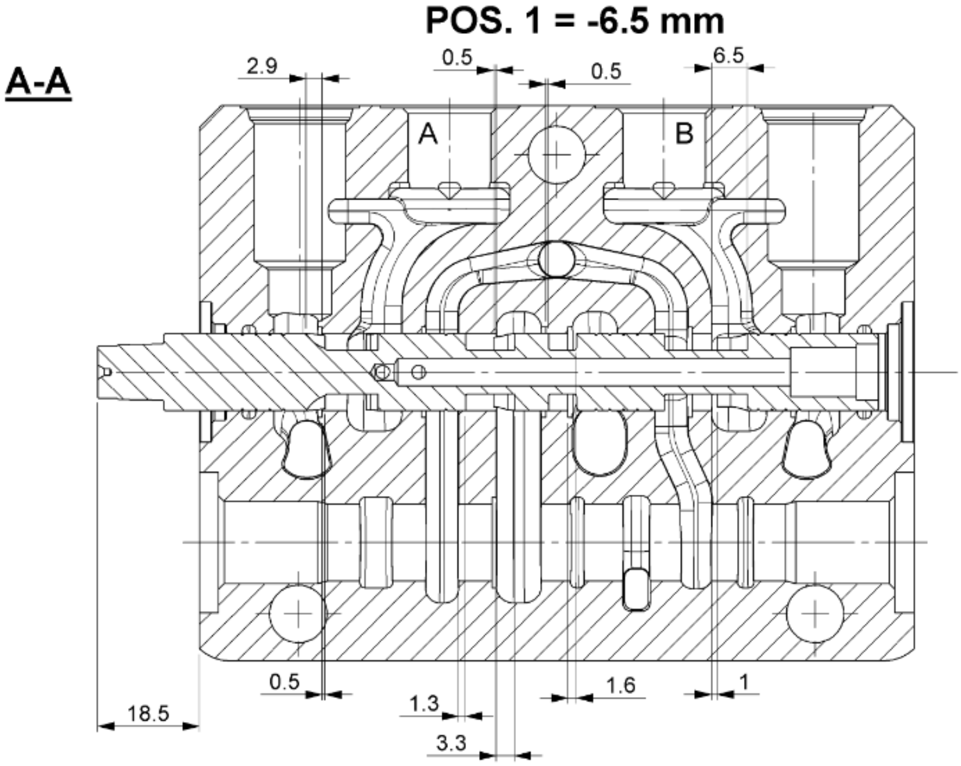

Figure 62. P-B; A-T Configuration with a regenerative function

The flow rate can only pass from A to the bridge and not vice versa, thanks to a check valve mounted inside the spool. Regeneration occurs only when the pressure in A is higher than the bridge pressure, a condition happening, for example, in case of overrunning loads. This flow rate will be added to that of the other user (B) going in fact to speed up the movement of the actuator with the same pump demand, therefore it is in effect an energy saving solution. The sizing of the regenerative is a very delicate process, since if you exaggerate with the regenerative flow, you will have negative effects on the controllability of the actuator and cavitation. The laws of area of the spool are shown below.

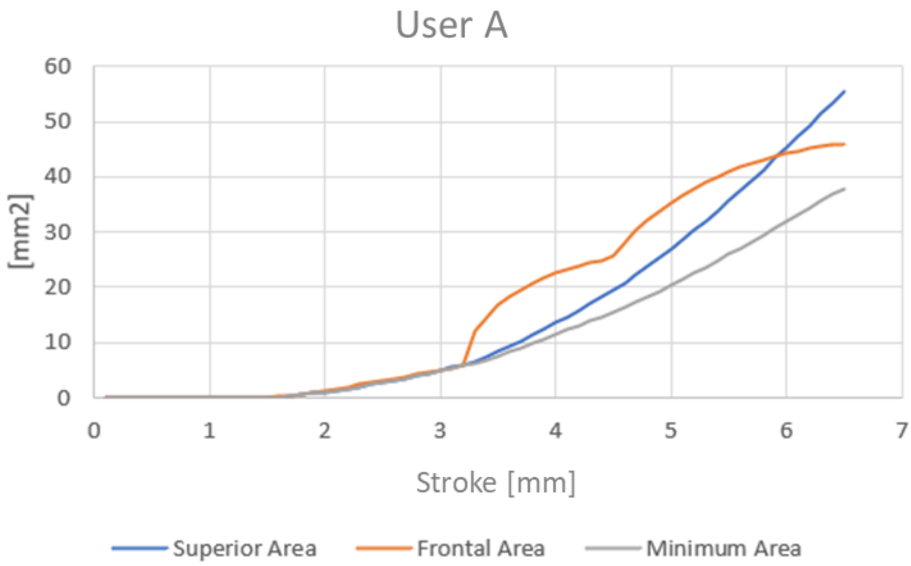

Figure 63. User A low of area, boom

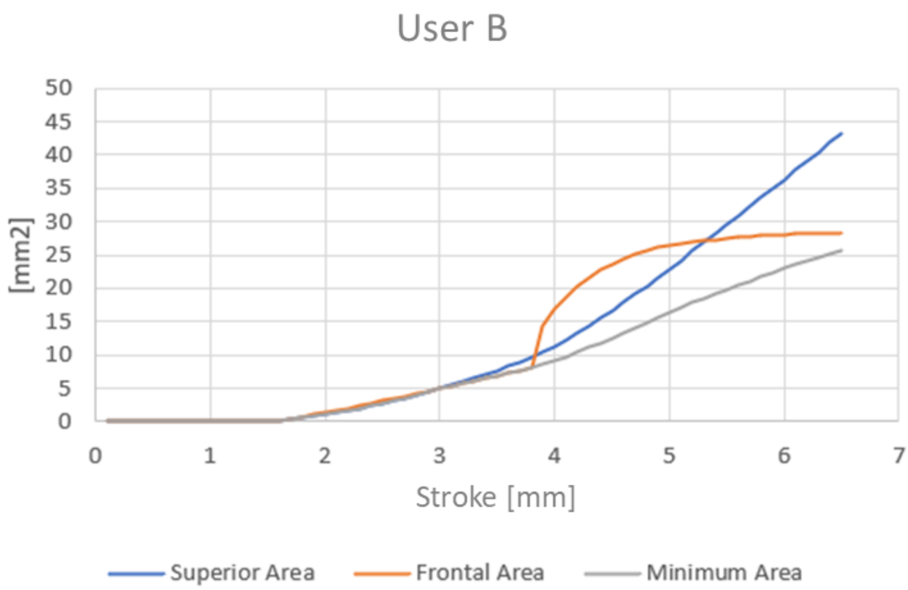

Figure 64. User B low of area, boom

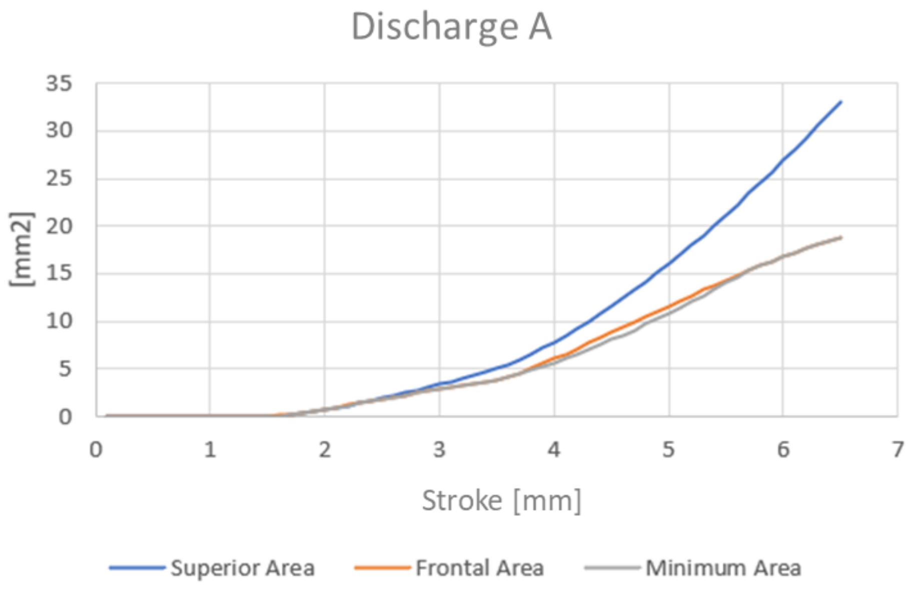

Figure 65. Discharge A low of area, boom

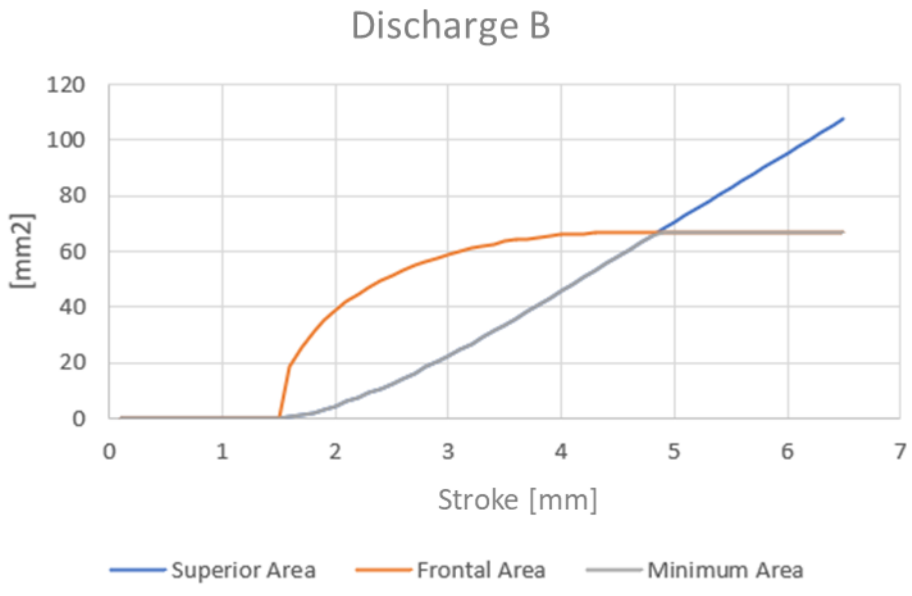

Figure 66. Discharge B low of area, boom

It should be noted that the minimum area of the discharge A is lower than that of the other notches, useful for creating back pressure in return, which is functional to ensure controllability and avoid cavitation in case of overrunning loads.

III.1.7.2 Arm

The dimensions of the arm cylinder and the connections with the DCV are shown in Table 8.

Cylinder - Arm	
Cylinder diameter	82.6 mm
Rod diameter	50.8 mm
Length	660.4 mm
Head side connection	User B
Rod side connection	User A

Table 8. Geometry features and hydraulic connections of the Arm

The main spool used in the arm section is shown in Figure 67.

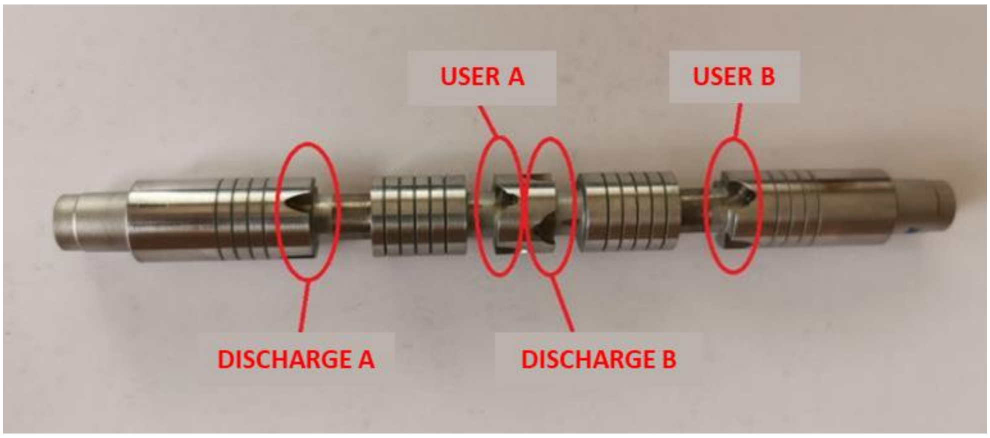

Figure 67. Arm section's main spool

This spool is of the standard type, without implementation of the regenerative function. The area laws are shown below.

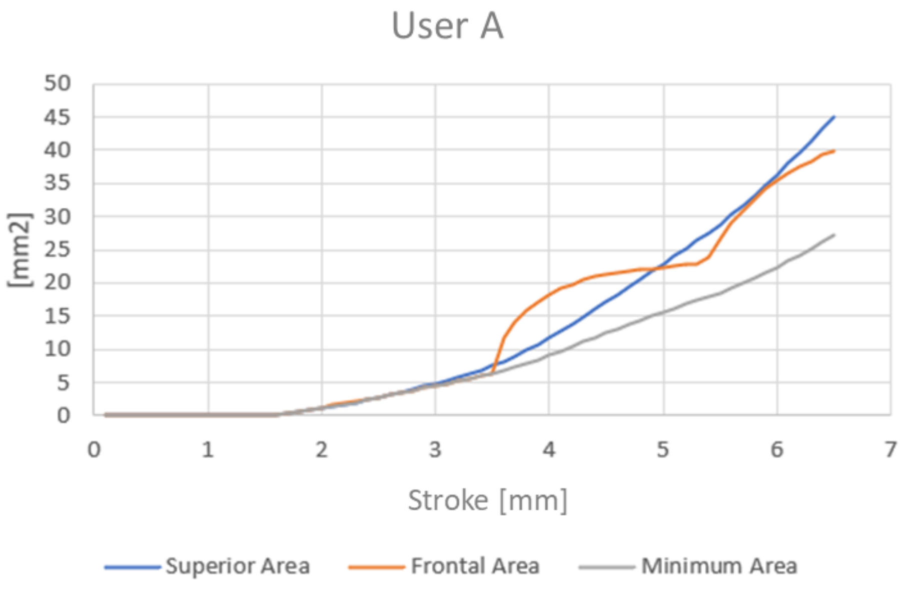

Figure 68. User A low of area, arm

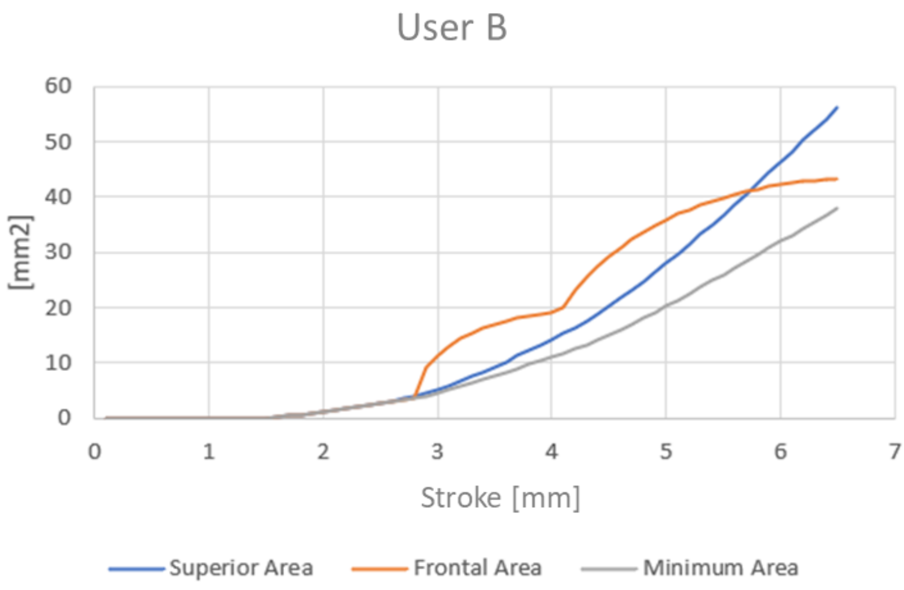

Figure 69. User B low of area, arm

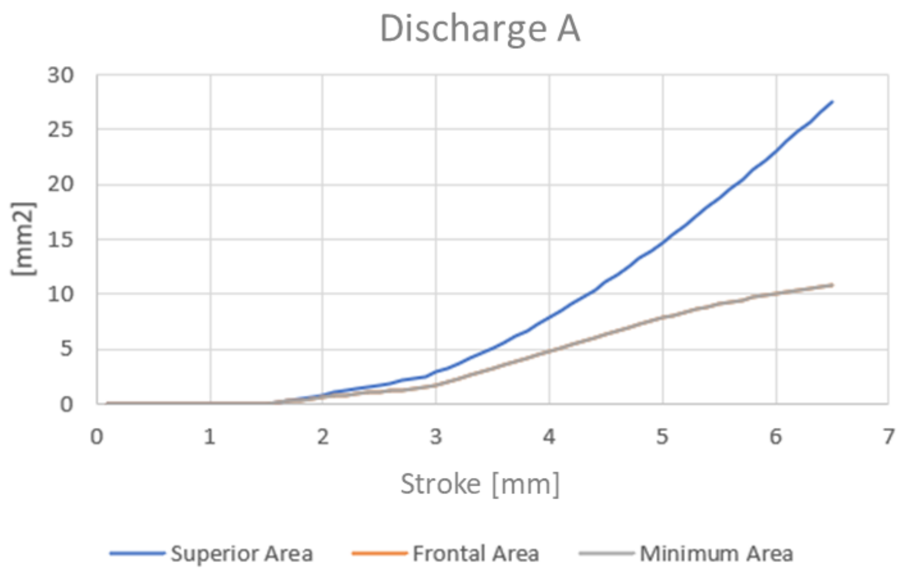

Figure 70. Discharge A low of area, arm

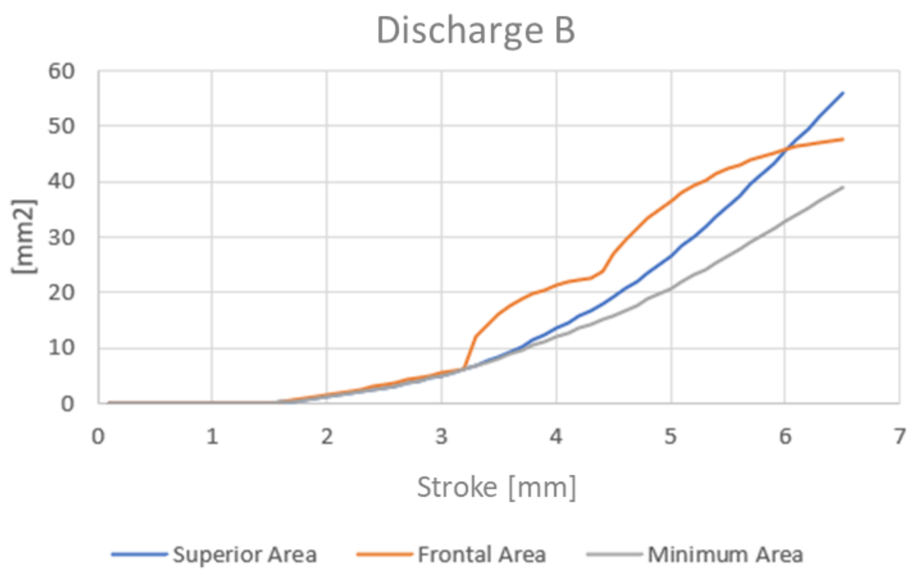

Figure 71. Discharge B low of area, arm

III.1.7.3 Bucket

The dimensions of the bucket cylinder and the connections with the DCV are shown in Table 9.

Cylinder - Bucket	
Cylinder diameter	76.2 mm
Rod diameter	44.5 mm
Length	524 mm
Head side connection	User B
Rod side connection	User A

Table 9. Geometry features and hydraulic connections of the bucket cylinder

The main spool used in the bucket section is shown in Figure 72.

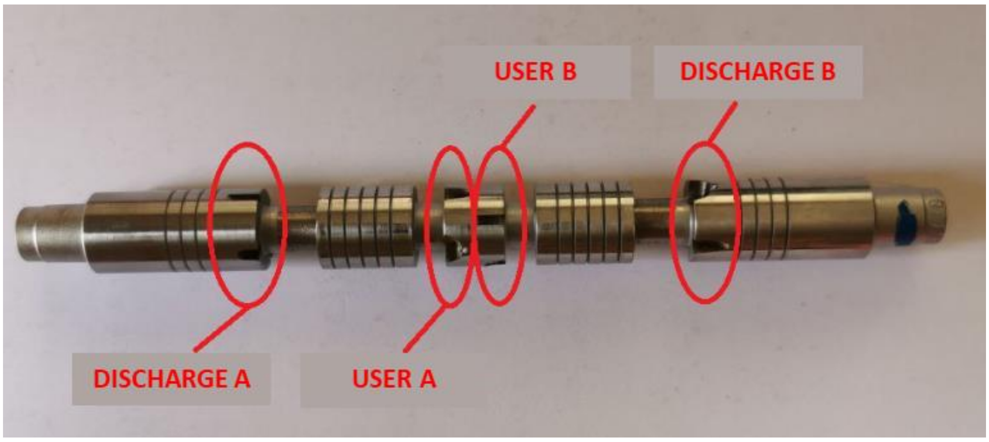

Figure 72. Bucket section's main spool

The bucket section also has a standard spool; the area laws are shown below.

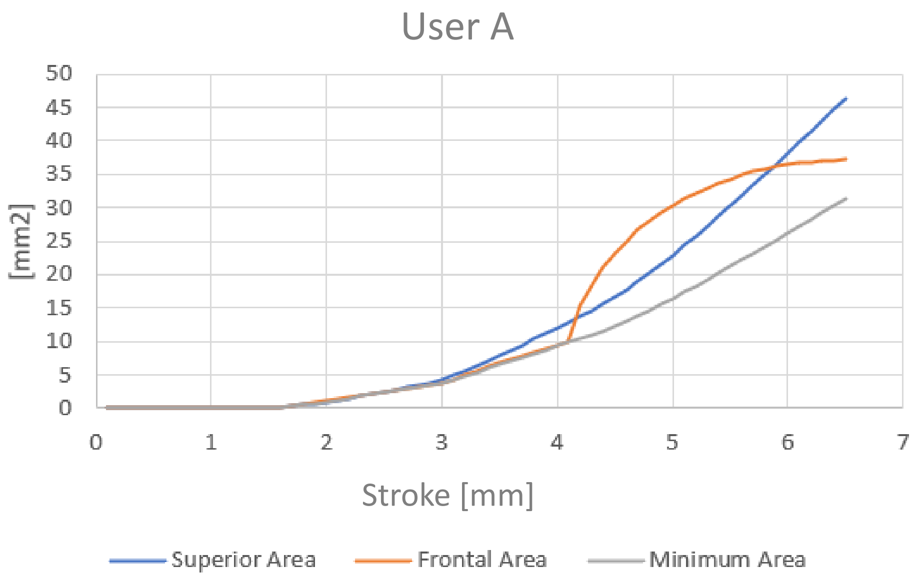

Figure 73. User A low of area, bucket

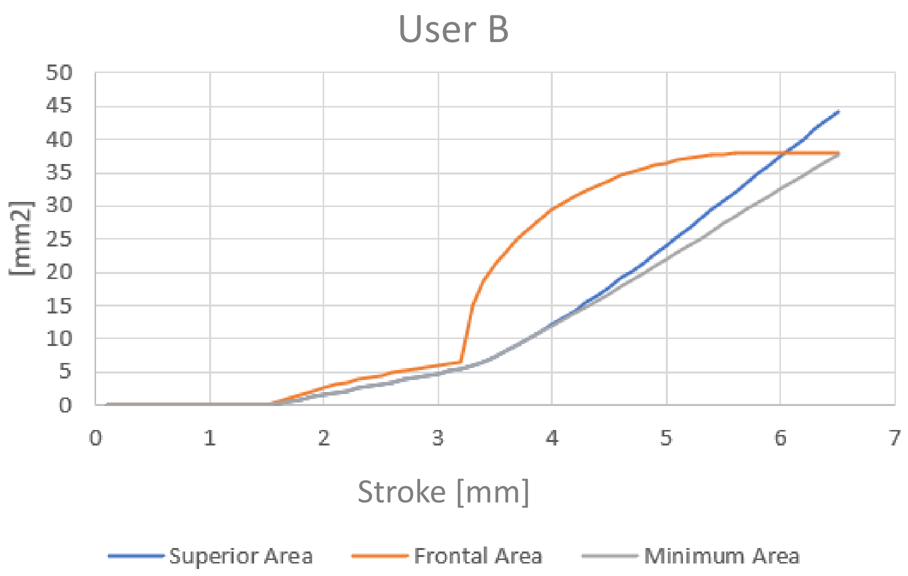

Figure 74. User B low of area, bucket

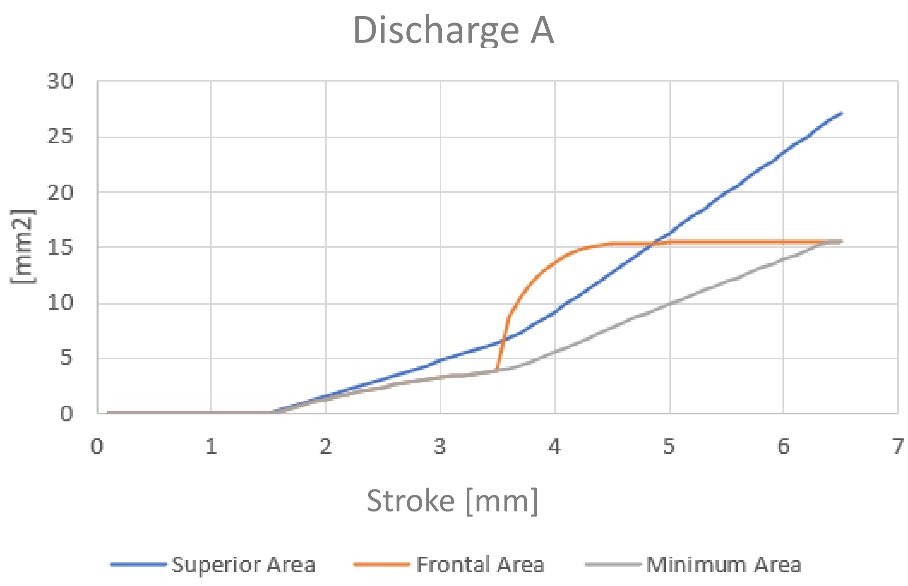

Figure 75. Discharge A low of area, bucket

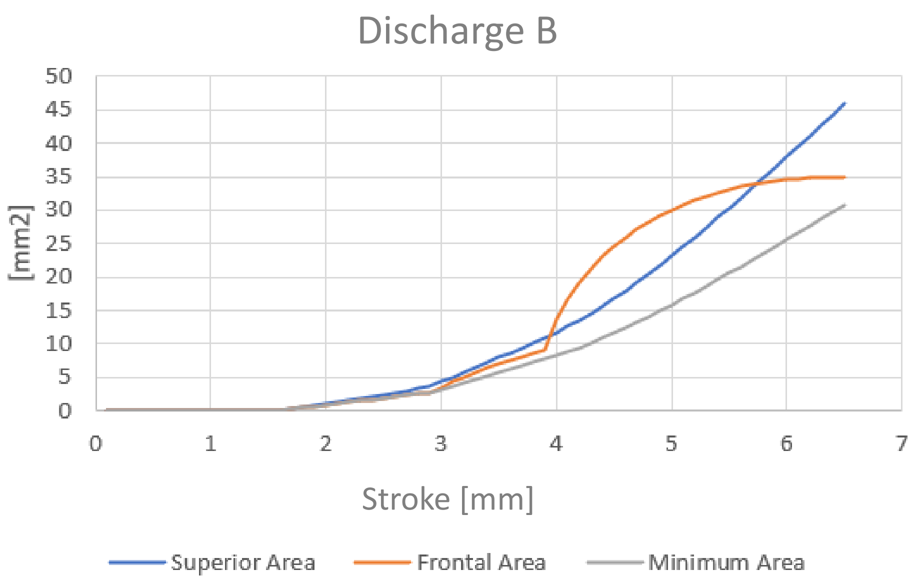

Figure 76. Discharge B low of area, bucket

III.1.7.4 Swing

Unlike the previous sections, the swing is not characterized by a linear actuator, but rather by a rotary actuator, which coupled to a suitable reducer, allows the rotation of the turret. The main spool used is shown in Figure 77.

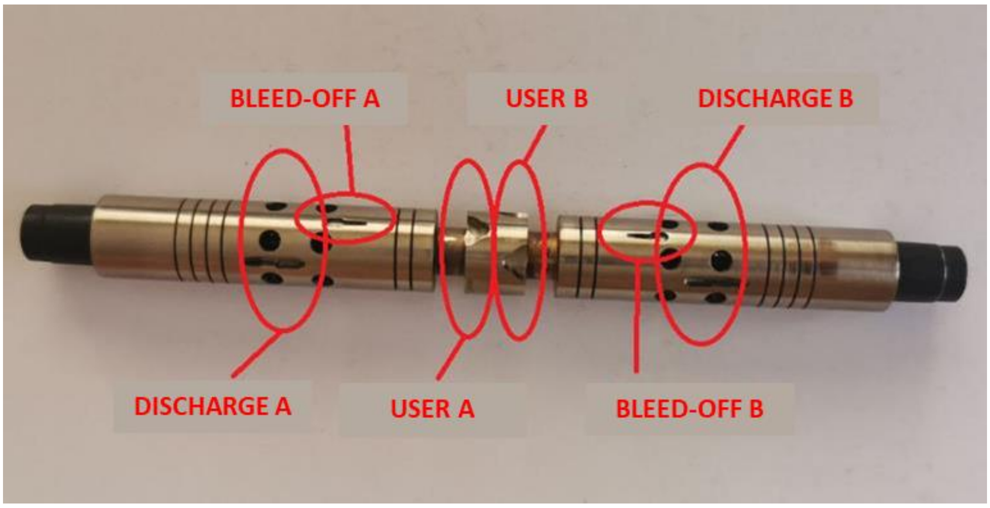

Figure 77. Swing section’s main spool

The spool is not standard, in fact there are two bleed-off slots; these elements perform the same function as the regenerative, that is to put in communication users A and B with the bridge. In this case, however, there are no elements that function as check valve, thus allowing the passage of flow in both directions; the effect given by the bleed-off is to make the actuator maneuvers less abrupt. As for the discharges, in addition to the slots that open in the first part of the stroke, there are holes (axially connected) that increase the crossing area near the limit end-stroke. The area laws are shown below.

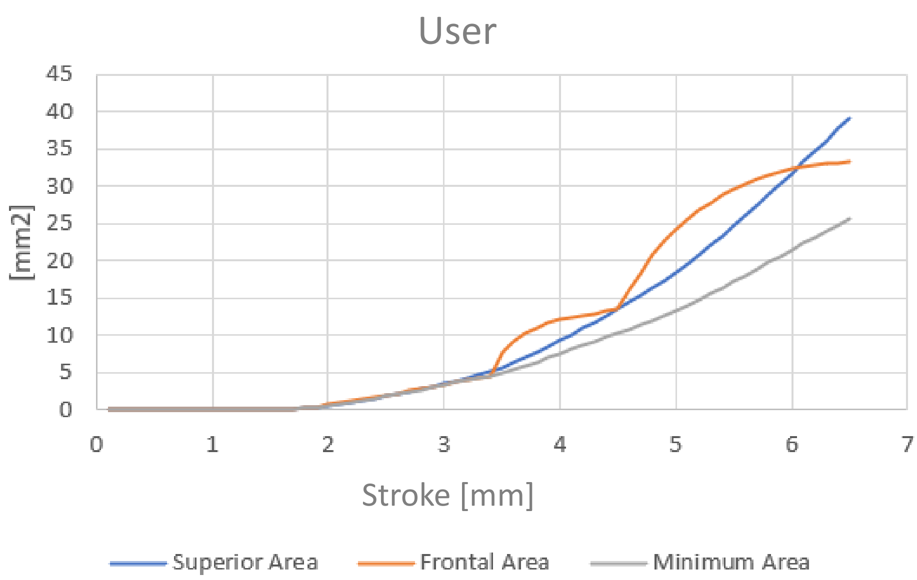

Figure 78. User low of area, swing

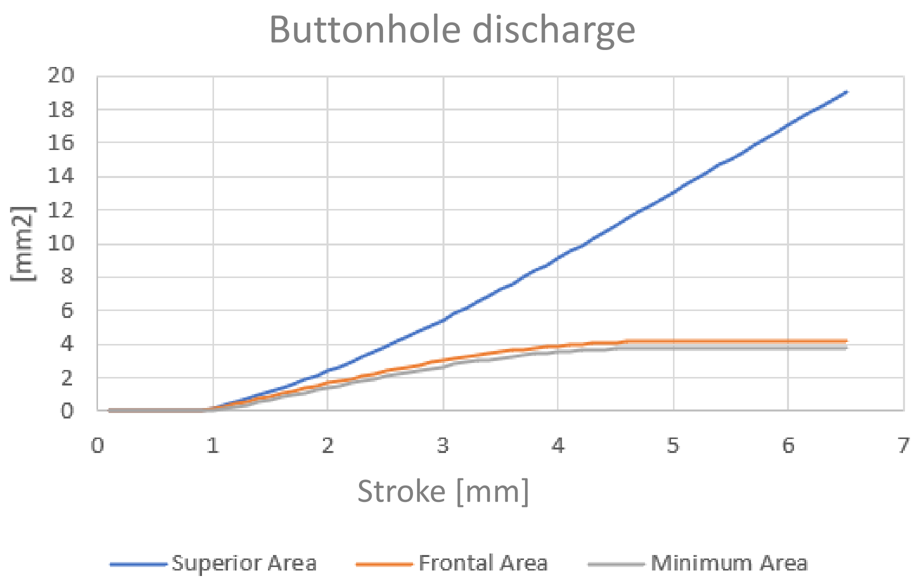

Figure 79. Buttonholes low of area, swing

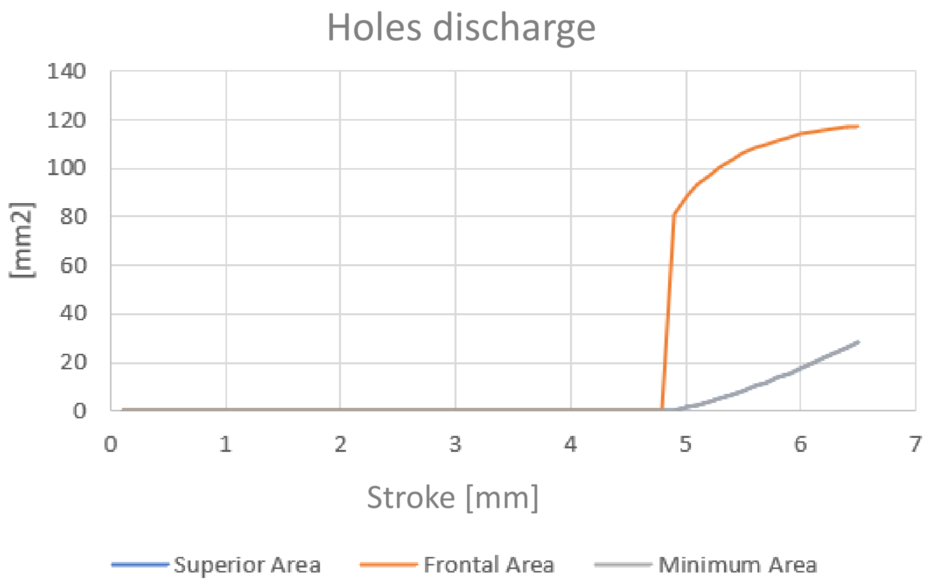

Figure 80. Discharge holes low of area, swing

The spool is symmetrical, the area laws are therefore identical for A and B.

III.2 Bench Test

III.2.1 Test 1 – Compensation in meter-in

The first bench test was performed with the new DCV aimed at energy recovery with manual drives (Figure 81).

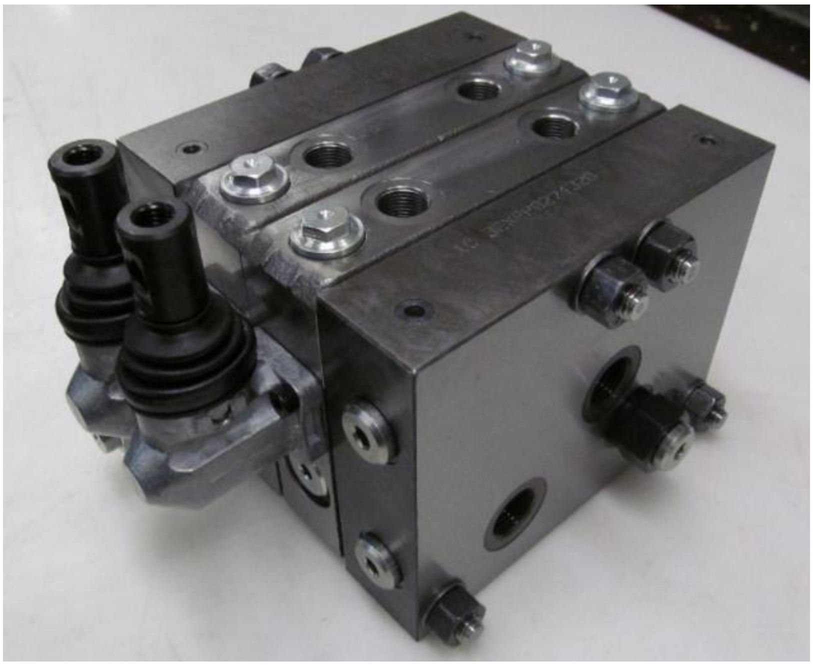

Figure 81. Energy recovery DCV

However, the compensator has been replaced with one that has the tank line T and the recovery line R always open and it also compensates in delivery to the actuator and not in return (Figure 82). In this way, since there is a check valve with a preloaded spring entering the R line, the return flow always goes to the tank T. Remember that the main spool of the new valve does not have any recess notches that can give back pressure, being in in this case, even the T-passage, which is always open, cannot be given even by the compensator. The purpose of this test is to verify that the compensator behaves like a DPX and subsequently (with simulations on a mathematical model) to evaluate the effect of the absence of bottlenecks in return.

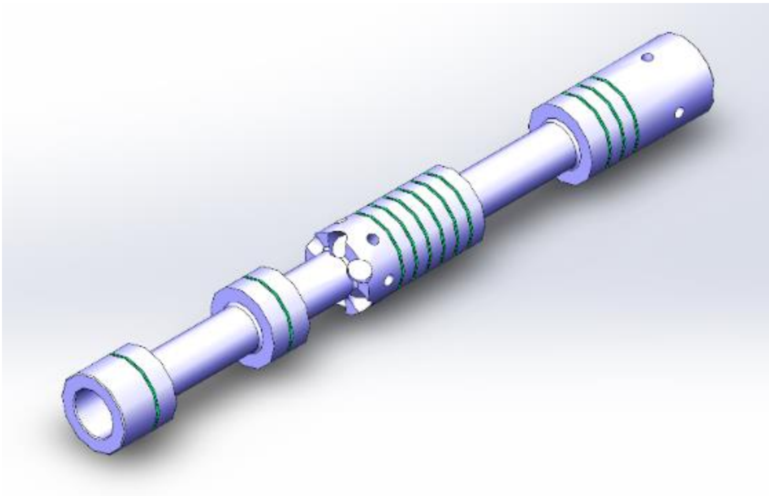

Figure 82. Compensator for DPX type operation without throttling in T

The bench set-up is shown in Figure 83.

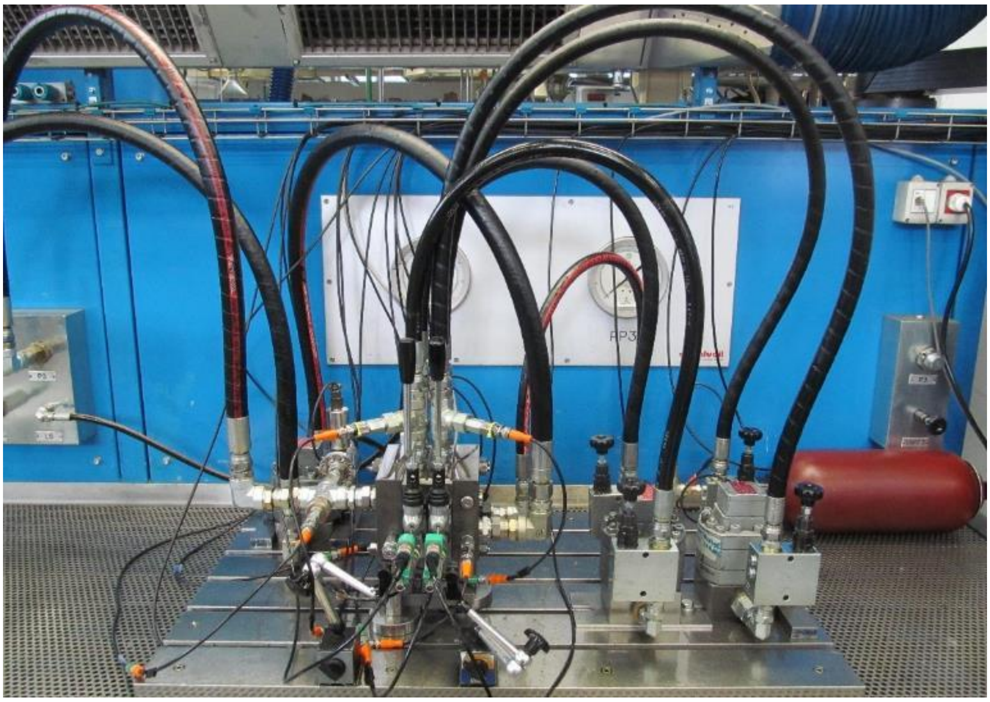

Figure 83. Test bench setup (test n.1)

The outlets of the two sections were connected to two filling valves (sequence) VDSRL; a 6 liters Hydac accumulator has been connected to line R, even if there is no flow rate; the system is powered by the screed LS pump.

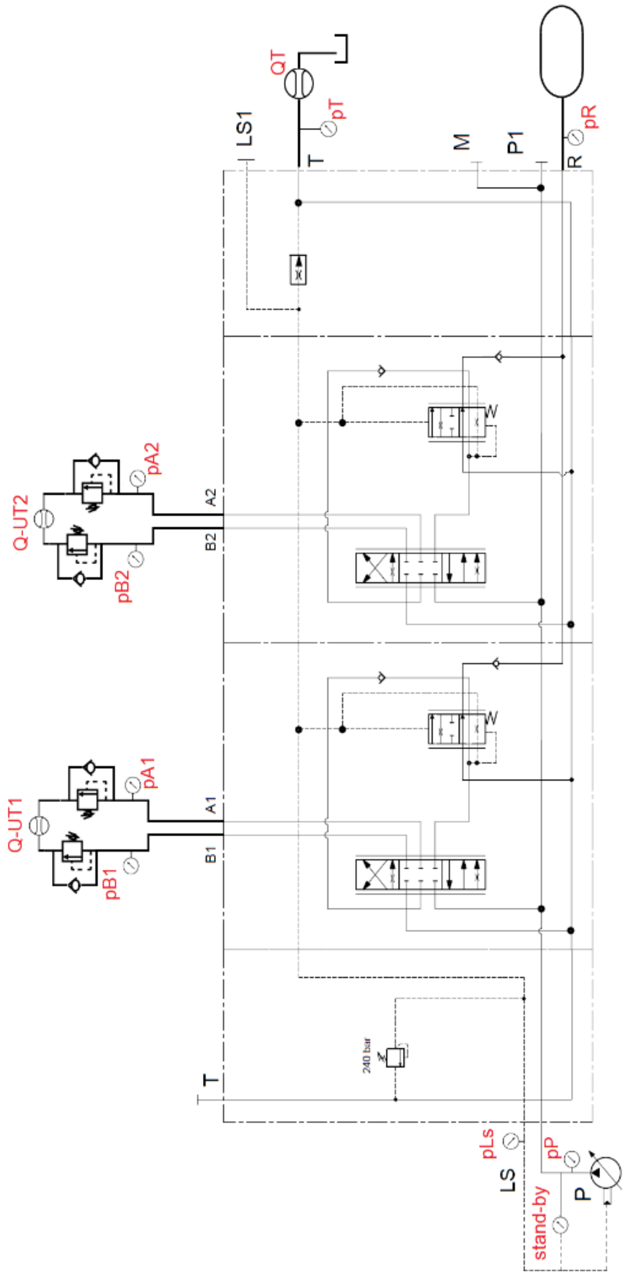

Figure 84. Hydraulic system diagram (test n. 1)

The pressure and flow sensors have been positioned according to the hydraulic scheme in Figure 84.

- **Sensitivity test**

The sensitivity curves of both sections were measured by setting the stand-by (p_P - p_{LS}) to 14 bar, moving the (symmetrical) spools gradually to the end of the stroke and without any load on the uses (VDSRL completely unbalanced).

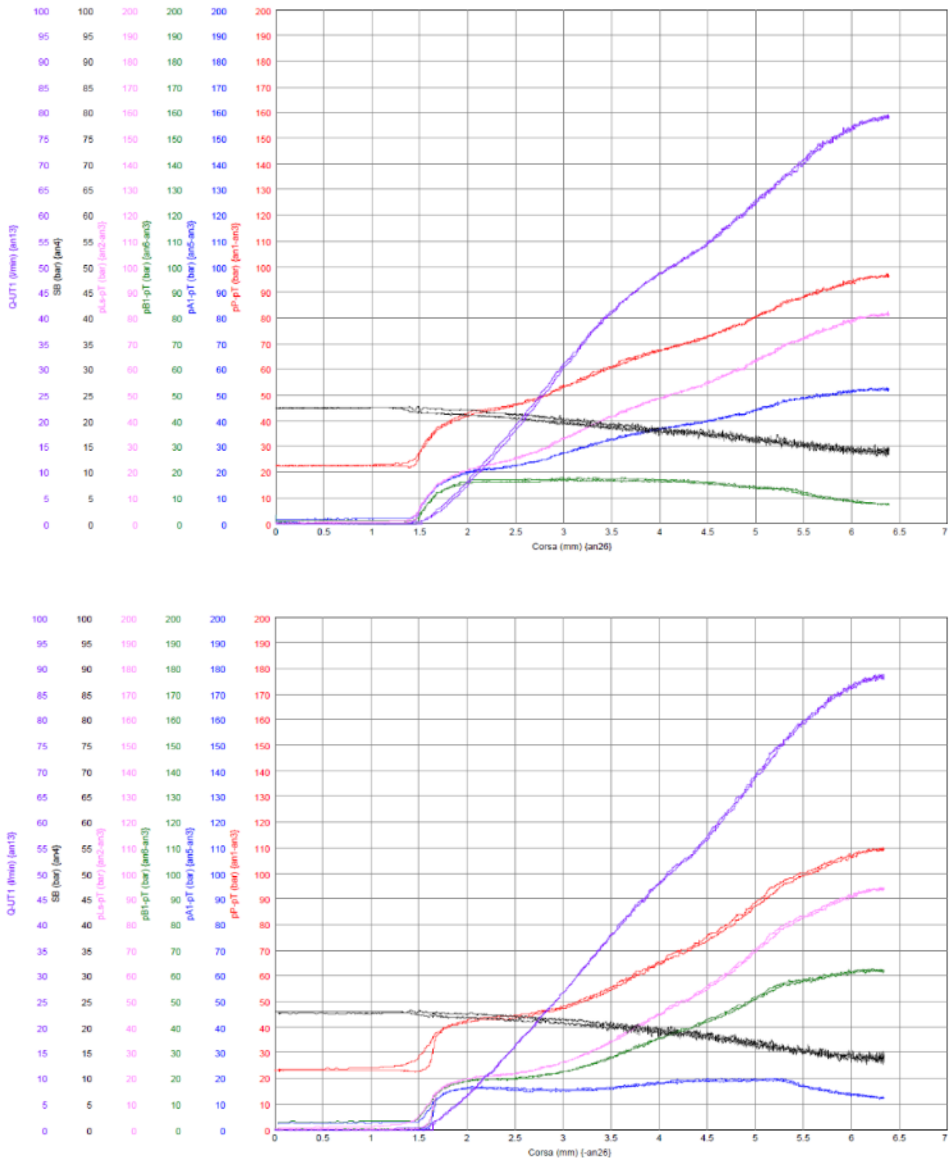

Figure 85. Sensitivity A (top) and B (bottom), section 1

The DCV achieves flow rates in line with a DPX100. There is a significant Δp between use and p_{LS}, probably caused by the geometry of the path between the compensator and the bridge.

- **Single compensation test**

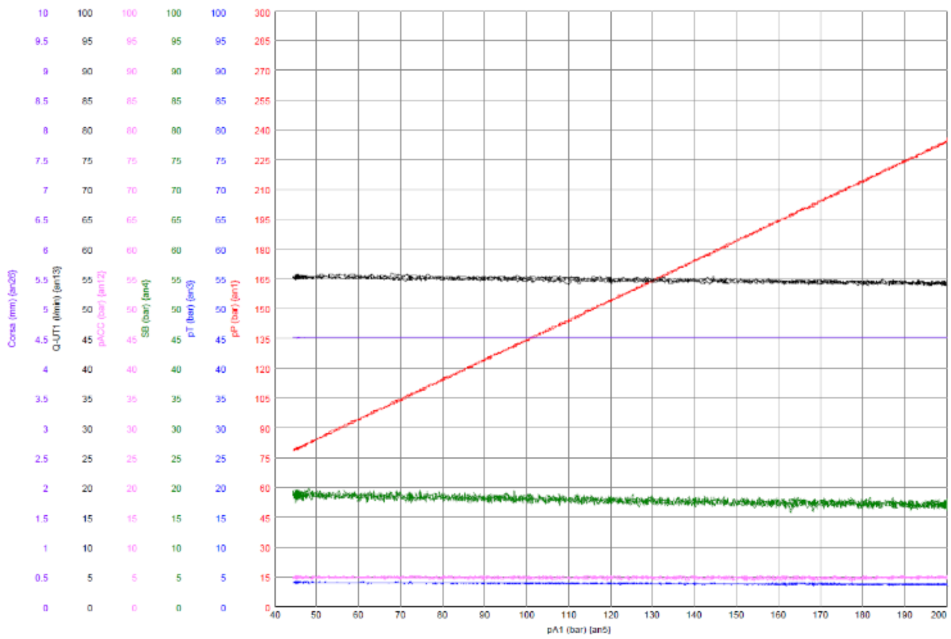

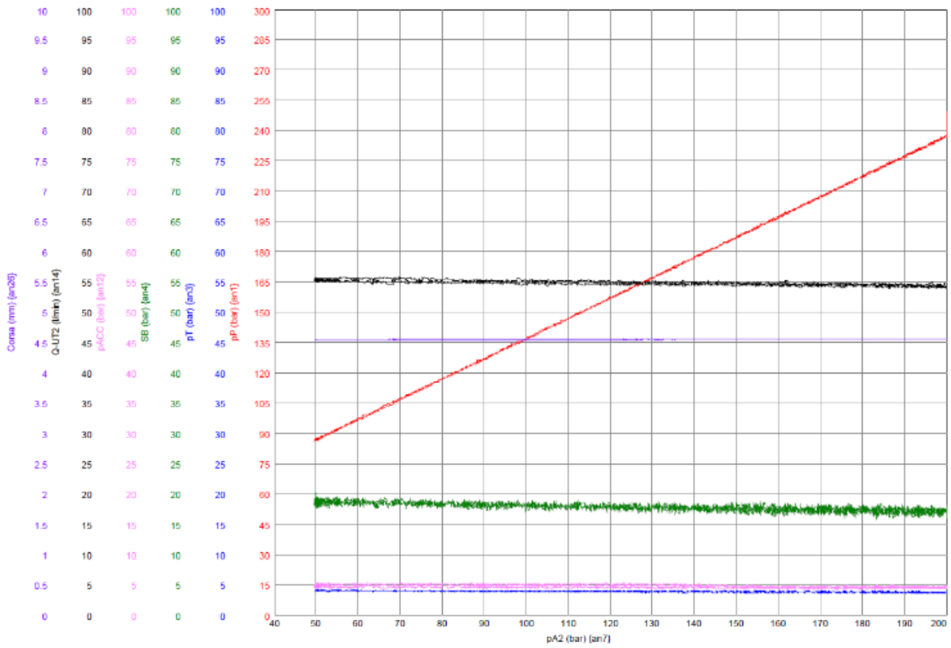

Figure 86. Single compensation section 1 (top) and section 2 (bottom)

The test was carried out by moving the spool towards A up to a stroke of 4.5 mm, then a loading ramp is carried out in A up to 200 bar. The correct operation of the LS logic (Q independent of the load) is observed.

- **Double compensation test**

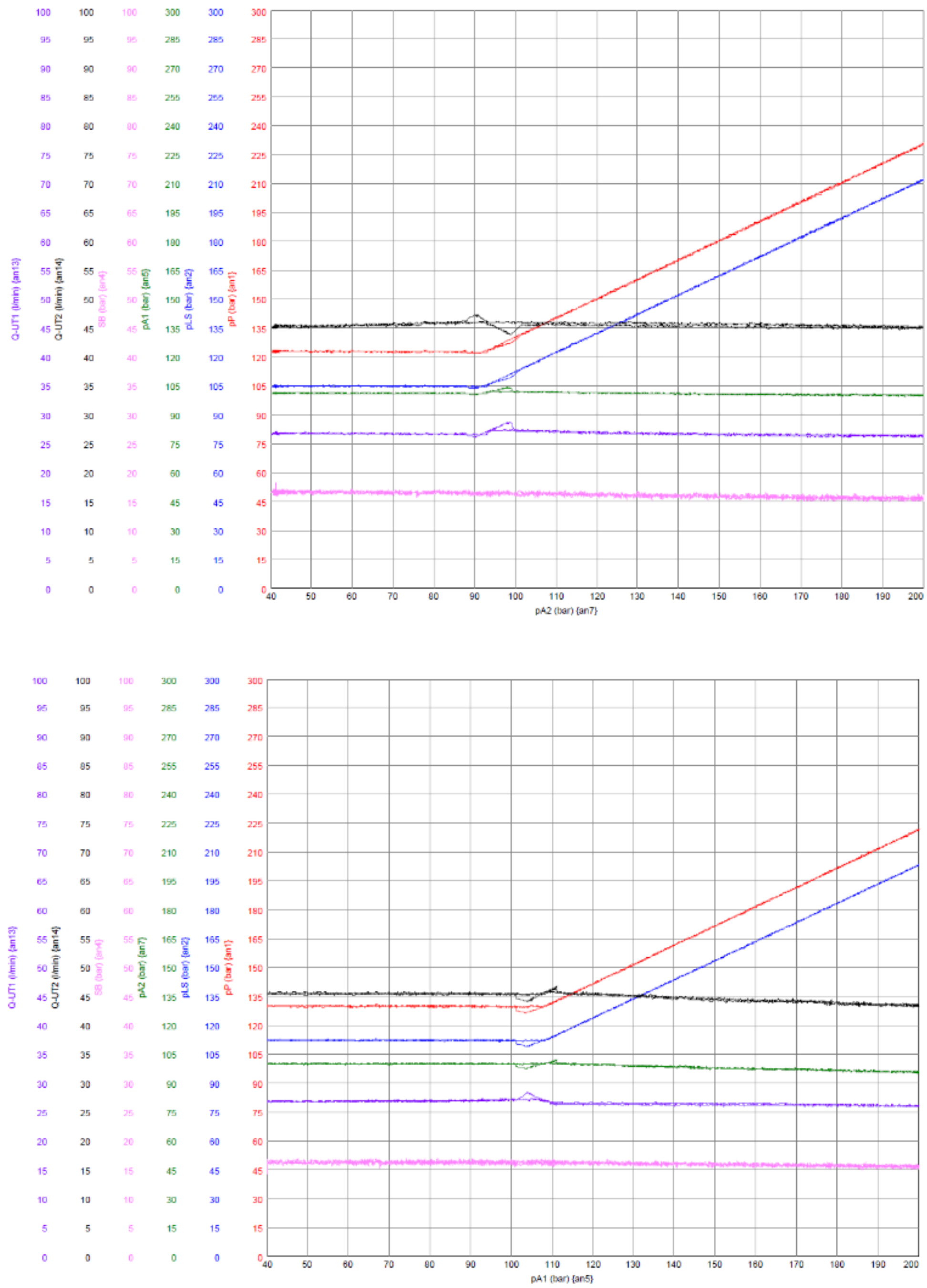

Figure 87. Double compensation with loading ramp in A2 (top) and A1 (bottom)

Test performed with section 1 at 3 mm stroke and load at 100 bar, section 2 at 4 mm stroke and loading ramp up to 200 bar; test repeated by reversing the sections. Correct operation of the compensators has been verified.

- **Double compensation test with flow saturation**

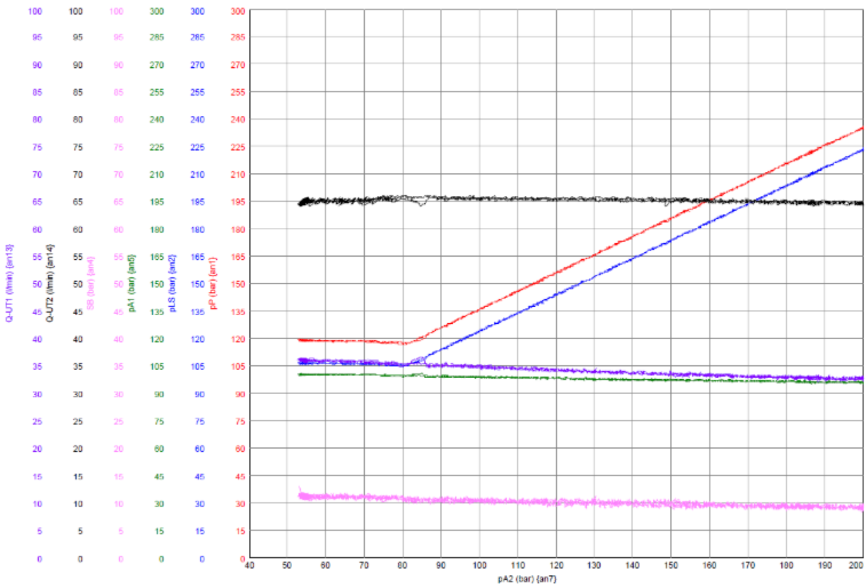

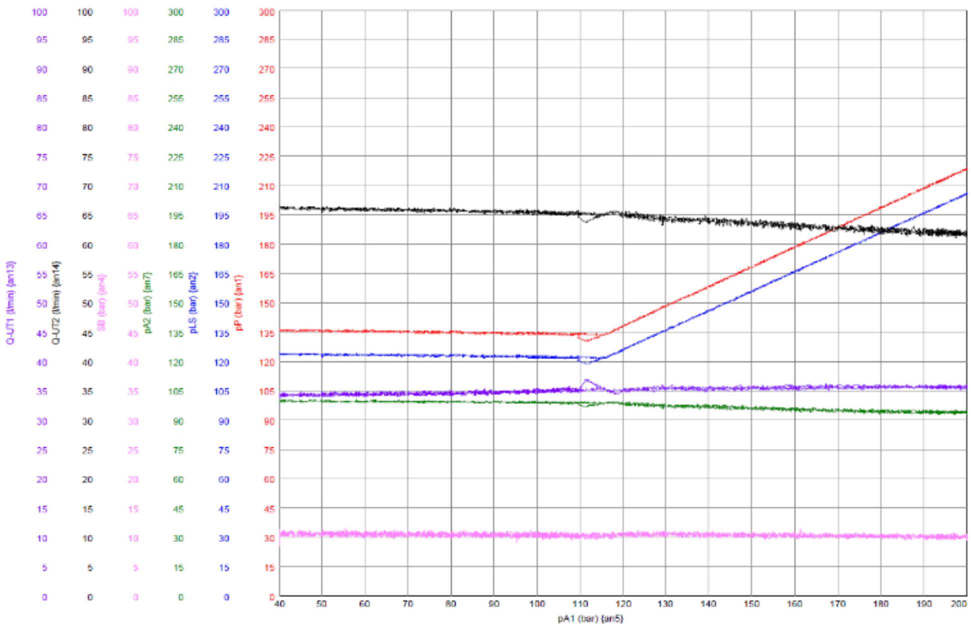

Figure 88. Double compensation in saturation with loading ramp in A2 (top) and A1 (bottom)

The pump that feeds the system is capable of delivering a maximum flow rate of 100 $\frac{l}{min}$. To reach the saturation condition, it is necessary to bring one of the two sliders to the limit switch; in particular, in one section a stroke of 4.5 mm was positioned with a load at 100 bar, in the other section a stroke of 6.5 mm and a loading ramp up to 200 bar. The correct functioning of the flow-sharing logic is observed, i.e. a reduction in flow rate, with respect to the value that can be read in the sensitivity curves, in both sections; even if the percentage reduction is not identical, it remains within the limits of acceptability. The correct behavior of the new distributor is therefore verified (with the use of an appropriate compensator) in line with the DPX100 (flow-sharing with post-compensation in meter-in); this compensator is not adequate if there are dragging loads, it is therefore necessary to implement adequate recess notches in the main spool, or, alternatively, to move the compensation to meter-out with the possible doping of the LS line when the latter it is very low (as explained above).

III.2.2 Test 2 – Compensation in meter-out

The second bench test was performed with the use of the same distributor used in the first bench test, to which compensators were replaced. The new compensator (Figure 89) no longer perform compensation in meter-in, but in meter-out (hydraulic diagram in Figure 90); this logic variation has the purpose of solving the problem of entrainment loads that occurs in the distributor when we use a spool that throttles in meter-in. In case of entrainment loads (low local p_{LS}), the compensator will throttle to copy the global p_{LS}, in this way all the pressures upstream of the restriction will be raised, thus counteracting cavitation; if the user in question is the only one that works, there will be the doping pressure in the LS line which will make the compensator work as if it was dominated. In this way there will be a "dynamic" return restriction which creates a back pressure, only if necessary.

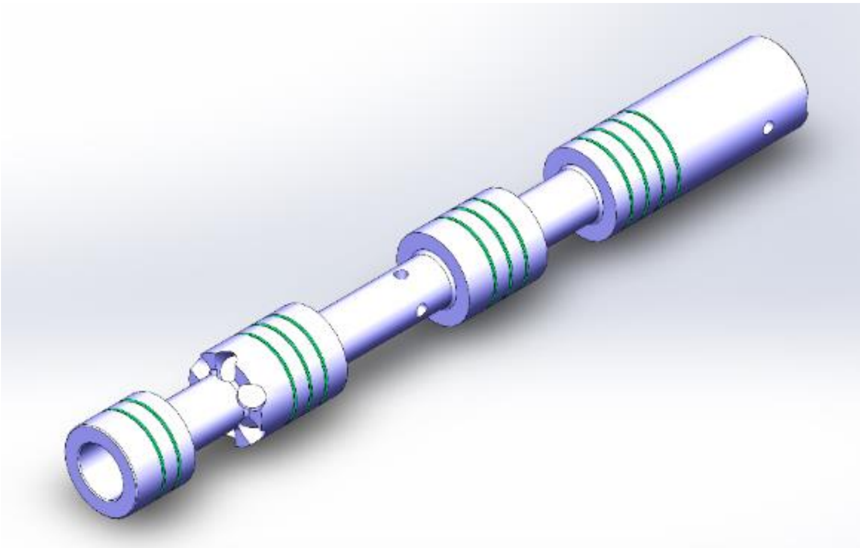

Figure 89. Compensator with choke in meter-out

The operation of the main spool is carried out again manually; the compensator keeps the passage to the R line closed; the restriction of the meter-out flow rate is therefore guaranteed by the T-shaped discharge notches. The hydraulic diagram and the set-up are shown below, respectively in Figure 90 and Figure 91.

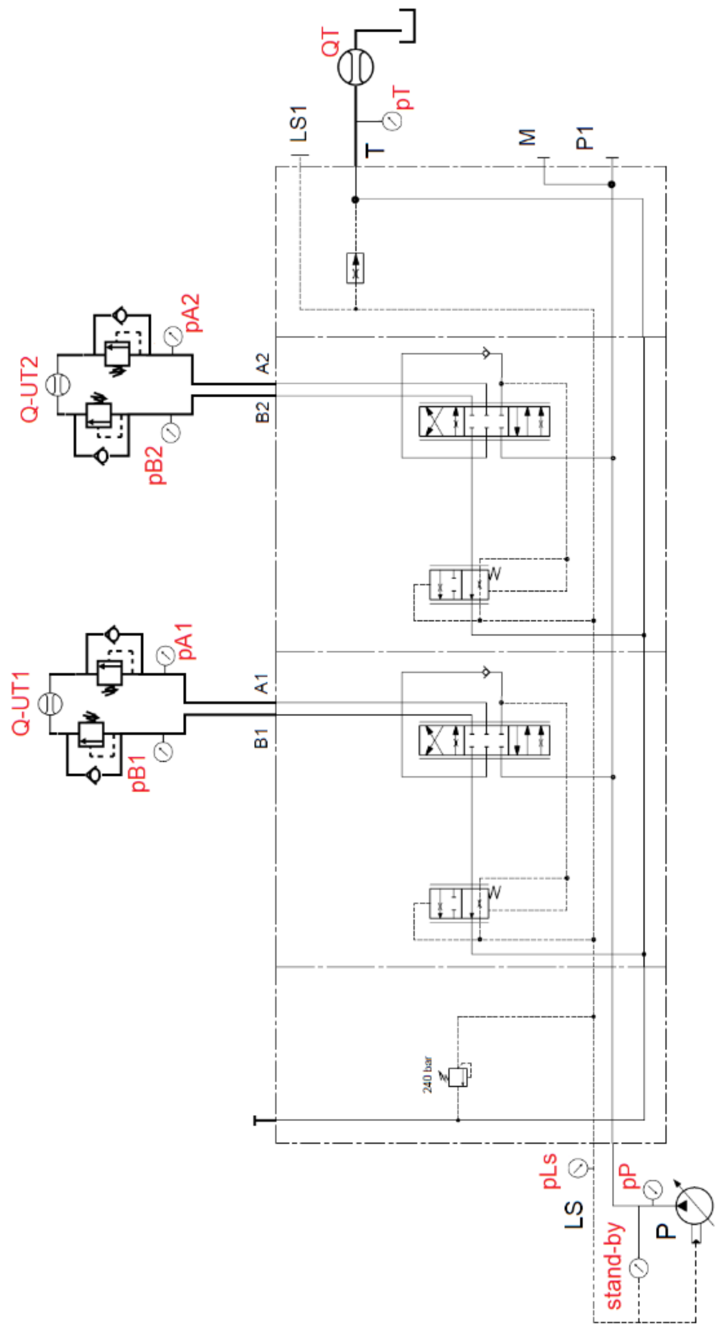

Figure 90. Hydraulic system diagram (test n.2)

Figure 91. Test bench setup (test n.2)

The system used for the bench test (Figure 91) is the same as the previous experimental test, with the only difference being the compensators. The objective of this test is to verify the correct functioning of the LS and flow-sharing logics, also expecting the phenomenon of the multiplication of pressures due to the meter-out compensation.

- **Sensitivity test**

The sensitivity curves of both sections were measured in the same way as in the first bench test, i.e. by setting the stand-by (p_P- p_{LS}) at 14 bar, gradually moving the spools to the end of the stroke and without any load on the uses. As in the previous test, there is a difference in the flow rates across the metering sections A and B, despite the symmetry of the main spool; this phenomenon is caused by the non-symmetry of the "paths" of the oil to reach the users and by the different direction of travel of the two metering notches by the fluid.

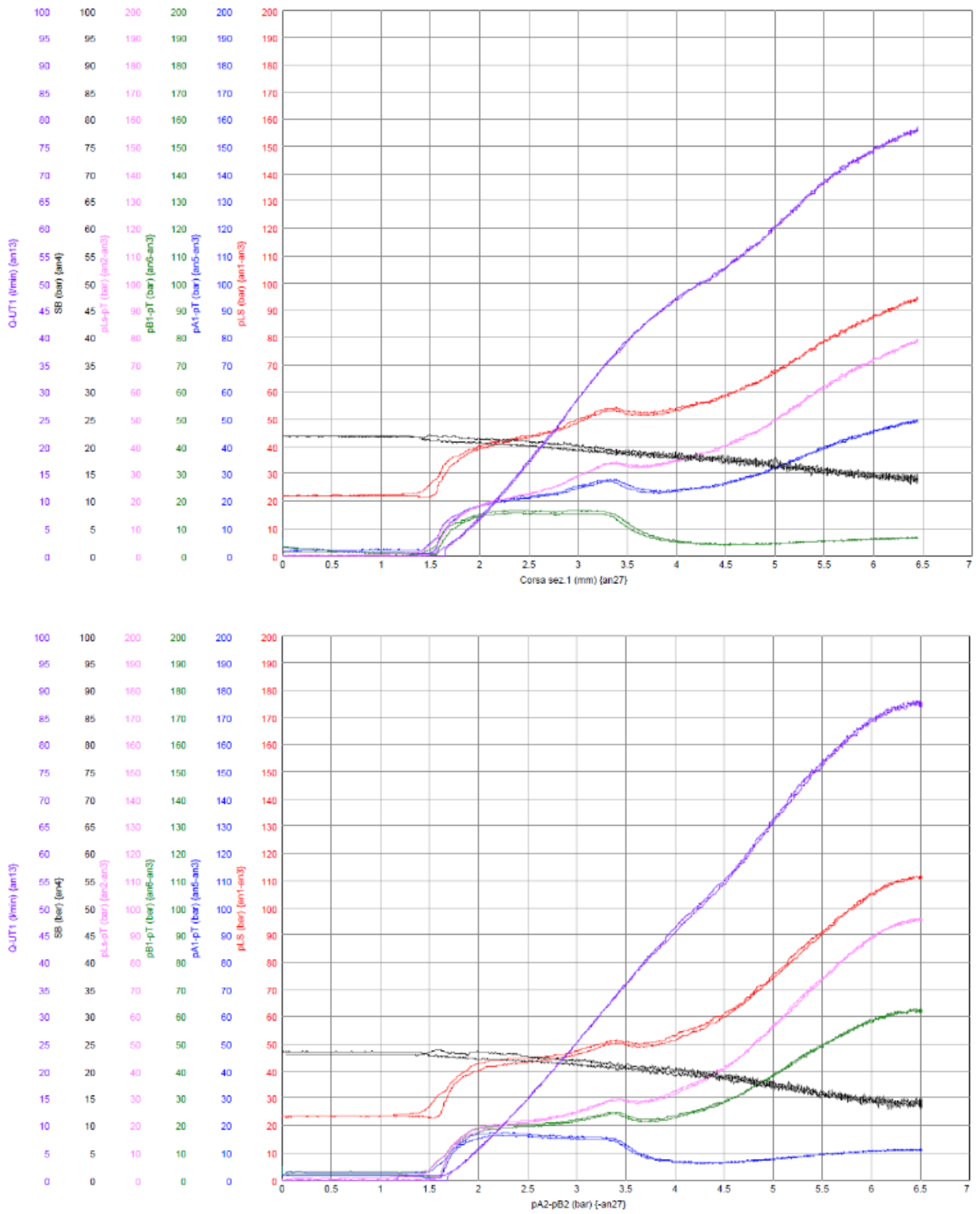

Figure 92. Sensitivity A (top) and B (bottom), section 1

The trends are in line with the previous test (same main spool), a sign that the compensator does not compromise the correct operation.

- ### Single compensation test

The test was performed by positioning the spool at 4.5 mm (feed A) and imposing a loading ramp at A up to 200 bar. The test was repeated for both sections.

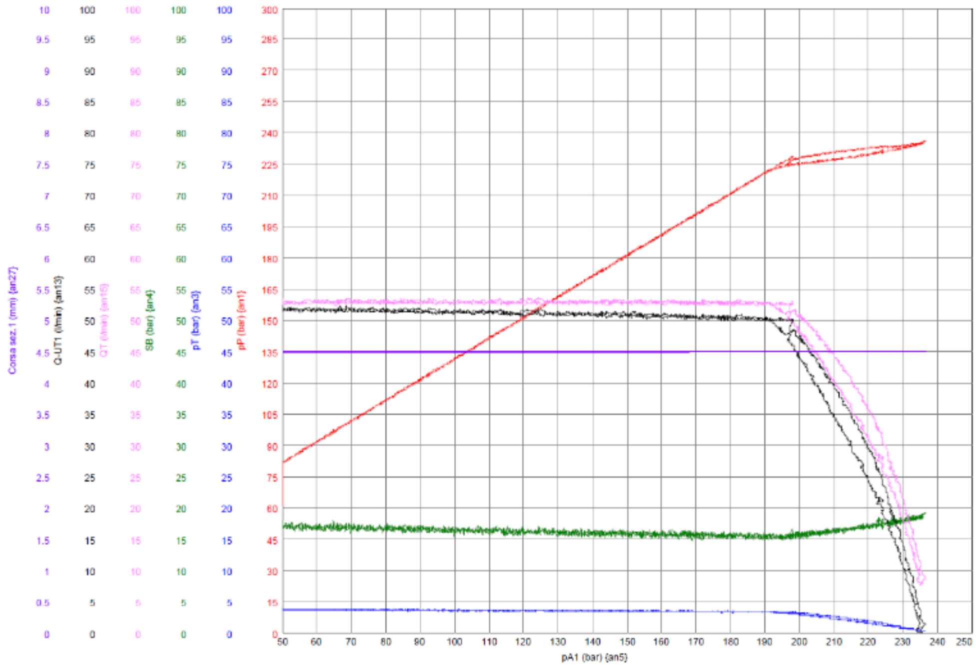

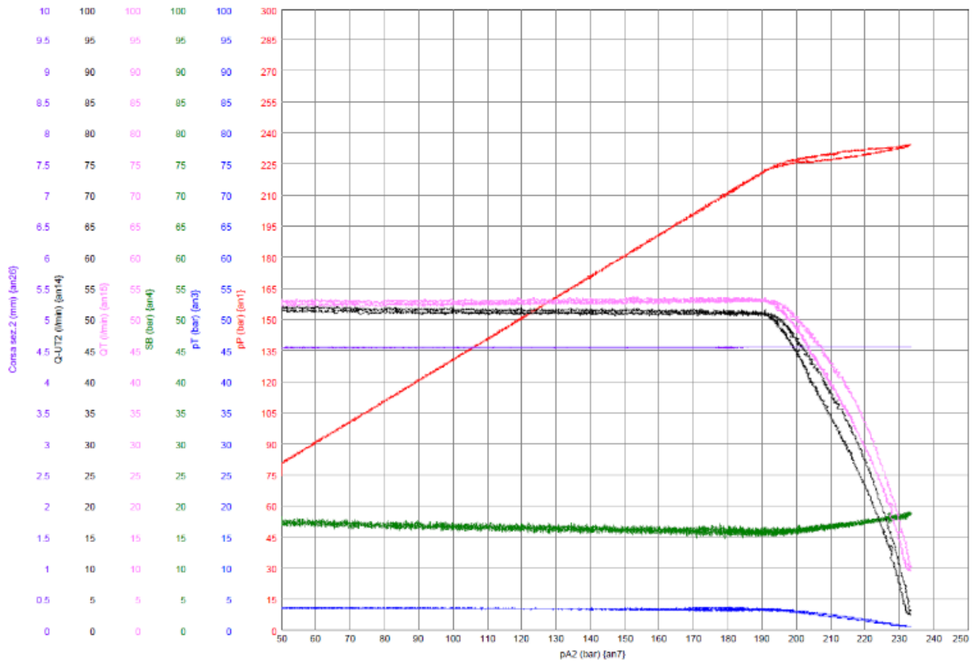

Figure 93. Single compensation section 1 (top) and section 2 (bottom)

The flow rate at use is proportional to the stroke of the spool, regardless of the load, thus implying the correct operation of the LS logic.

- ○ **Double compensation test**

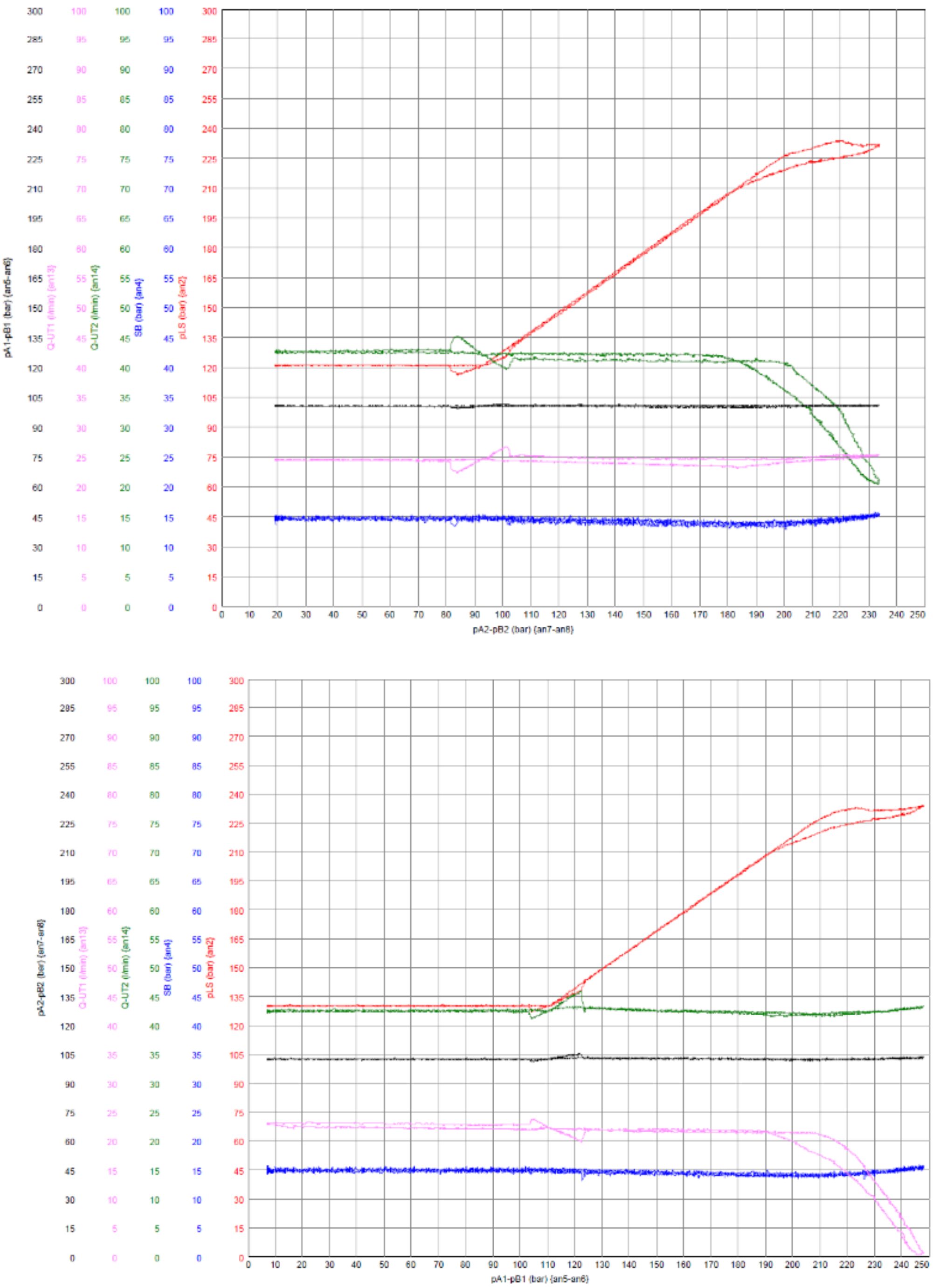

Figure 94. Compensation with loading ramp in A2 (top) and A1 (bottom)

The test was performed by positioning the first section at 3 mm stroke and the second at 4 mm, a load of 100 bar was subsequently applied to the first section and a ramp to the second; the test was repeated by reversing the sections. Due to the phenomenon of the multiplication of pressures, it would not be possible to distinguish the dominated and the dominant section from the pressure upstream of the load valve, it was therefore decided to graph as a function of the differential pressure in the load valve (pA-pB), in so as to discriminate the contribution on pB given by the compensator when it throttles; also in this case the correct operation with load reversals has been verified. To better understand the multiplication of pressures, see Figure 95, where the pressures pA1 and pA2 are shown as a function of time; the load pressures (less than the peak, due to the opening of the VLP on the side calibrated at 220 bar) "copy" the value of the maximum load between the two sections (one constant at 100 bar, the other with a forward loading ramp and back), becoming virtually indistinguishable.

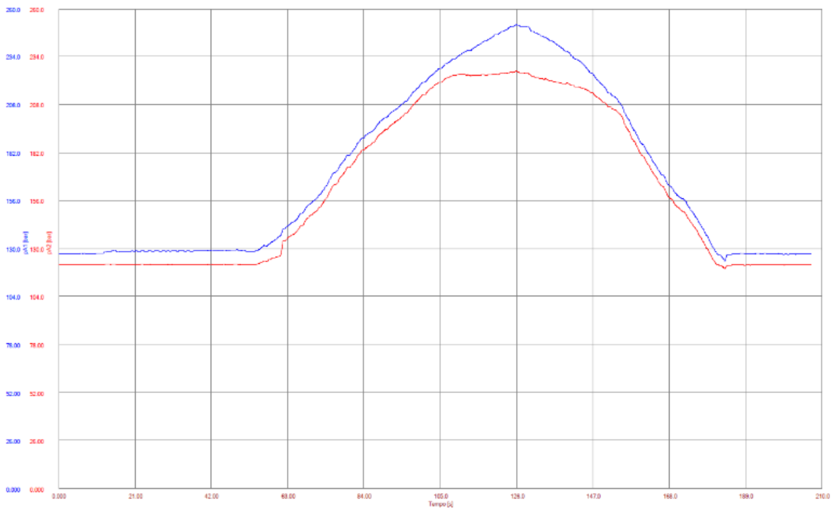

Figure 95. Phenomenon of the multiplication of pressures due to the meter-out compensation

- **Double compensation test with flow saturation**

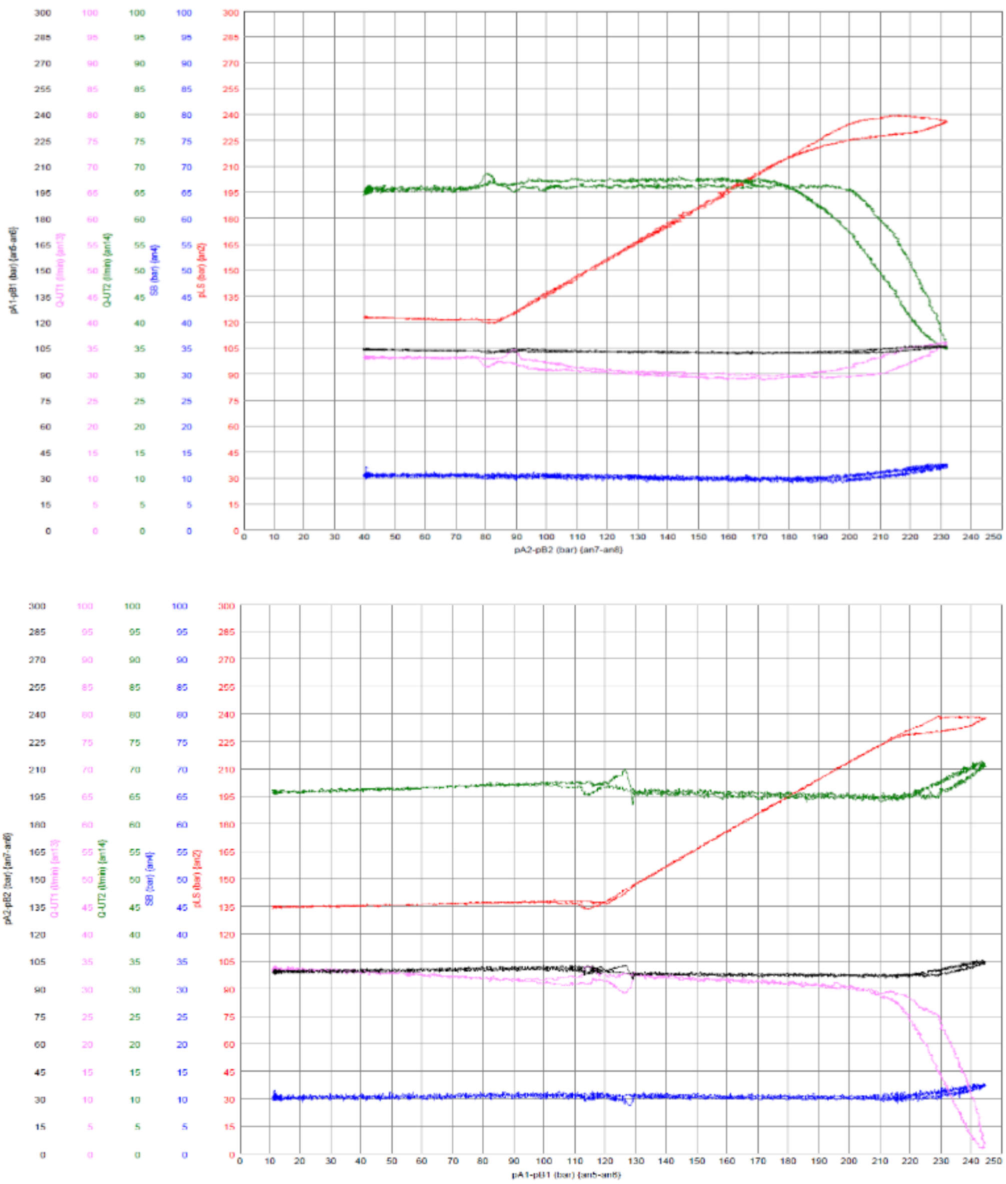

Figure 96. Double compensation in saturation with loading ramp in A2 (top) and A1 (bottom)

Test carried out with section 1 at 4.5 mm stroke and 100 bar load, section 2 at 6.5 mm stroke and loading ramp; the pump delivers a maximum of 100 $\frac{l}{min}$ and the test was repeated by reversing the conditions to the sections. Also in this case, the operation of the flow-sharing logic has been verified, which reduces the flow rate to all sections in saturation conditions.

III.2.3 Test 3 – Energy recovery

The third bench test is aimed at evaluating the behavior and performance of the distributor with energy recovery, this time mounting the compensator (Figure 97) which allows the energy recovery function.

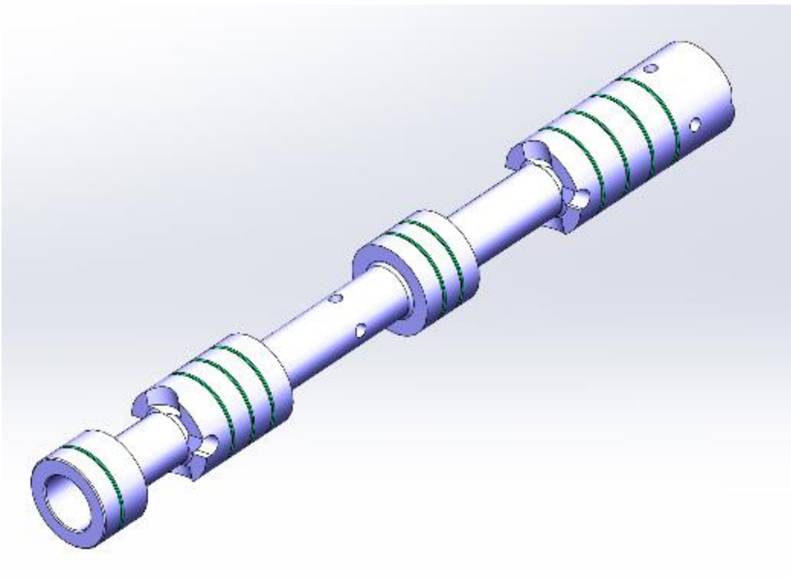

Figure 97. Compensator for energy recovery

The bench set-up is shown in Figure 98.

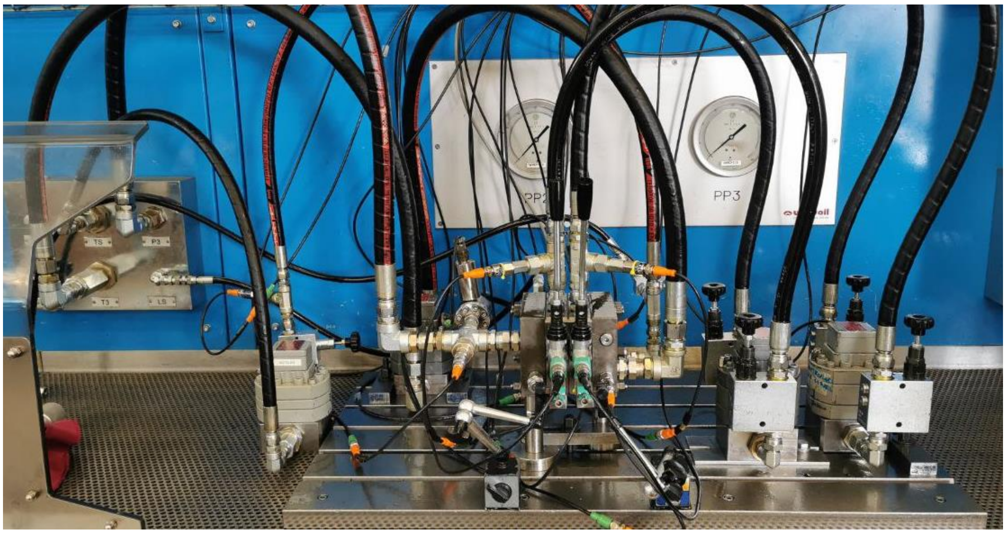

Figure 98. Test bench set-up (Test n.3)

As in the previous tests, the uses of the two sections were used with VDSRL load valves to impose the load. An additional loading valve has been connected to the R line (on the left, in Figure 98), capable of increasing the pressure of the line itself, simulating the effect of the resistant load of a hydraulic motor. The hydraulic scheme of the system is shown below in Figure 99.

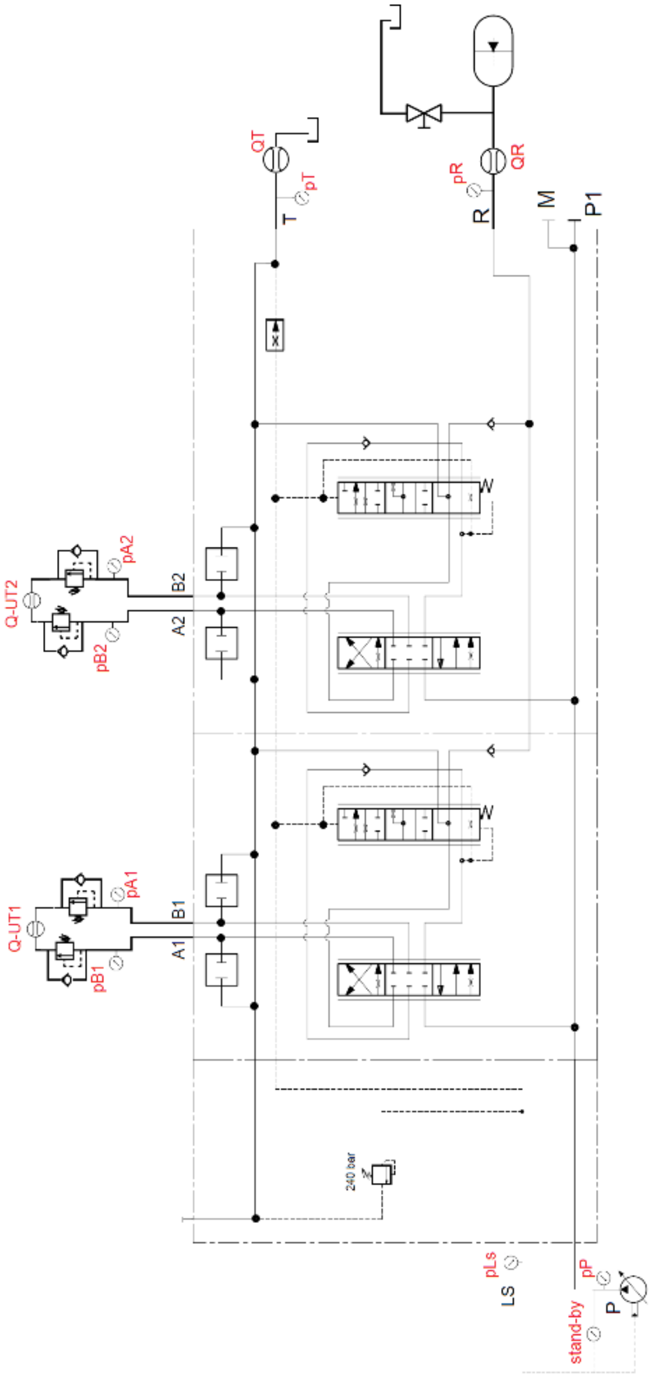

Figure 99. Hydraulic circuit (test n.3)

As in the previous tests, sensitivity, single compensation, double compensation tests, with and without saturation, were performed in order to evaluate the correct behavior of the DPX-R. Then, tests on the energy recovery function were then carried out.

- ### **Sensitivity test**

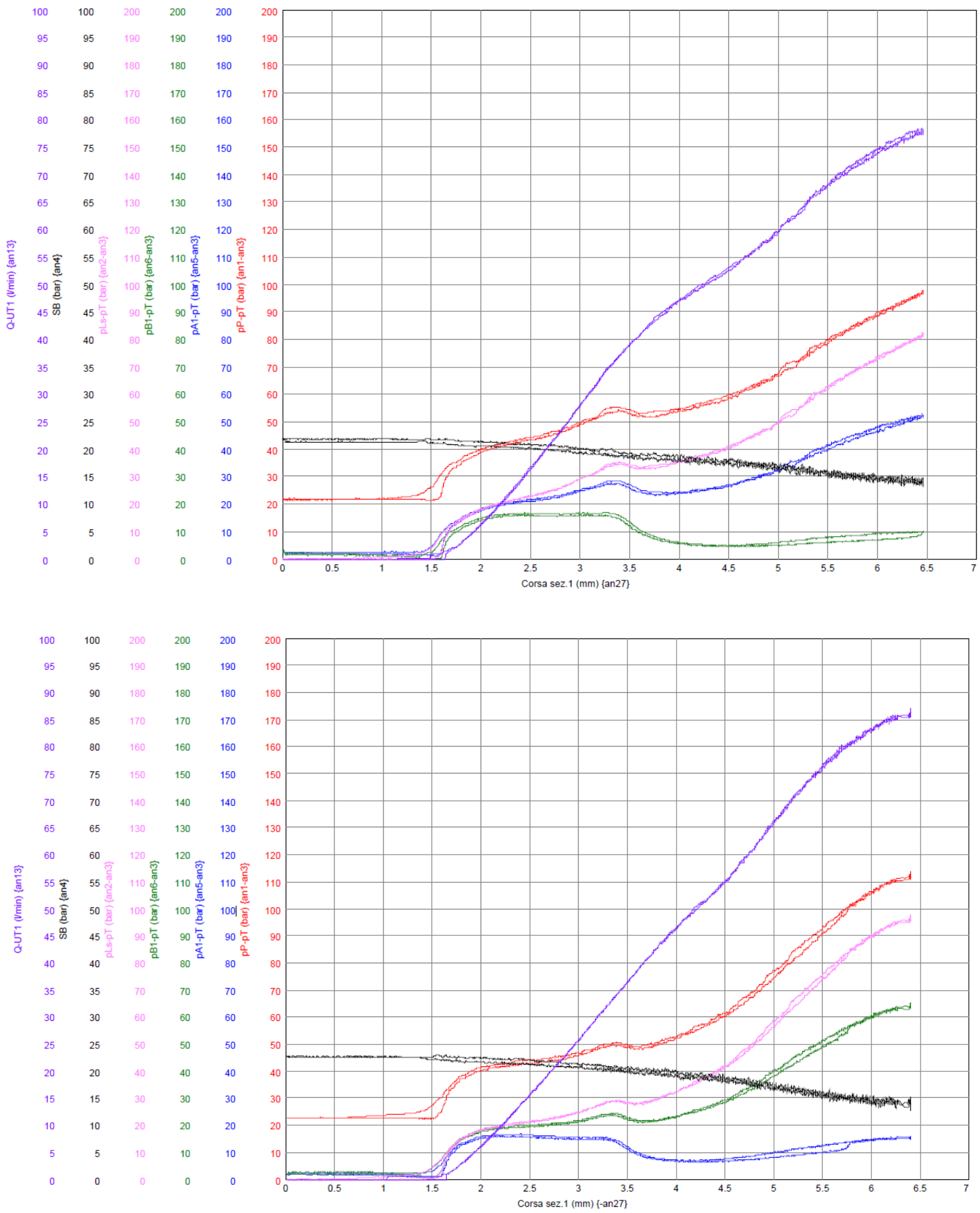

Figure 100. Sensitivity A (top) and B (bottom), section 1

Also in this case the correct functioning of the main spool has been verified.

- ### **Single compensation test**

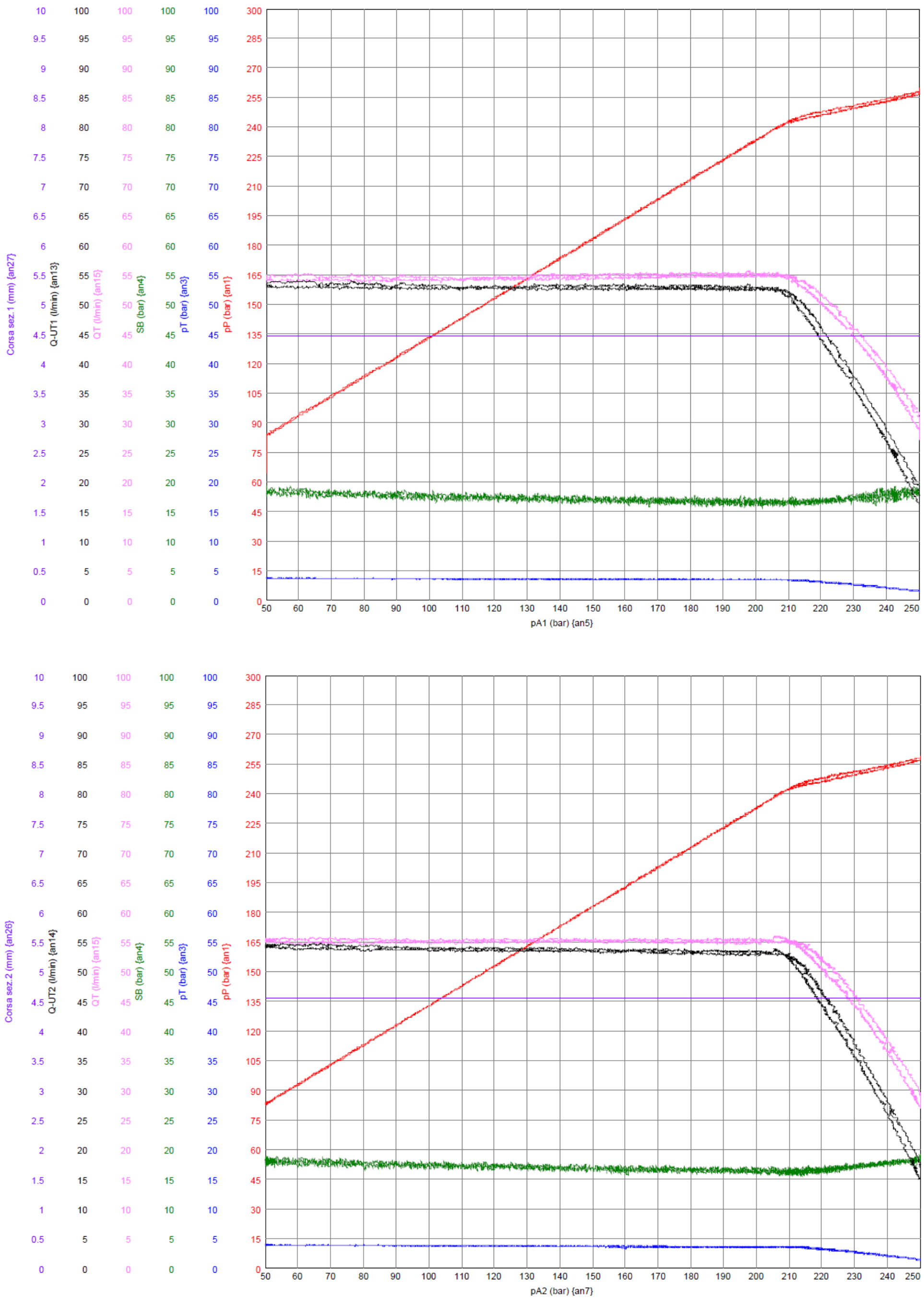

Figure 101. Single compensation section 1 (top) and section 2 (bottom)

Test performed with the main spool stroke at 4.5 mm, the independence of the load capacity is observed, the correct functioning of the sections is then verified (as shown in Figure 101).

○ Double compensation test

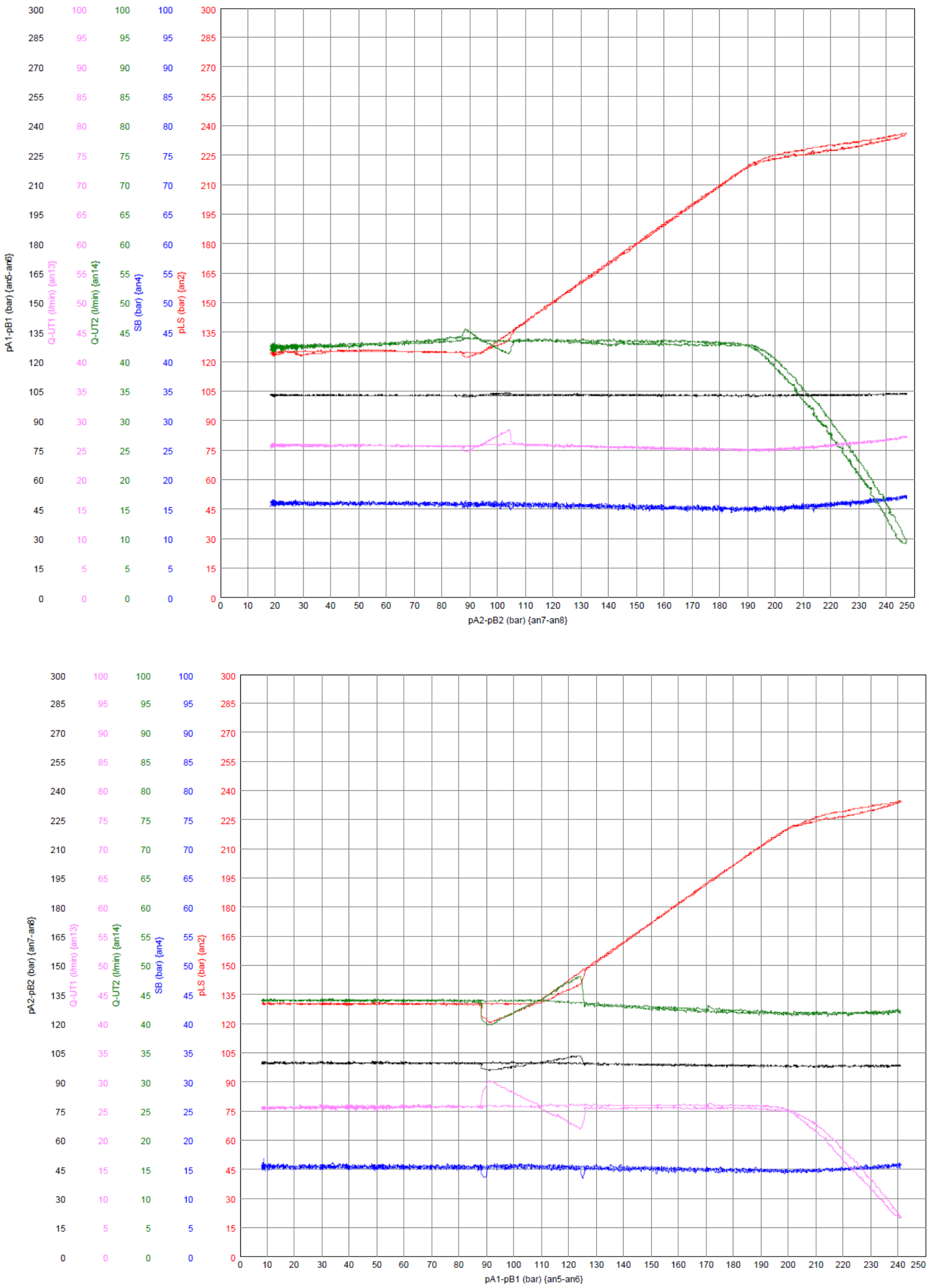

Figure 102. Compensation with loading ramp in A2 (top) and A1 (bottom)

The double compensation tests were performed under the same conditions as the previous tests. The trends shown in Figure 102 are in line with the correct functioning of the vending machine load-sensing logic.

- **Double compensation test with flow saturation**

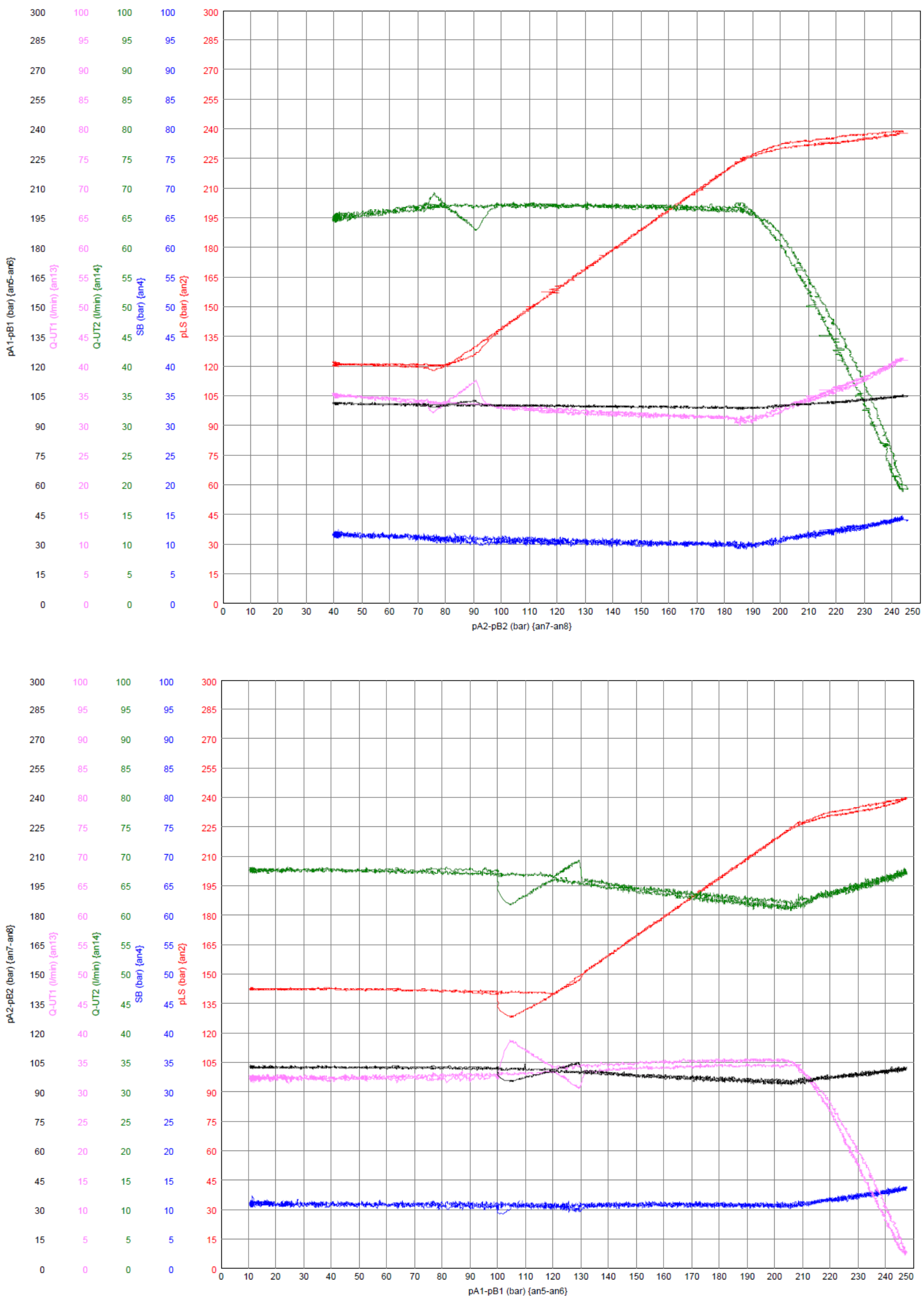

Figure 103. Double compensation in saturation with loading ramp in A2 (top) and in A1 (bottom)

The double compensation tests with flow saturation were also performed under the same conditions, as previously described. The trends found, in Figure 103, once again show the correct functioning of the flow-sharing function.

- **Energy recovery test**

Before proceeding to the explanation of the tests concerning energy recovery, the laws of area of the notches for unloading on the T and R lines of the compensator used are introduced (Figure 104).

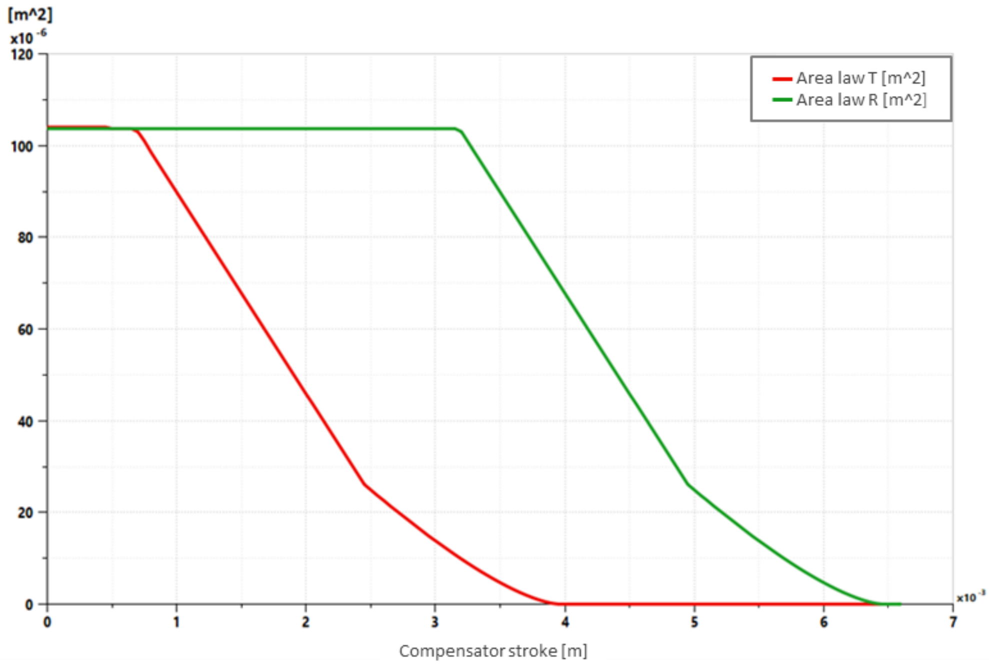

Figure 104. Notches T and R laws of area of the compensator for energy recovery

The T-shaped drain remains open in the first compensation section (up to a stroke of 3.95 mm stroke) while the connection to the R line remains open for almost the entire compensator stroke (up to

6.45 mm), remembering that at 0 mm there is no compensation and at 6.6 mm the maximum degree of compensation.

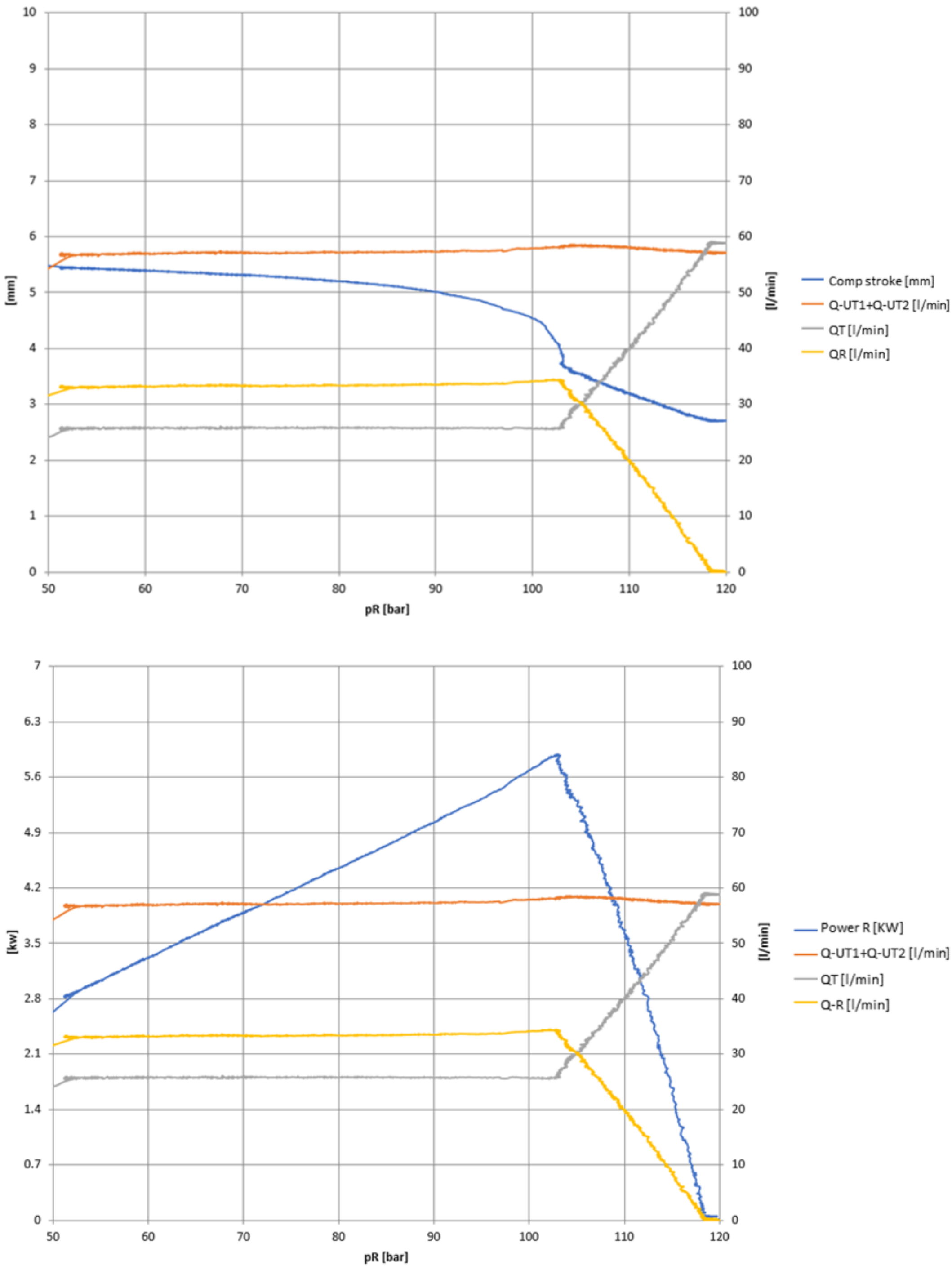

Figure 105. Energy recovery test

The test was performed by positioning the spool of section 1 at 3.5 mm with a load of 50 bar, while section 2 at 3.0 mm with a load of

150 bar; section 1 is therefore the dominated one and consequently the one which by compensation will allow energy recovery. Through the filling valve on the R line, the pressure upstream of it was raised, thus evaluating the behavior of the system as a function of pR (Figure 105). The position of the compensator was measured through an LVDT, whose characteristic is represented in Figure 106.

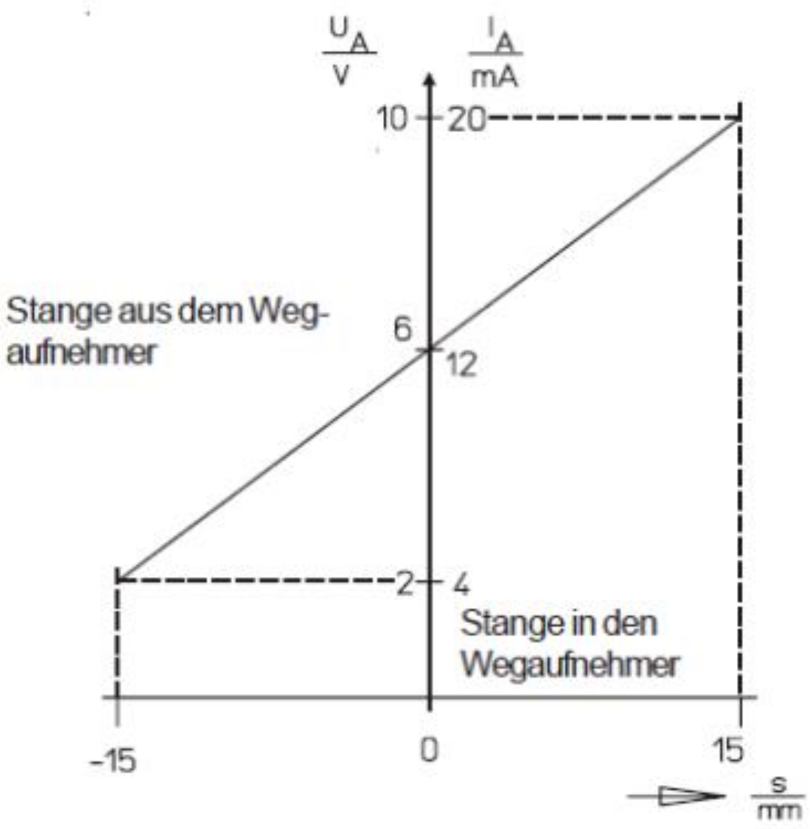

Figure 106. LVDT characteristic

By observing the course of the compensator, it is noted that the increase in p_R "decreases" the compensation requested from the compensator, bringing it closer and closer to the rest position. This aspect leads to an increase in the crossing area to the R line (see low of area), and therefore also to an increase in the power on R (p_R), since:

$$P_R = Q_R \cdot p_R \tag{17}$$

As soon as the compensator stroke falls below 4 mm, the flow rate at R and PR drop and the flow rate at T increases. As can be seen from the laws of area, this is the result of the opening of the connection to the drain T in the dominated section 1. Tests were subsequently carried out at different flow rates and Δp imposed on the users, with the aim of defining the recovery efficiency of the compensator at different positions of the latter, the result is shown in Figure 107.

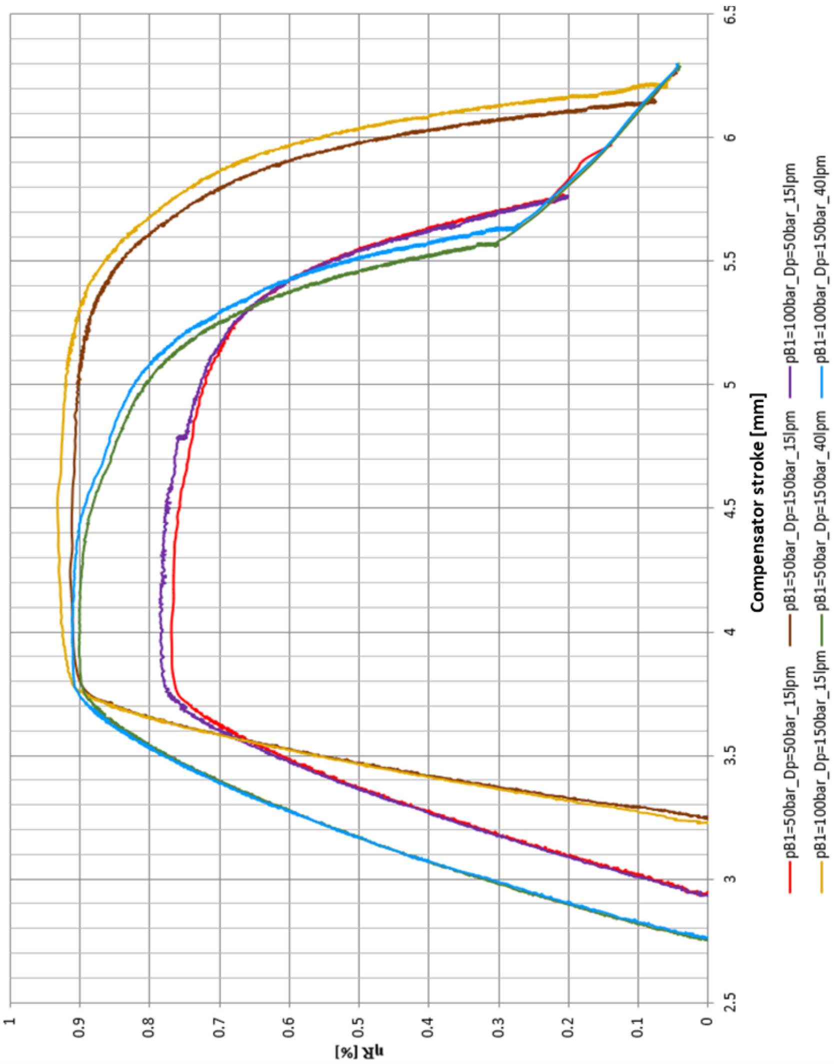

Figure 107. Efficiency recovery system

The efficiency of the recovery system ηR in the single section was defined as:

$$\eta_R = \frac{Q_R \cdot p_R}{Q_r \cdot p_r} \tag{18}$$

where Q_R and p_R are the flow rate and the pressure in R, while Q_r and p_r are the flow rate and the pressure returning to the section being compensated. The results shown in the graph are extremely encouraging, in fact it appears that the efficiency remains at a very high and almost constant value for a wide range of compensator positions (approximately from 3.8 mm to 5.0 mm). This condition guarantees a great advantage in the control of the hydraulic motor on the R line in the future, since to maximize the recovered energy, it will be necessary to control the resistant torque to keep the compensator in a range of values and not at a fixed value. From the graph it can be seen that the various performance curves reset to zero at different stroke values, this behavior can be explained by analyzing the equation of the orifice:

$$Q = c_d \cdot A \cdot \sqrt{\frac{2 \cdot \Delta p}{\rho}} \tag{19}$$

Taking the red and brown curves as the first example, the two curves have the same conditions unlike the Δp-differential; taking into consideration the reasoning made in the previous chapters on post-compensated systems in meter-out and the previous equation, in the case of the brown curve we will find ourselves having a Δp straddling the notch T higher than that of the red curve, therefore with the same of A (directly related to the position of the compensator as shown in Figure 106) will discharge much more flow rate at T, thus more quickly zeroing Q_R and consequently ηR. The same reasoning if we compare the brown curve to the green curve, differing only the flow rate Q, if the Δp across the niche T is the same, for the same A (therefore stroke) the same will be discharged; since there is more flow in the case of the green curve, it will require a greater A to discharge more Q to T, and consequently a stroke closer to 0 mm to cancel Q_R and ηR.

III.3 Digging cycle experimental data

III.3.1 Digging cycle

The digging cycle used to carry out the simulations on the numerical model and to validate it was provided by the Maha Fluid Power Lab of the Purdue University, in the United States of America.

This cycle performed by a Bobcat 435 ZHS model is visible in the captures in Figure 108.

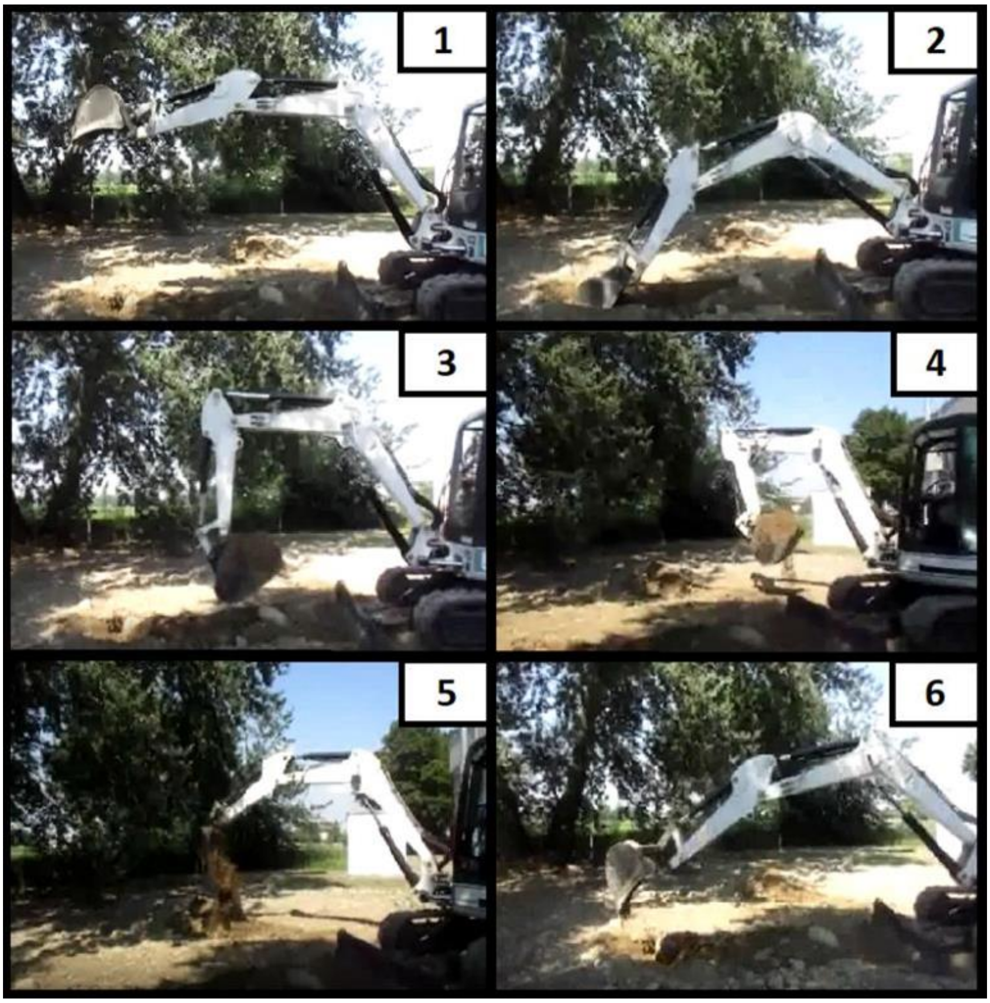

Figure 108. Digging cycle with Bobcat 435 ZHS

The experimental data that we had available from this cycle were the pressures on the head side and rod side of each actuator and the cylinders strokes (in the case of the swing, the angular rotation).

In the following Figures (109, 110, 111 and 112), the experimental pressure trends are shown:

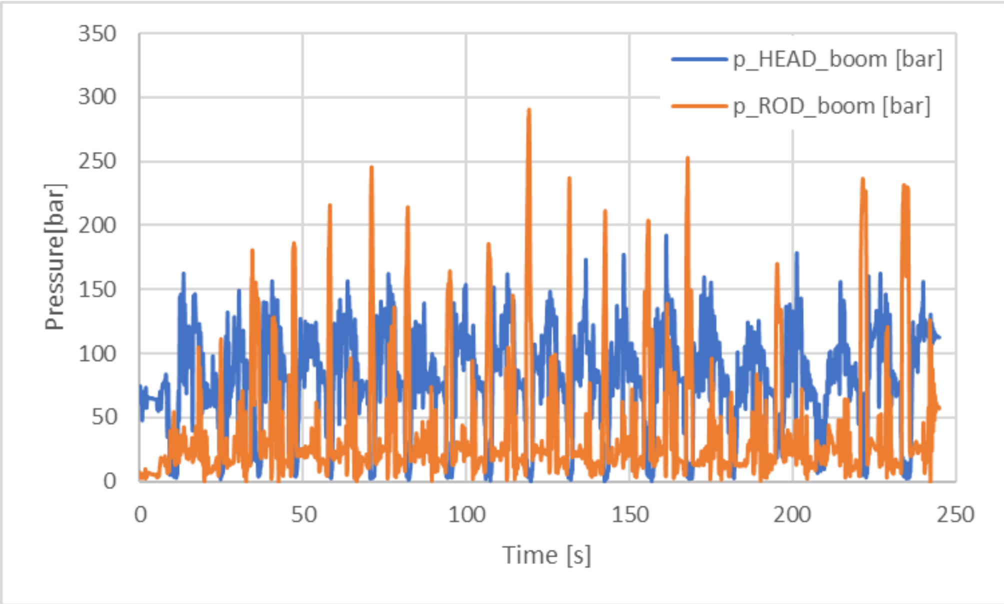

Figure 109. Pressure trends - BOOM

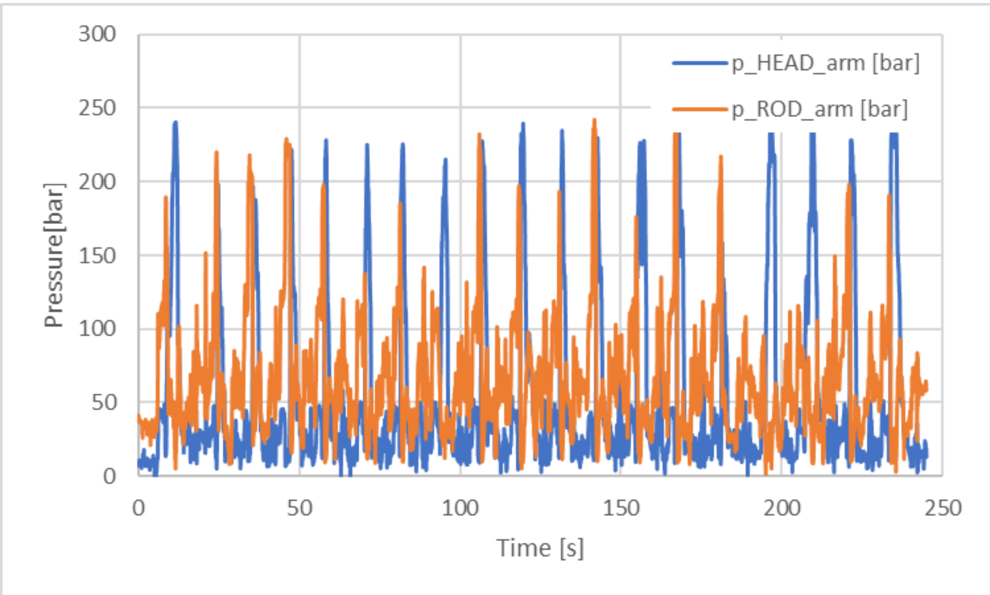

Figure 110 - Pressure trends - ARM

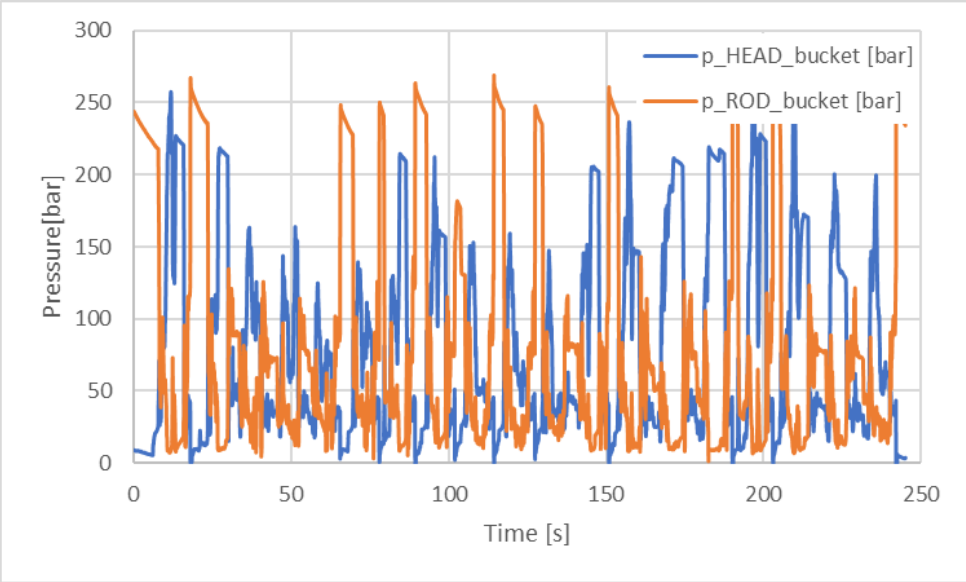

Figure 111. Pressure trends - BUCKET

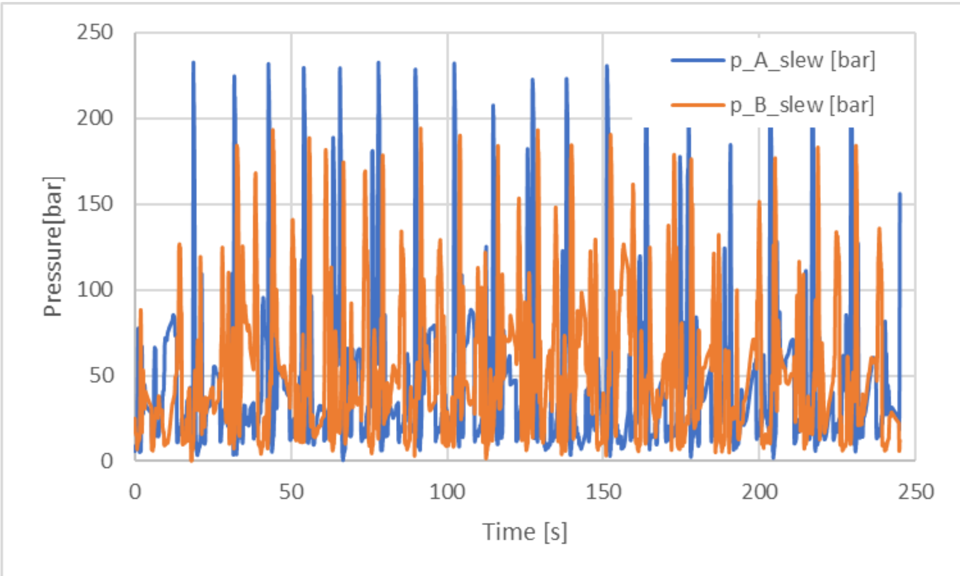

Figure 112. Pressure trends - SWING

In Figure 113 the trends of the actuator's displacement are shown.

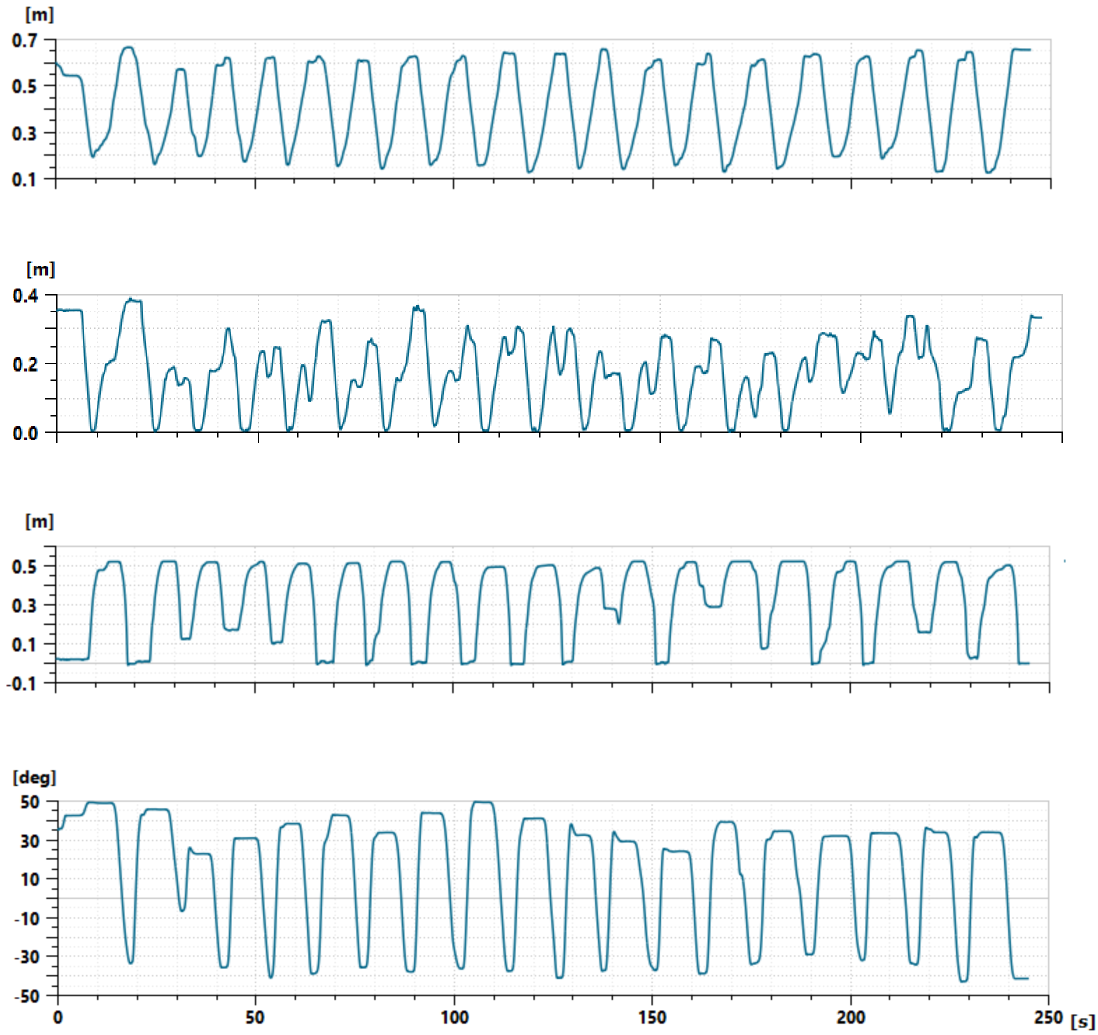

Figure 113. Actuator's displacements Bobcat 435 ZHS

The data entered as input to the numerical model (explained in the next chapter) are two:

- the load applied to the actuators;
- the mechanical control of the main spool strokes.

In particular, the data relating to pressures were used to calculate the loads [N] applied on each actuator in this cycle.

The actuator stroke trends were used with inverse formulas to calculate the main spool strokes. The experimental activity of this project is continuing at the Walvoil S.p.A. Test Department with tests on bench of other components of this energy recovery system.

The final goal of this activity, the entire tested recovery system will be applied and tested on the machine. To anticipate the results of the experimental activity and to speed up the energy analysis on the potentiality of this system, a detailed numerical analysis accompanied the experimental activity from the beginning. In particular, the detailed numerical model developed in a lumped and distributed parameter software will be explained in the next chapter.

Chapter IV: **Numerical model**

IV.1 Introduction of the numerical model

The lumped and distributed parameters model described above has been implemented using the commercial code Simcenter Amesim® developed by Siemens (5800 Granite Parkway, Suite 600, Plano, TX – 75024, USA). It allows the zero and one-dimensional modeling of multi-domain systems and their analysis. In particular, the software package consists of a suite of tools used to model, analyze and make predictions on the performance of mechatronic systems. The models are described through time-dependent nonlinear analytical equations; compared to a 3D CAE modeling, this approach makes it possible to analyze the behavior of the system even without detailed CAD geometry. The modeling (with lumped parameters) takes place through a block diagram, with the use of submodels which, once properly connected, will also define the causality of the system. The submodels are divided into various physical libraries, the main ones being: control, electrical, mechanical, pneumatic, hydraulic and thermal. The simulation process takes place in four different steps:

1. **Sketch mode**

   The components are chosen and connected to each other;

2. **Submodel mode**

   The physical sub-models associated with each component of the model are defined;

3. **Parameter mode**

   The parameters of each submodel are defined;

4. **Simulation mode**

   The mathematical simulation is performed and the results are analyzed.

Referring to Figure 114, the structure of the numerical model of a single section can be understood. In the blue box there is the LS pump that supplies all the sections of the DCV. The pump (not analyzed in detail in this work) has two hydraulic connections: an output corresponding to the delivery and an input corresponding to the LS signal coming from the common LS line to all sections.

In the red box there is the main spool whose stroke is mechanically controlled by the input data entered in the model (through the red "signal blocks"). The geometric data of the spool are indicated in Chapter III. In the yellow box there is the actuator which, depending on the specific section, can be a cylinder or a hydraulic motor. The geometric characteristics of the actuators have been listed in the tables of Chapter III. In the green box there is the innovative component of this DCV: the local compensator of the section. This element is the only one that varies in the three double compensation tests that will be shown in the next paragraph. In the pink boxes, two relief valves are modeled, one of which is located downstream of the compensator towards the energy recovery line (in these preliminary tests it ends with a tank, but subsequently it will be connected to an energy recovery system).

IV.1.1 Double compensation tests

As already described in the previous chapter, the new DCV with energy recovery was tested on bench with three different compensators, while always maintaining the same main spools. The Amesim models of the three configurations therefore only differ in the modeling and laws of area of the compensators.

The validation of the models was performed by replicating and comparing the experimental tests (in particular, the double compensation test, with constant load on section 1 and loading ramp on section 2) carried out on test bench. Only the results of the numerical models in the conditions of meter-in compensation and meter-out compensation without recovery will be represented (Figure 115 and Figure 117). The numerical model in condition of meter-out compensation with energy recovery will be described in detail because is the main goal of this thesis project.

- **Model with compensation in *meter-in***

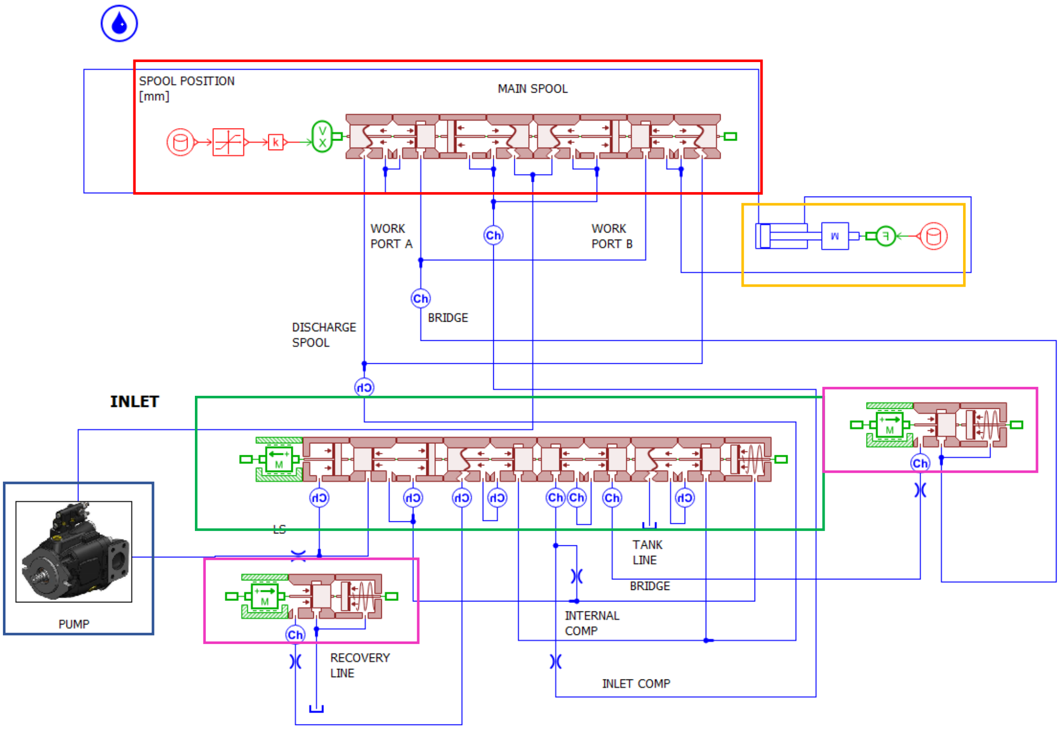

Figure 114. DCV model with Energy Recovery- compensation in meter-in

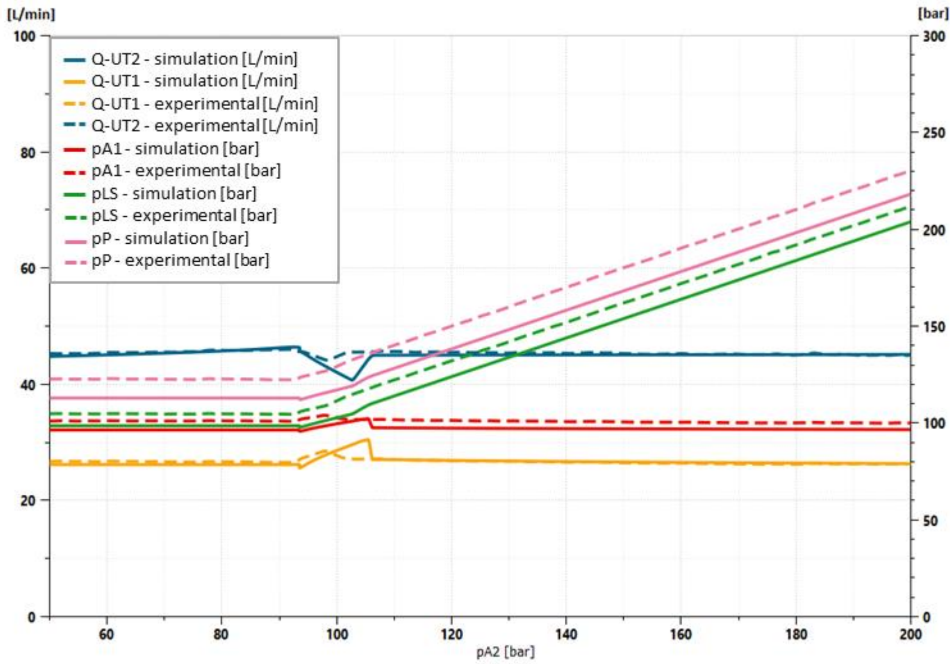

Figure 115. Model validation – meter-in compensation

- **Model with compensation in *meter-out* without recovery**

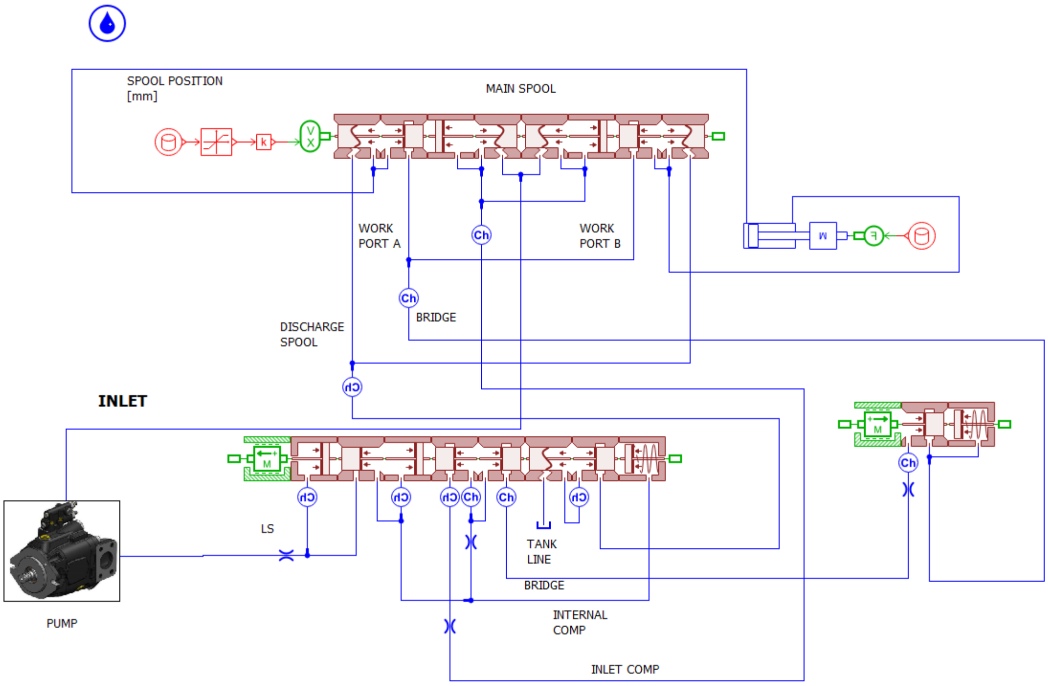

Figure 116. DCV model with Energy Recovery - meter-out compensation without recovery

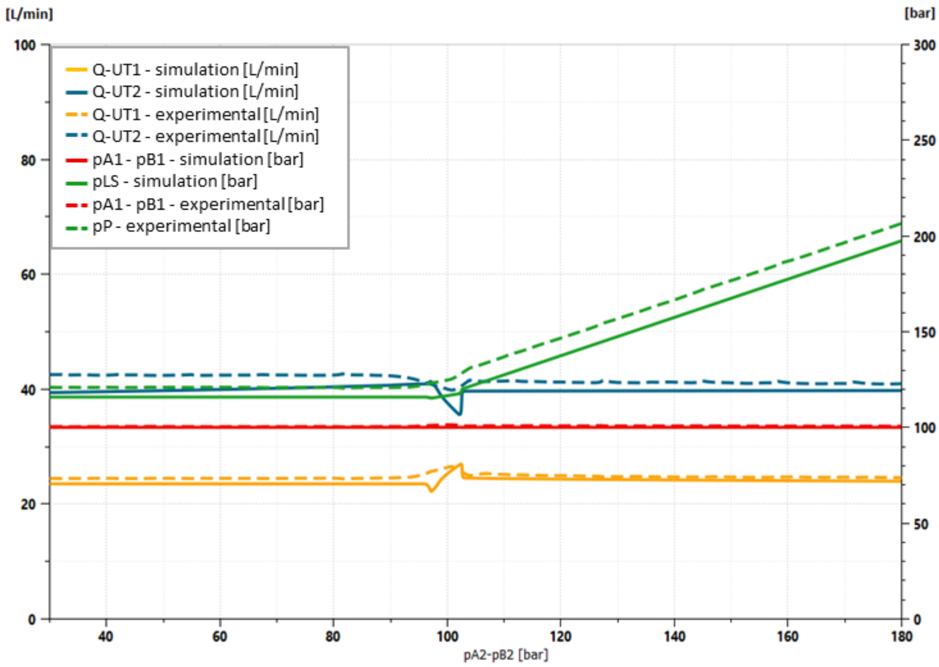

Figure 117. Model validation - meter-out compensation without recovery

- **Model with compensation in *meter-out* with recovery**

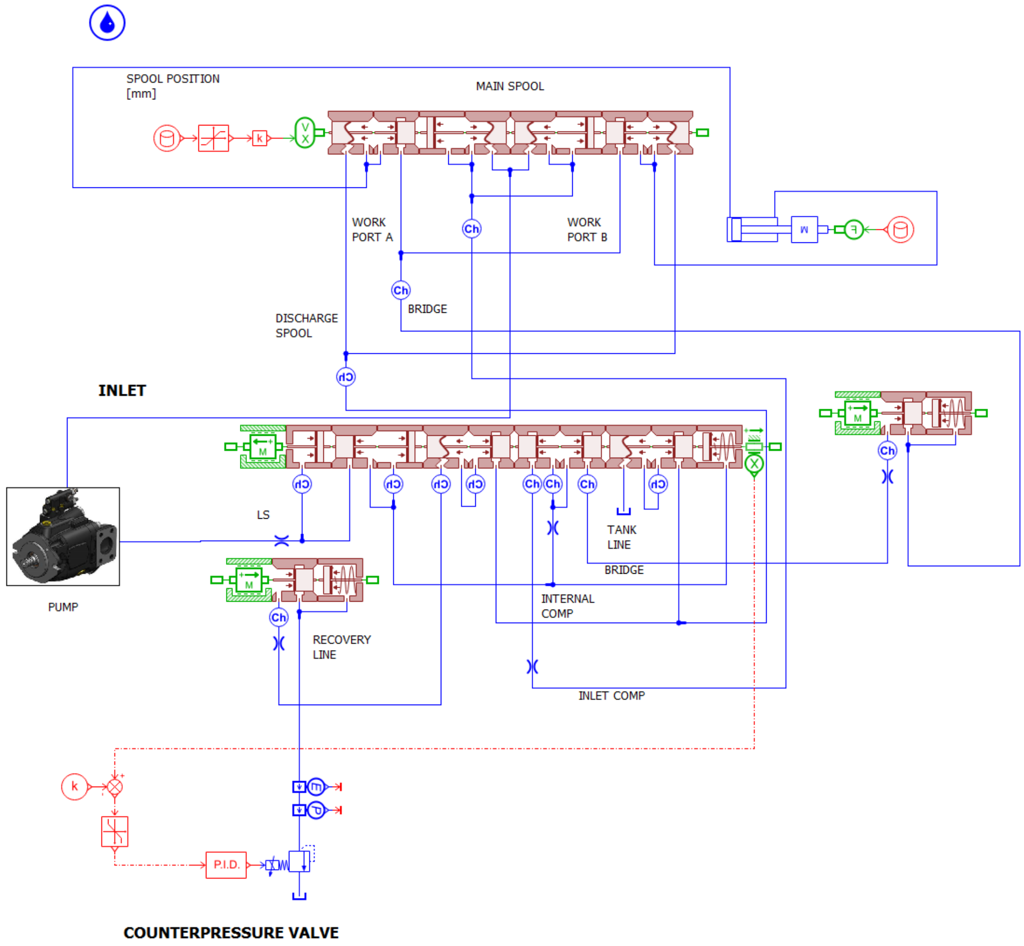

Figure 118. DCV model with Energy Recovery - meter-out compensation with recovery

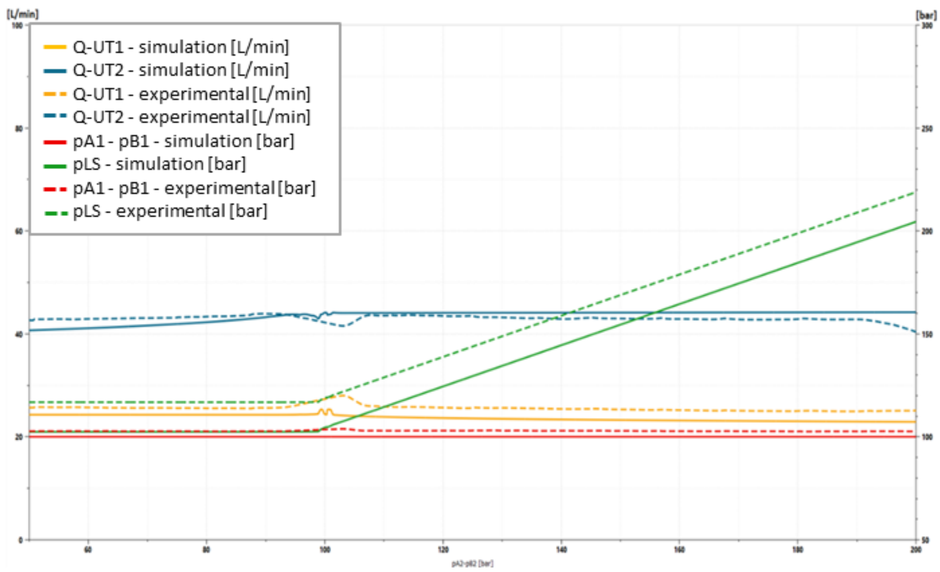

Figure 119. Model validation - meter-out compensation with recovery

Naturally, these simulations that reply the double compensation tests were carried out by connecting the models of the individual sections as shown in Figure 120.

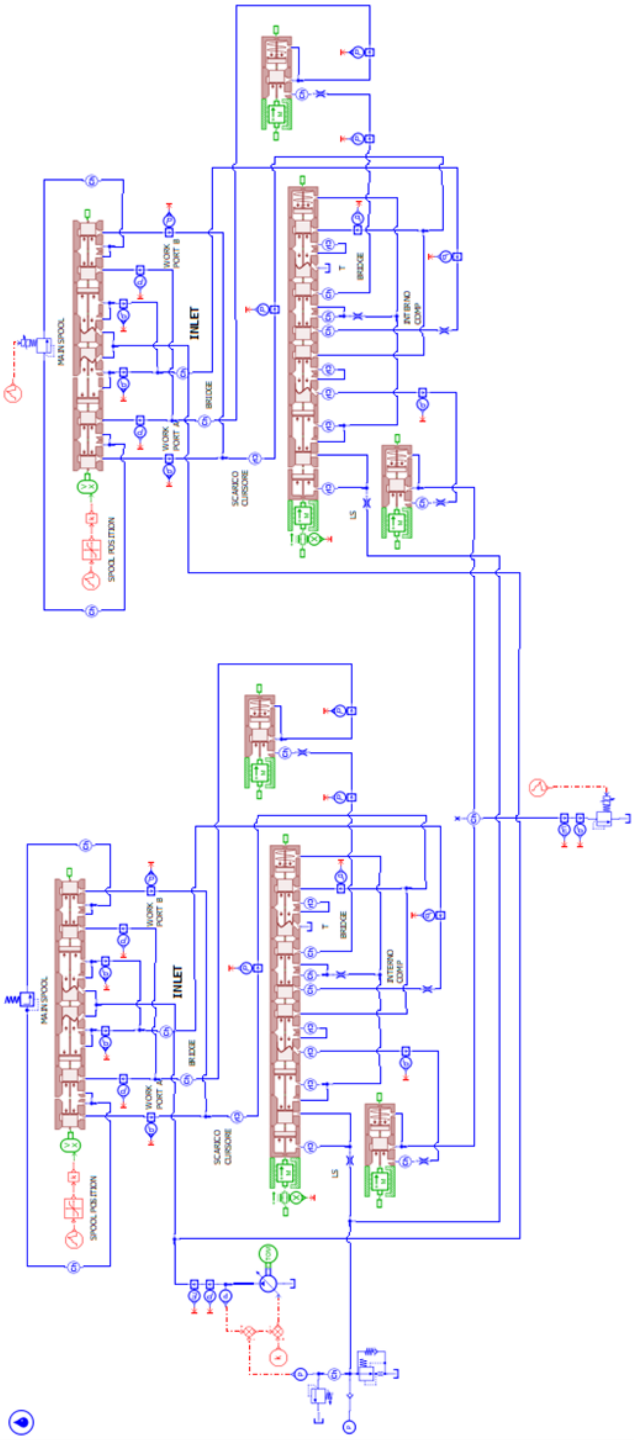

Figure 120. DCV model with Energy Recovery – 2 sections

In the previous figures (Figures 114, 116, 118) a single section has been shown with the relative results that see the comparison of the compensation condition in experimental and numerical tests. Of course, not all four sections are shown as they are identical to each other (the main spool does not have dedicated exhaust notches yet and it is the same for all sections. The same reasoning applies to the compensator which provides for compensation on the meter out for all sections).

The geometric features of the hydraulic cylinders (shown in Tables 7, 8, 9) are the only differences between these sections; naturally the only section with a different actuator is the swing (Figure 121) modeled through a functional block of a hydraulic motor with the characteristics listed in Table 10.

Swing parameters	
Displacement [cm^3/rev]	820
Volumetric efficiency	0.95
Hydraulic-mechanical efficiency	0.9

Table 10. Hydraulic motor swing characteristics

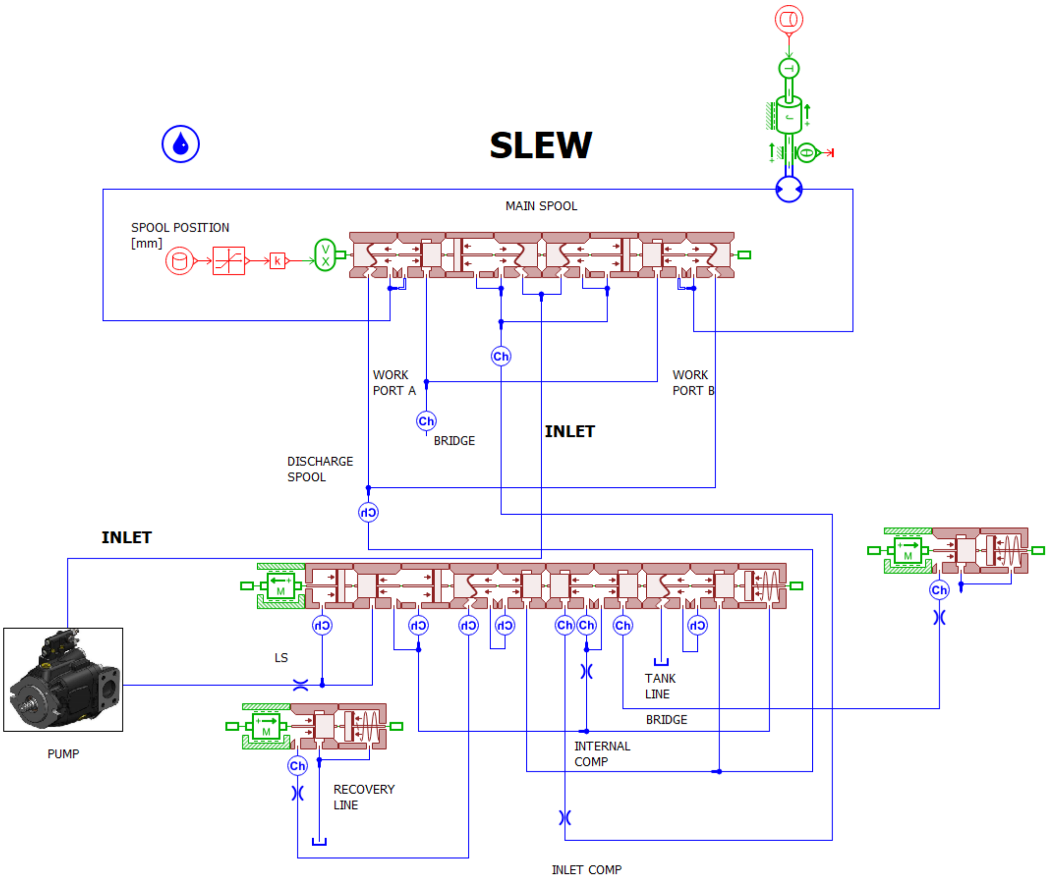

Figure 121. DCV model with Energy Recovery - meter-out compensation with recovery (slew/swing)

IV.1.2 Digging cycle tests

The numerical activity, proceeding faster than the experimental one, allowed us to predict the behavior of the new DCV and of the total energy recovery system that will be applied on the final machine (Bobcat 435 ZHS), thanks to the modeling of a real cycle.

As anticipated in the previous chapter, a complete digging cycle (Figure 113) of 245 s was implemented in the model consisting of 18 rather repetitive cycles, carried out by an expert operator on the Bobcat ZHS 435.

This cycle was kindly made available by the Maha Fluid Power Lab of Purdue University (USA).

For these simulations, the complete model of the machine was realized with the union of all its four main sections supplied by the same LS pump (Fig.122).

Figure 122 shows the complete model consisting of 4 sections, the supplying system (pump) and a recovery line, in a preliminary phase controlled by a relief valve. This valve is able to control the pressure on the R line thanks to an input command, function of the compensators strokes. This operation will be explained in *IV.1.2.1.*

In second phase it will be seen that the Relief valve will be replaced by the Energy Recovery components, explained in detail in the next pages.

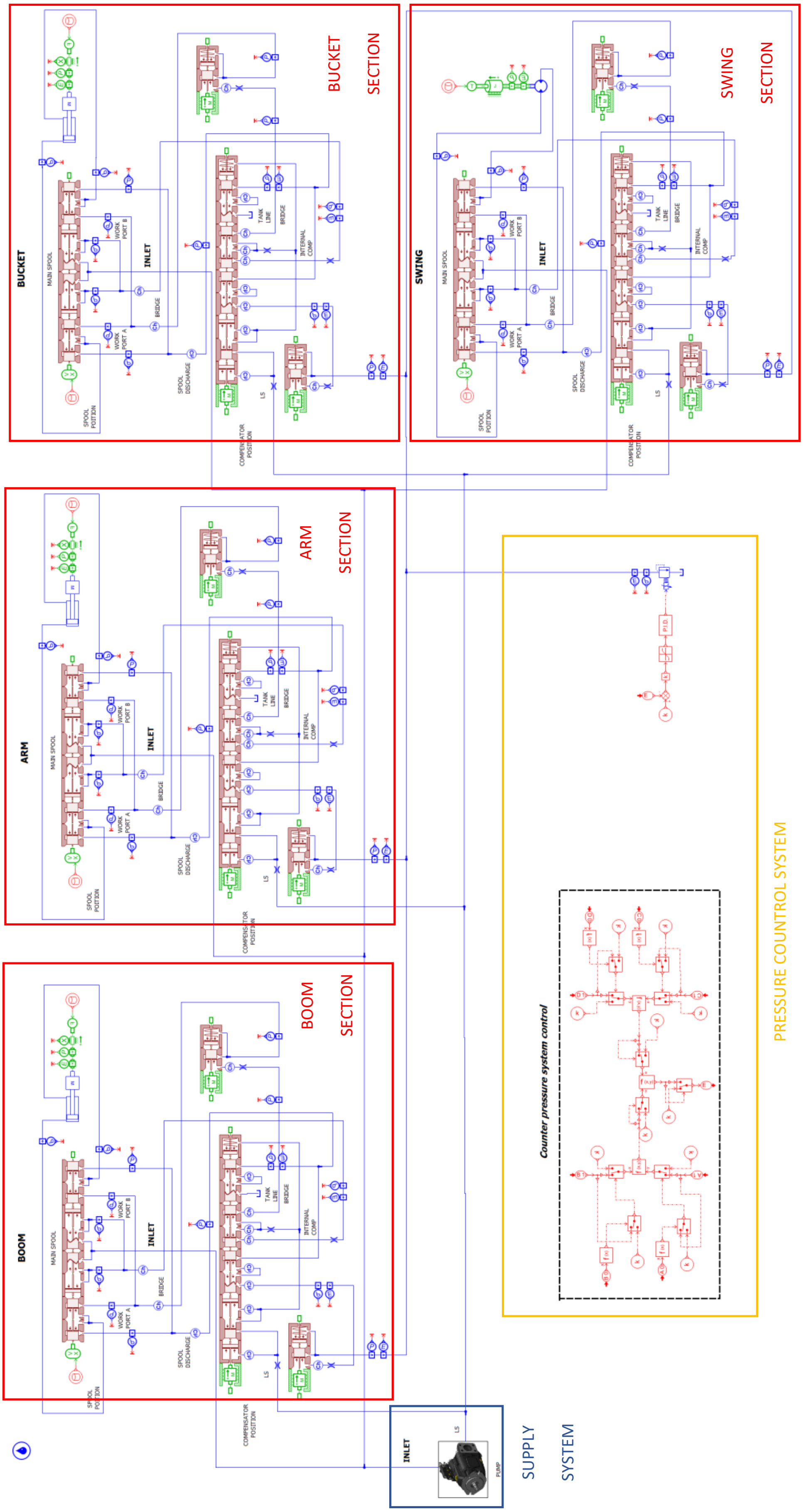

Figure 122. DCV model with Energy Recovery – 4 sections

IV.1.2.1 Counter pressure system control

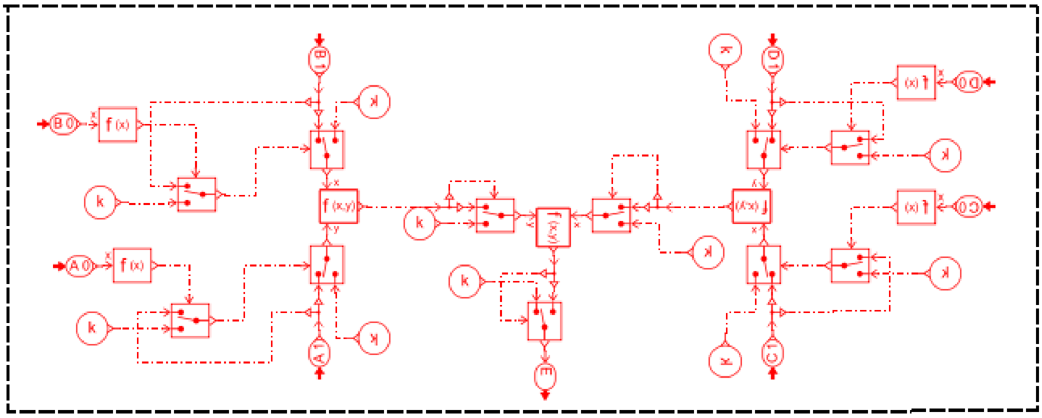

Figure 123. Counter pressure system control

The Figure 123 shows a detail of the system implemented in the Relief Valve torque control model. This set of functions is only a simple preliminary control system before to develop a more sophisticated one, actually in elaboration phase. This system, which temporarily replaces a control unit (ECU), reads the compensator stroke through position sensors located on each individual local compensator itself.

These position sensors read the compensator strokes and send this signals to a counter pressure control shown in Figure 123.

The position signals of the compensators enter the logic only if the sections concerned are active (information available from the position of the main compensator). The incoming position signals that will pass to the next level of logic are those that exceed a set stroke value (4.5 mm) and the minimum value is taken from the latter; the signal obtained will be compared with the set-point (also at 4.5 mm) and will generate the input to the PID that controls the pressure relief valve (functioning as a load valve). In this way, the sections with the compensator stroke over 4.5 mm are brought into a position of greater recovery efficiency, without opening the T-line in any of the aforementioned sections.

The model of Figure 122 was validated through the digging cycle already shown in Figure 113 and below described. As explained in detail in *III.3.1* the inputs to the system are:

- the loads applied to the actuators (calculated by the digging cycle data of the pressures on the head and on the rod of each of four actuators);
- the mechanical control of the main spool strokes (calculated by the flow rates to the port A and B of each actuator).

The pressures and the flow rates of the digging cycle were supplied by Maha Fluid Power Lab.

In Figures 124 and 125 the experimental (blue line) and the numerical trends (red line) of pressures on both sides of the boom actuator show the validation of the model for a single section.

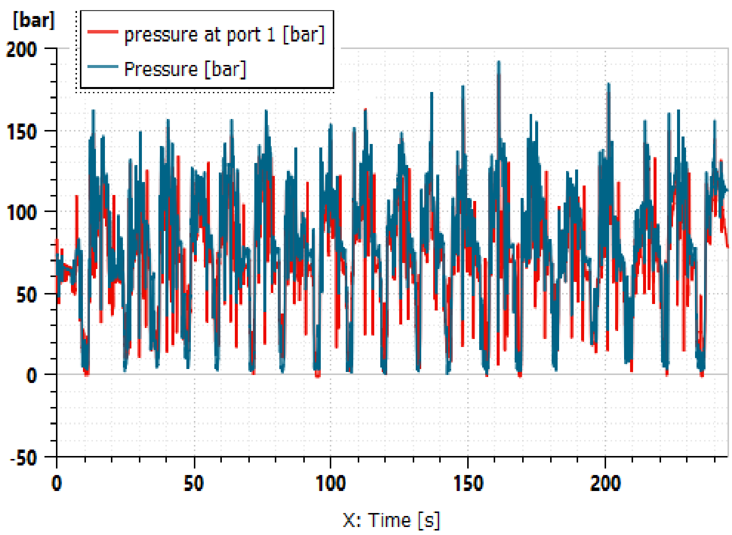

Figure 124. Experimental and numerical pressure trend, port A (boom)

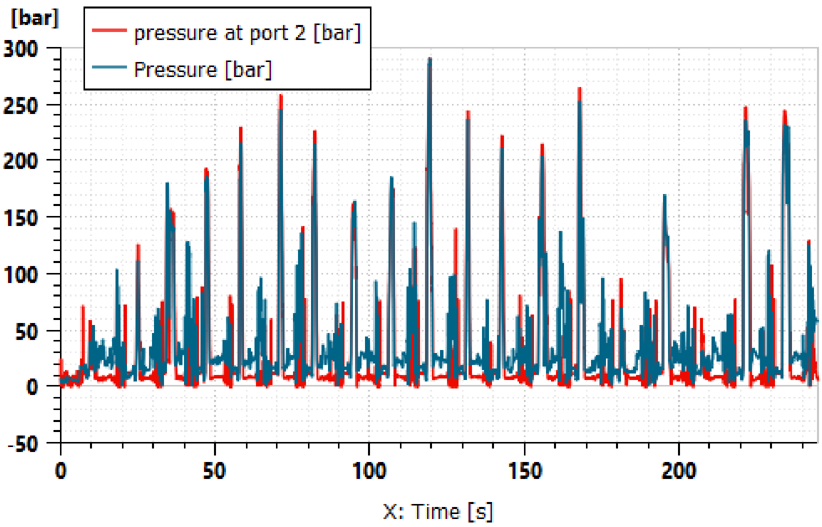

Figure 125. Experimental and numerical pressure trend, port B (boom)

In Figure 126 the validation of the complete model with the application of the digging cycle is shown:

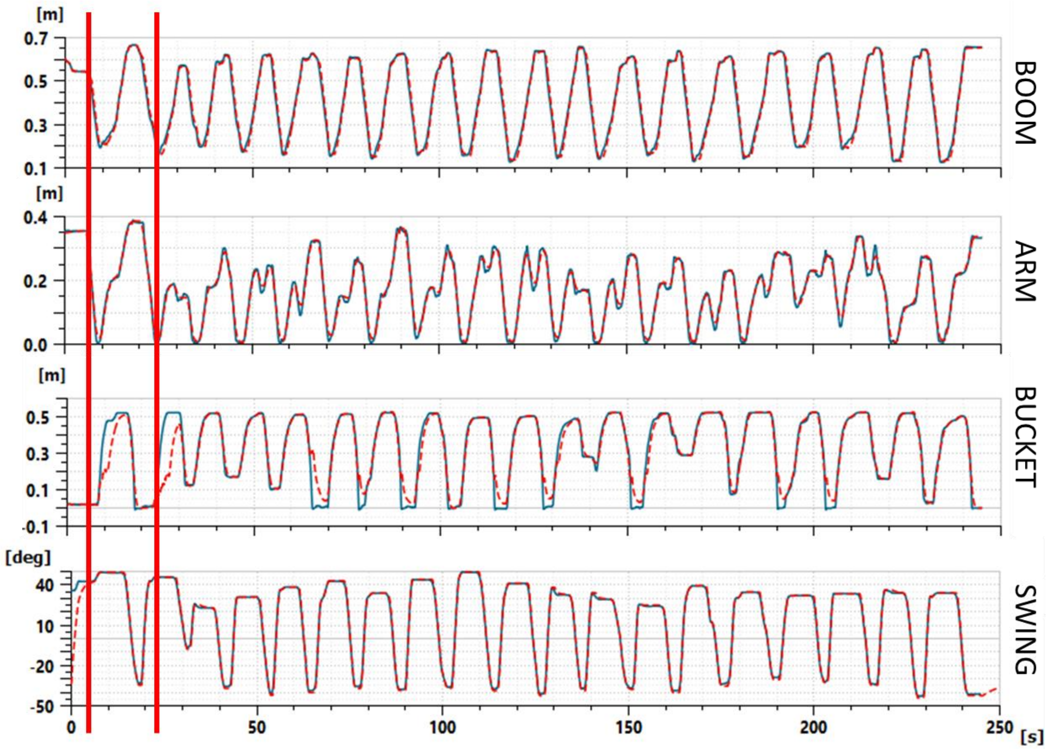

Figure 126. Digging cycle (cylinders strokes and swing angular displacement)

The solid blue lines represent the experimental results and the red dashed lines represent the numerical results. As can be seen from the figure the trend shows one of the outputs of the simulation, respectively the stroke of the 3 cylinders (arm, boom and bucket) and the angular displacement of the swing over a total time span of 245 s, the model is validated.

The details of the system have been already explained in *II.2.6.*

The working cycle taken in consideration, as said before, is more or less the same for about 18 consecutive equal cycles for a total time of 245 s. To analyze the system downstream of the DCV, therefore, only the first cycle was taken into consideration, ranging from 5 s to 22 s for a total time of 17 s, because it is more or less similar to the following ones.

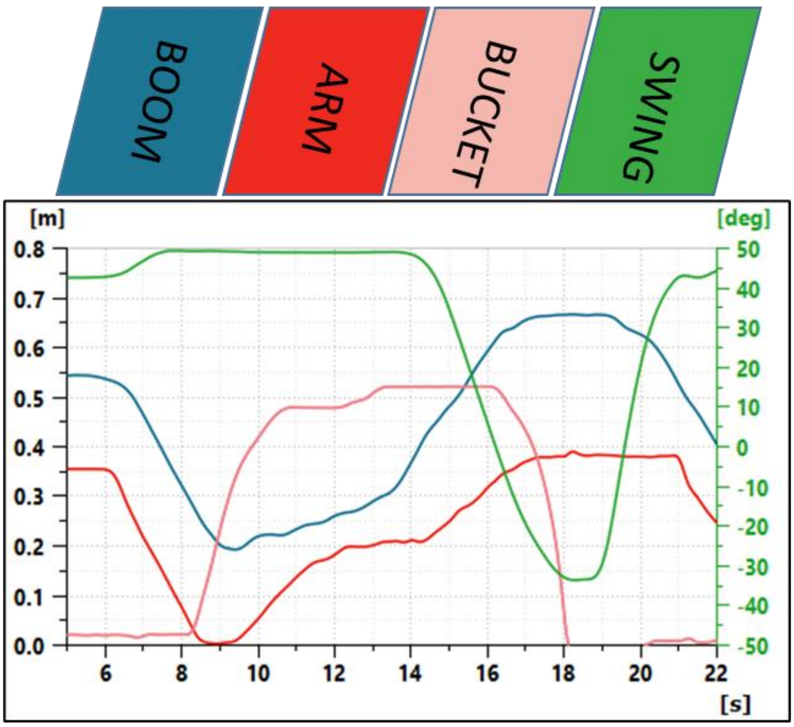

Figure 127. Digging cycle (single cycle)

In Figure 127, for the reference cycle, the strokes of the cylinders and the angular rotation of the swing of the reference cycle can be seen in a single graph.

In particular:

- blue line: boom cylinder stroke
- red line: arm cylinder stroke
- pink line: bucket cylinder stroke
- green line: swing angular displacement

After the validation of the model, the Relief Valve was replaced with a system able to recover and then reuse this energy. Different analysis conducted the research to insert in the numerical model, on the recovery line, the following components (shown in the green box of Figure 128):

- hydraulic motor;
- AC motor/generator with inverter;
- battery.

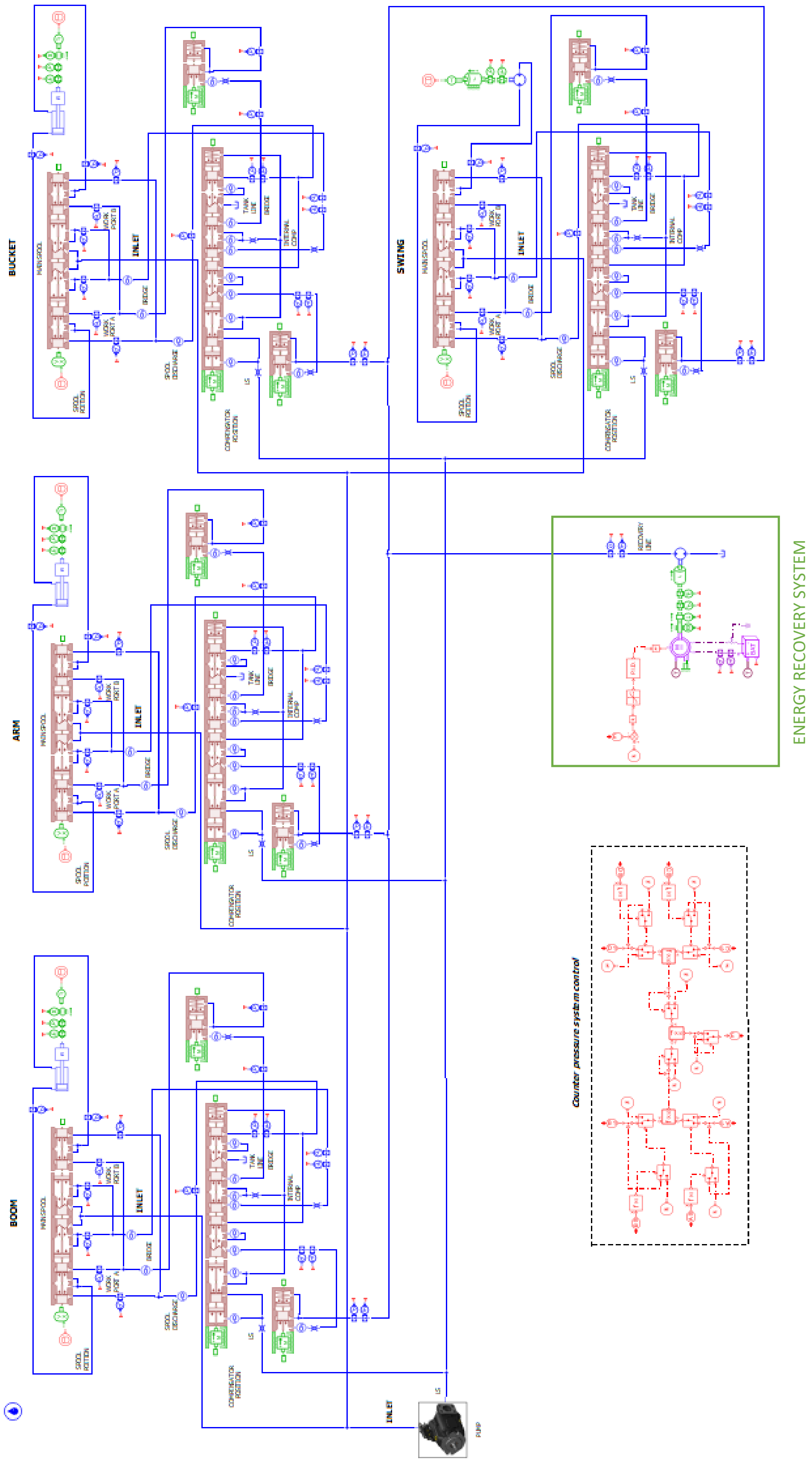

Figure 128. Complete excavator numerical model

In particular, the hydraulic motor is coupled to an AC generator which charges a Battery thanks to an inverter. The components in this configuration will be used in the next experimental tests of this activity, once purchased from other manufacturers. The adaption of this numerical model permits us to estimate in advance the main features of all these components. The characteristics of the Hydraulic motor, Electric-Motor Inverter and of the Battery used in these numerical simulations are shown in the following Tables:

HYDRAULIC MOTOR	**Hydraulic motor displacement [*cc*]**	15
	Global efficiency (η)	1

Table 11. Hydraulic motor parameters

ELECTRIC MOTOR + INVERTER	**Speed_nom [*rev/min*]**	2000
	Torque_nom [*Nm*]	20
	Efficiency_nominal values (η)	0.94
	pmax [*KW*]	20
	Torque_max [*Nm*]	80
	Voltage (*V*)	400
	Overall efficiency (*h*)	0.91
	Losses_inverter	Effic_map

Table 12. Electric motor parameters

BATTERY	**Cells_Voltage [*V*]**	3.47		
	N_cells_series	115		
	N_cells_parallel	1	2	3
	Cell_capacity [*Ah*]	31.5		
	Total_capacity [*Ah*]	31.5	63	94.5
	Total_voltage [*V*]	399.05		
	Internal resistance [*Ohm*]	0.009		

Table 13. Battery parameters

Chapter V: **Energy Analysis and Numerical results**

The final phase of the activity is focused on the collection of results and the development of various energy analysis using the numerical model. All the graphs showed in this chapter are the results of the simulations realized on the numerical model, already explained and validated through the experimental tests (Figure 122). Moreover, the digging cycle of Figure 113 was used to realize these numerical tests.

The idea was to consider the total system as a black box for which the sum of the input rates is equal to the sum of the outlet rates.

In particular, the energy input to the system is composed of the sum of the following energies:

- pump energy (En_{pump})
- energy gained from overrunning loads (En_{overr_loads})

The energy output is composed of the sum of:

- recoverable energy ($En_{recoverable}$)

- energy spent for resistive loads (En_{resist_loads})
- energy dissipated in the system ($En_{dissipated}$)

For the above, in the first analysis, if we consider the energy introduced into the system as 100% (Figure 129):

- 90% is the energy that the pump spent to complete the reference working cycle;
- 10% is the energy obtained from the overrunning load condition of all sections.

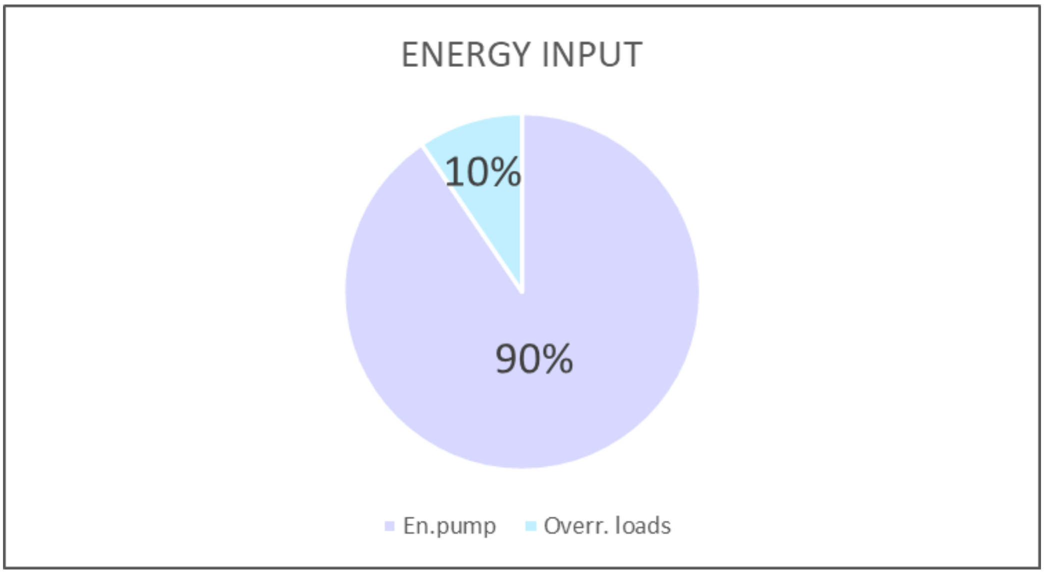

Figure 129. Energy input to the system

These calculations derive from the following equations:

$$En_{pump}[\%] = \frac{En_{pump}}{En_{pump} + En_{overr\_loads}} \cdot 100 \tag{20}$$

$$En_{overr\_loads}[\%] = \frac{En_{overr\_loads}}{En_{pump} + En_{overr\_loads}} \cdot 100 \quad (21)$$

As for the output energy (Figure 130):

- 33% of this energy is spent for resistive loads;
- 29% is the energy recoverable[1] from the hydraulic circuit, thanks to the new DCV;
- 38% are the dissipation losses in the system.

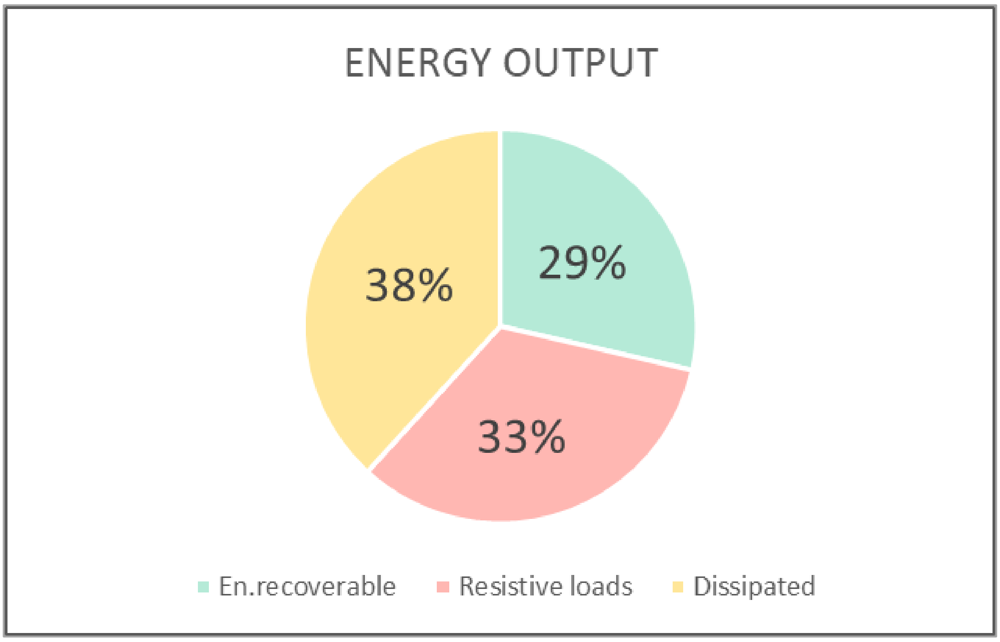

Figure 130. Energy output from the system

The graph in Figure 130 is the result of the following equations:

[1] The so-called *recoverable energy* is the energy that the new DCV is able to recover thanks to the particular functioning of the compensator which directs the spool's meter out flow preferably towards a recovery line rather than towards the discharge line. This energy corresponds to the largest part of the energy that would have to be dissipated in a traditional valve without recovery.

$$En_{recoverable}[\%] = \\ = \frac{En_{recoverable}}{En_{recoverable} + En_{resist\_loads} + En_{dissipated}} \cdot 100 \quad (22)$$

$$En_{resist\_loads}[\%] = \\ = \frac{En_{resist\_loads}}{En_{recoverable} + En_{resist\_loads} + En_{dissipated}} \cdot 100 \quad (23)$$

$$En_{dissipated}[\%] = \\ = \frac{En_{dissipated}}{En_{recoverable} + En_{resist\_loads} + En_{dissipated}} \cdot 100 \quad (24)$$

It is observed that the recovered energy exceeds that of the driving loads, thanks to the fact that, being more active sections, we have the contribution of the energy recovery given by the compensation.

The boom is the section that provides the greatest contribution to energy recovery. In fact, it is able to recover in overrunning load e in simulation compensation conditions for a total contribution of 67% to the total recoverable energy from the system. In Figure 131 the minor contributions from the other sections are shown (14% by arm section, 12% by bucket section and only 7 % by the swing section).

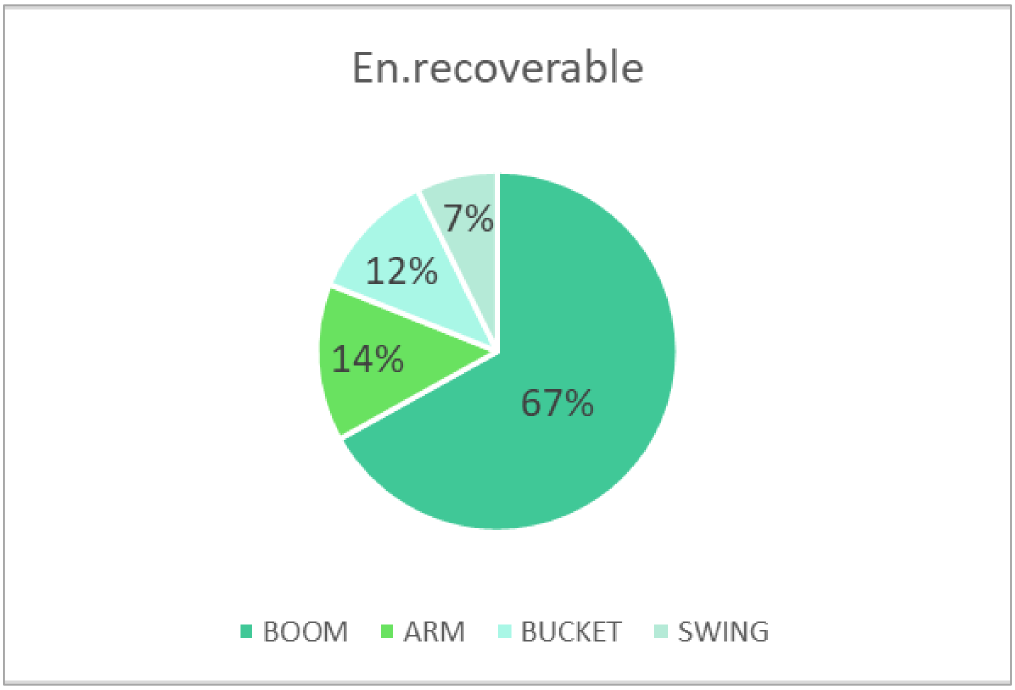

Figure 131. Energy recoverable from all sections

The contributions in Figures 131 are obtained from power sensors applied in the numerical model downstream of each section and visible in Figure 122. Specifically, the numerical model allowed us to distinguish the energy spent for the resistive loads and that recovered from the overrunning loads for each single section (Figure 132).

In the boom it can be seen that the two contributions are almost equal, then it is also deductive to think that it is the section from which the most quantity of energy is recovered in overrunning load condition.

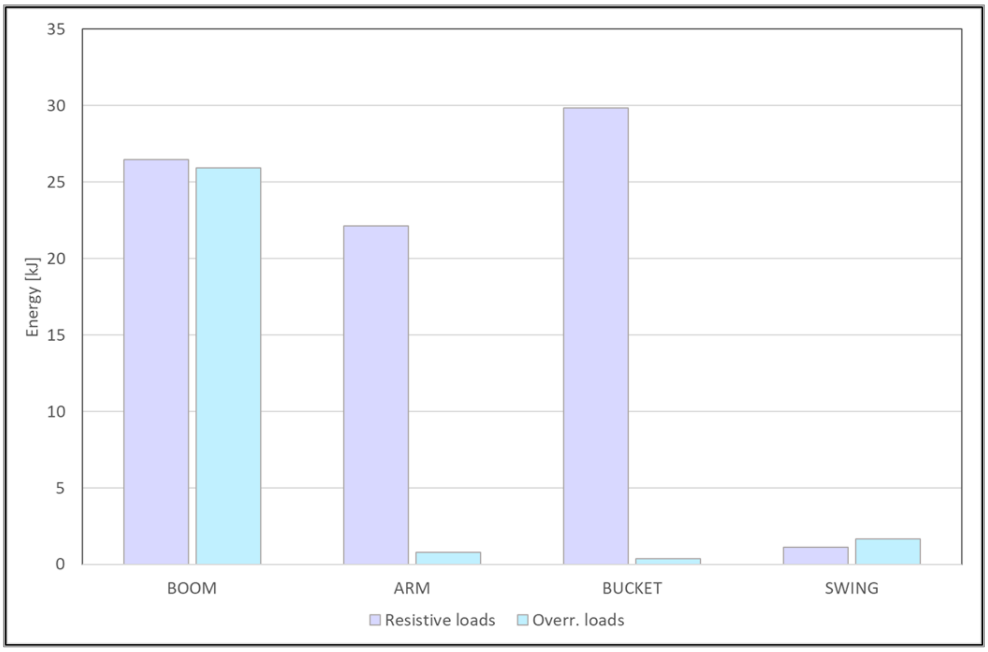

Figure 132. Resistive and Overrunning loads of the four sections

Furthermore, this result is also justified in compensation conditions; it is enough to observe the cycle in Figure 120 to understand that the compensator of the boom section in the range from 9 s to 18 s moves together with the arm and since the section is dominated, it is the section that manages the downstream back pressure system which optimizes the opening of one of the compensators towards the recovery line, in this case the boom.

A further analysis concerns the energy comparison between a traditional Load Sensing Flow Sharing valve and the new DCV with energy recovery. The intuitive result clearly emerges from the comparison visible in Figure 133.

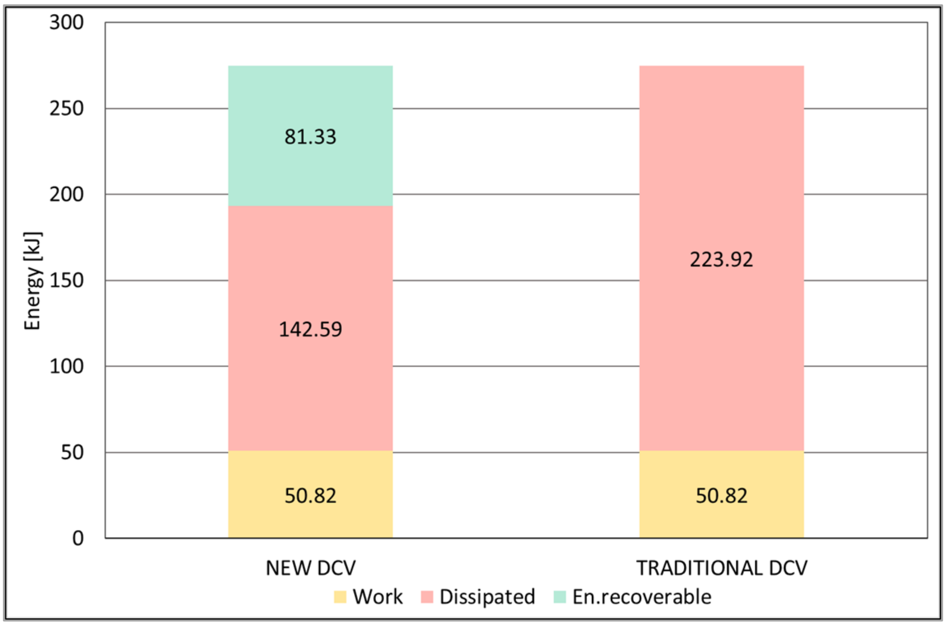

Figure 133. New DCV vs Traditional DCV

In the numerical model the two valves were subjected to the same real cycle that we are considering as a reference (Figure 127).

Referring to Figure 131 the pump (the same for both) spends 277 kJ to complete this working cycle (17 s). Since the cycle is the same, the two simulations do the same work, almost 50.82 kJ. The remaining energy from the total one delivered by the pump is completely dissipated in the traditional valve (223.92 kJ) because it has no system capable of recovering flow. With the new valve 81.33 kJ of 277 kJ are transformed into recoverable energy while only 142.59 kJ are losses.

It must be considered that the energy recovery DCV not only dissipates less energy, but also recovers an amount equal to 81.33 kJ of the energy required by the pump. This energy can potentially be reused in subsequent cycles, supporting the pump, making the system even more efficient.

A further interesting analysis concerned the energy recovered in relation to that actually spent by the pump (thus excluding the input due to overrunning loads). This energy was calculated by the following equation:

$$En_{recovered}[\%] = \frac{En_{recovered}}{En_{pump}} \cdot 100 \tag{25}$$

As can be seen from Figure 134, the new DCV recovers 32% of the energy spent by the pump. This energy value refers to all the energy recovered from the hydraulic system upstream of the electrical recovery system. Naturally, the electrical recovery system explained above is equipped with components that generate further energy dissipations. However, it is precisely the energy contribution made available by the electric motor / generator in the form of electrical energy that is the fundamental data of the whole study.

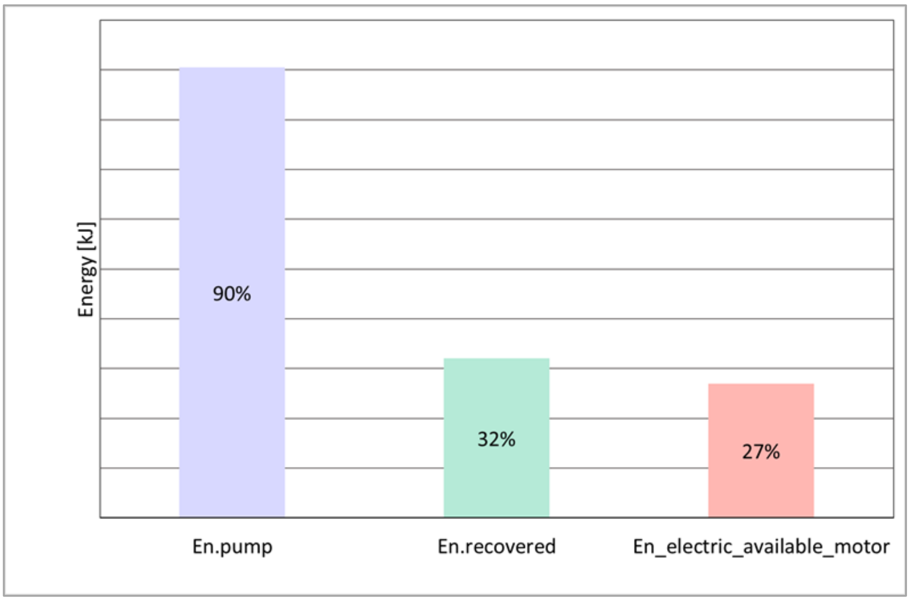

Figure 134. Energy spent vs Energy recovered

This data was calculated through a power sensor placed between the electric motor / generator and the battery pack in the numerical model. The histogram of Figure 132 shows that this energy value is equal to 27% of the energy spent by the pump.

With the battery (whose characteristics are shown in Table 13) chosen for this numerical test, we made a calculation of its charging condition. In this preliminary phase we only have calculated the overall battery charging time, excluding any conditions of reuse of the latter. Therefore, the calculation was carried out on the complete non-use of the latter as until now it was simply considered an energy storage system. Then the recovered electricity (27%) recharges the battery for a single reference cycle (17s) of 0.075%. If the initial state of charge of the battery (SOC) is 0.2 (thus 20%), at the end of the first cycle it will be 20.075% (Figure 135).

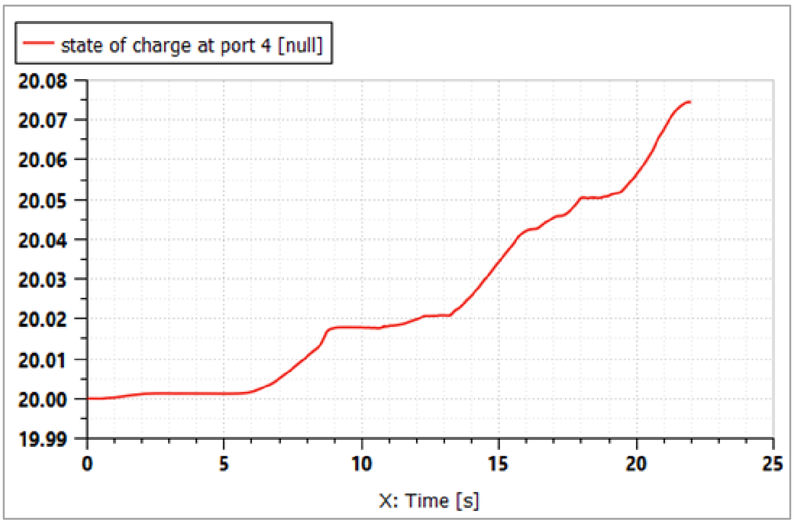

Figure 135. Battery state of charge in 17 s

Assuming we want to run the excavator for many hours, through simple mathematical calculations made on this cycle, we can conclude that the reference battery in these operating conditions, after 5 hours and starting from a state of charge of 20% in complete inactivity, will be completely recharged.

More detailed studies on this part of the energy recovery system, expecially on the electric motor and on the battery will be conducted in the project that Walvoil S.p.A is developing.

Nomenclature

Acronyms

DCV	Directional Control Valve
ECU	Electronic Control Unit
ICE	Internal Combustion Engine
INV	Inverter AC-DC
MRV	Main Relief Valve
PRV	Pressure Reducing Valve
SOC	Battery State Of Charge

Symbols

Name	*Description*	***Unit***
A1, B1…	Work ports	[-]
A_0	Orifice cross section	[mm^2]
A_{in}	Spool meter-in Area	[mm^2]
A_{out}	Spool meter-out Area	[mm^2]
A_R	Local compensator Area of way towards recovery line R	[mm^2]

A_T	Local compensator Area of way towards tank T	[mm²]
$A_{(x)}$	Crossing area	[mm²]
C	Generator torque	[Nm]
C_d	Discharge coefficient	[-]
D_{IN}	Line Downstream spool meter-in	[-]
D_{OUT}	Line Downstream spool meter-out	[-]
Δp_{LS}	Pressure Difference p_P - p_{LS}, or pump margin	[bar]
G	AC Generator	[-]
LS	Load Sensing, highest pressure among working sections	[-]
M	Hydraulic Motor	[-]
p_A, p_B	Work port A, B pressure	[bar]
P_{lost}	Power Lost	[W]
p_{LS}	Load Sensing pressure	[bar]
p_P	Pump pressure	[bar]
p_R	Pressure in recovery line R	[bar]
P	Variable Load Sensing Pump	[-]
P_{spent}	Power Lost	[W]
PS	Position Sensor	[-]
P_{spent}	Power Spent	[W]
p_u	Pressure requested by the user	[Pa]
P_{useful}	Useful Power	[W]
p^*	Calibration pressure	[Pa]
Q	Volumetric Flow rate	[l/min]
Q_0	Pump maximum deliverable flow rate	[l/min]
Q_A, Q_B	Work port flow rate, or meter-in flow	[l/min]
Q_{OUT}	Flow rate from the actuator, or meter-out flow	[l/min]
Q_R	Flow rate in the recovery line R	[l/min]
Q_u	Flow rate requested by the user	[l/min]

R	Energy Recovery line	[-]
s	Compensator stroke	[mm]
SP	Compensator stroke set point	[mm]
X	Pilot line fed by the Pressure Reducing Valve	[-]
T	Tank line	[-]
V_{max}	Pump maximum displacement	$[{}^{m^3}/_{rad}]$
V_0	Pump displacement	$[{}^{cm^3}/_{rev}]$
w	Angular displacement	[deg]
X	Command signal	[-]
ηR	Efficiency of recovery system	[adim]
Δp	Pressure difference	[bar]

Conclusions

This thesis present the development of an efficient Energy Recovery system for Off-Road vehicles. In detail, an innovative Directional Control Valve has been implemented and developed which allows the recovery of flow rate in the hydraulic circuit, that otherwise would be dissipated.

This valve is based on the concept of the positioning of a "3-ways Downstream Compensation" on the actuators return line with the purpose to control and recover the return flow into a dedicate energy line R.

The 3-ways compensator allows to recover energy into the recovery line R in presence of:

- overrunning loads;
- simultaneous operations at different pressures, thanks to the DCV compensation action.

An important aspect is that, thanks to this design, the controllability and the flow regulation of the DCV is not minimally affected by the recovery action; in case the recovered hydraulic power cannot be reused or stored, the compensator simply vent to tank the return flow.

Compared to a traditional flow sharing DCV, the new design allows to perfectly control the overrunning loads without any risk of cavitation.

The particular embodiment of the compensator is characterized by the presence of three ways, which allow the main spool discharge line to be connected respectively to the system tank T or to an energy recovery line R (typically feeding a hydraulic accumulator). The compensator spool rest position has both ways (A_R and A_T) open. Along its stroke (X_{COMP}), it first closes the notch A_T and then the notch A_R, so as to achieve a throttling function which preferably conveys the meter out flow towards the energy recovery line R.

The complete numerical model of this innovative DCV was developed in a lumped parameter environment; the numerical simulations allowed us to make important energy considerations. The model was validated through a comparison between the numerical results and experimental measurements obtained through the activities on test bench. A further development of this architecture led to the creation of a numerical model of an excavator with its four main actuators: boom, arm, bucket and swing. The machine chosen for this analysis is a 5t mini-excavator (Bobcat 435 ZHS model).

A complete digging and unloading cycle of this machine has been implemented in the numerical model through the pressures and flow rates experimentally measured. Subsequently, the model has been validated, comparing the flow rates and pressures at the actuator in the cycle with those obtained from the simulation.

Moreover, a system of control signals has been developed in the software to replace the accumulator and to generate on R line the ideal counter pressure value in order to maximize the energy obtained through the flow rate recovery on this line.

In a second phase, in the numerical model an Energy Recovery system was inserted on R line. This system includes a hydraulic motor coupled to an AC generator which charges a Battery thanks to an inverter.

In particular, the generator resistant torque is managed by an electronic control that, reading the compensator stroke, regulates the backpressure on the recovery line. Managing this backpressure, it allows one of the compensator to the ideal position where the efficiency is maximum.

In fact, in this position the tank notch is completely closed and the recovery notch is at its maximum opening.
When the compensator goes over this position the tank notch is always closed, but the recovery notch too begins to be almost completely closed.

Then this control system read this compensator stroke through a position sensor and generates on this line the ideal pressure to conduct the compensator as closer as possible to this position.

This ideal backpressure leads one of the compensator to the position of maximum recovery and avoid excessive dissipation through the downstream compensators.

The Energy Efficiency Analysis has been developed following this criterion.

The system was considered like a black box with Input and Output energies:the Energy spent for Pump operation and Overrunning loads are considered as input energy and Energy recoverable, Resistive Loads and Dissipated are considered as output energy.

In a final analysis this Energy Recovery System is able to recover the 27 % of the overall spent energy spent, that otherwise in a traditional DCV should be dissipated.

Unfortunately, the pandemic crisis that affected the globe during this tremendous year slowed the whole project down for what concerns the experimental support. These experimental activities are still in plan but they will be done in 2022.

The study here presented and in particular the numerical model has created a potential tool that will be used from the company for the development of this activity and the optimization of actual designs.

Reference

[1] TS Kwon, SW Lee, SK Sul, CG Park and et al., “Power Control Algorithm for Hybrid Excavator With Supercapacitor", Vols. vol. 46, no. 4, pp. 1447–1455, IEEE Transaction of Industry Application, 2010.

[2] S. Lee, J. Lee, H. Lee and H. S. Lee, "Modeling and Control of Plug-In Hybrid Excavator", vol. pp. 4653–4659, IECON 2013 - 39th Annual Conference of the IEEE Industrial Electronics Society, 2013.

[3] A. Bedotti, F. Campanini, M. Pastori, L. Riccò and P. Casoli, "Energy saving solutions for a hydraulic excavator", Vols. vol. 126, pp. 1099–1106, 72nd Conference of the Italian Thermal Machines Engineering, 2017.

[4] T. Wang, Q. Wang, and T. Lin, "Improvement of boom control performance for hybrid hydraulic excavator with potential energy recovery", Vols. vol. 30, pp. 161–169, Automation in Construction, 2013.

[5] M. Vukovic, S. Sgro and H. Murrenhoff, "Steam - A mobile hydraulic system with engine integration", Vols. no. October 2013, 2013, ASME/BATH 2013 Symposium on Fluid Power and Motion Control FPMC, 2013.

[6] M. Vukovic, R. Leifeld and H. Murrenhoff, "STEAM – a hydraulic hybrid architecture for excavators", vol. pp. 151–162, 2016.

[7] K. Sahlman and Heybroek and M., "A hydraulic hybrid excavator based on multi-chamber cylinders and secondary control – design and experimental validation", Vols. vol. 19, no. 2, pp. 1–15, International Journal of Fluid Power, 2018.

[8] E. Hughes, C. Wlliamson, J. Zimmerman and M. Ivantysynova, "Displacement-Controlled Hydraulic System for Multi-fucntion Machines", Vols. 8,191,290 B2, 2012.

[9] J. Zimmerman, E. Busquets and M. Ivantysynova, "40% Fuel Savings By Displacement Control Leads To Lower Working Temperatures - a Simulation Study and Measurements", National Conference on Fluid Power, 2011.

[10] Ivantysynova and J. Zimmerman and M., "Hybrid Displacement Controlled Multi-Actuator Hydraulic Systems", vol. pp. 952–978, The Twelfth Scandinavian International Conference on Fluid Power, 2011.

[11] Ivantysynova and R. Hippalgaonkar and M., "Optimal power management of hydraulic hybrid mobile machines - Part I: Theoretical studies, modeling and simulation", Vols. vol. 138, no. 5, Journal of Dynamic Systems, Measurement and Control, Transactions of the ASME, 2016.

[12] Ivantysynova and E. Busquets and M., "Toward Supervisory-Level Control for the Energy Consumption and Performance Optimization of Displacement-Controlled Hydraulic Hybrid Machines", vol. pp. 163–174, 10th International Fluid Power Conference, 2016.

[13] M. Vukovic, J. Schmitz and J. Zhou, "Systematic Data Analysis for Optimal System Design", Aachen: 11 International Fluid Power Conference, IFK, 2018.

[14] Hwasu-Dong, Dong-Gu, Incheon and Elchingen, "Application of Power Regenerative Boom system to excavator".

[15] P. Marani, Milani M., Mesturini, D. and Busani, U., "Experimental Evaluation of the New Meter Out Sensing Architecture", Aachen, Germany: 11th International Fluid Power Conference, 2018.

[16] J. G. M. Siebert, "Reduction of System Inherent Pressure Losses at Pressure Compensators of Hydraulic Load Sensing Systems", Dresden, Germany: 10th International Fluid Power Conference, 2016.

[17] Walvoil, ALS Adaptive Load Sensing, http://www.walvoil.com/products/valves-for-special-applications/als-2, 2016.

[18] U. Lenzgeiger, Maier, U. and Schmuttermair, P., "Electronic Load-Sensing for Tractors", Aachen, Germany: 11th International Fluid Power Conference, 2018.

[19] S. Fu, Li, Z., Lin, T., Chen, Q. and Ren, H., "A Positive Flow Control System for Electric Excavators Based on Variable Speed Control", 2020.

[20] B. Thompson, H. Yoon, J. Kim, and J. Lee, "Swing Energy Recuperation Scheme for Hydraulic Excavators", Vols. no. 2014-01–2402, SAE Technical Paper, 2014.

Ringraziamenti

Con questa tesi di Dottorato si conclude, così, il Terzo Capitolo del mio percorso accademico.

Sono passati 8 lunghi anni ed ho cambiato 3 matricole da quando per la prima volta ho varcato la soglia dell'Università Federico II di Napoli e solo ora, dopo un lungo ed intenso viaggio, sono pronta a chiudere alle spalle quelle porte. Tanto mi ha insegnato e ancor di più io devo a quest'università; gli anni di studio non sono stati mai semplici, per lo più aggravati dalle varie peripezie che accadevano puntualmente ogni giorno per raggiungere quell'aula. Ma nonostante tutto, mai mi son pentita delle scelte fatte perché anche quando al bivio sceglievo la strada più difficile, era sempre la mia scelta e dunque quella per me più facile.

Mai una volta mi sono arresa, mai una volta mi son fermata, sono andata forte come un treno perché tanta era la voglia di correre. Ero una ragazzina quando quei primi giorni in aule stracolme di studenti e di pochissime studentesse, avevo vergogna anche solo ad alzarmi. Oggi, invece, sento di essere una donna forte, determinata ed intraprendente.

E' proprio oggi che dopo otto lunghi anni sto sciogliendo quel cordone ombellicale che mi ha tenuta fortemente legata a quell'Università che mi ha proclamata Dottoressa, Ingegnere ed ora anche Dottore di Ricerca.

Ma prima di farlo non posso che ringraziare delle persone speciali.

Devo tanto soprattutto alle persone incontrate, ai colleghi che poi son diventati amici e con i quali le giornate e gli esami avevano un sapore diverso; devo tanto ai professori che prima di ogni cosa mi hanno insegnato come funzionava la Vita fuori da quelle mura. Loro mi hanno insegnato che nulla poteva essere regalato ma che piuttosto il sudore e la fatica poteva donare poi gioie ancora più grandi, e ad oggi posso solo confermare che è vero.

Ringrazio due persone di un immenso spessore e calibro quali il professor Nicola Bianco ed il professor Vincenzo Naso, che, sebbene non siano mai stati miei insegnanti, mi hanno spesso accolta ed ascoltata con umiltà, elogiata e considerato il mio percorso universitario un esempio per gli altri studenti; non posso che dirvi grazie, vi stimo davvero tanto.

Non posso non ringraziare il professor Adolfo Senatore, colui senza il quale questo percorso non avrei neanche pensato di iniziarlo. E' stato colui che me l'ha proposto, colui che ha sempre creduto in me dal primo giorno, colui che mi ha sempre motivata anche quando gli altri non lo facevano. Come un padre ha sempre saputo lavare i panni sporchi in casa e davanti al mondo elogiare i proprio "figli". A lui devo tanto, non saprò mai come ringraziarlo abbastanza per essere stato il mio mentore, colui che con maestria e sapienza coordina il Fluid Power Research Group di Napoli.

Ringrazio Emma Frosina, dapprima mia professoressa, poi tutor, poi diventata un'amica, semplicemente Emma. A tutte le volte che dicevi di rivedere in me il tuo percorso, alle tue chiamate da sorella maggiore, ai tuoi consigli, a tutte le volte che mi hai detto "brava" perché sapevi che mi faceva bene sentirlo. A tutti i tuoi consigli sinceri, a quanto le tue parole mi hanno fatta crescere e soprattutto a tutte le risate che non sono mai mancate ai congressi o in differita. Sei stata la mia ancora di salvezza tante volte, ti voglio bene.

Ringrazio tutto il gruppo FPRG ed i vari dottorandi e tesisti che si sono susseguiti, in particolare Luca e Gianluca, i due moschettieri al mio fianco. E' stato stupendo condividere questo percorso con voi. Vi ringrazio perché camminando davanti mi avete sempre spianato la strada. Per me siete stati sempre i due pilastri di riferimento, non ho mai esitato dal chiedervi informazioni e voi mai una volta vi siete tirati indietro dal farlo. Grazie per l'immensa pazienza che avete avuto ogni volta, sono stata proprio fortunata.

Grazie a tutto il team di Walvoil, una squadra di cavalieri che mi ha accolta e coccolata ogni giorno come una principessa. Grazie perché con tutti voi ho capito che Reggio era Casa e neanche per un istante mi son sentita sola. Un grazie particolare va a Davide, con la tua pazienza ed i tuoi insegnamenti son cresciuta tanto. In un percorso che per me doveva essere soprattutto formativo, la tua grande umiltà e cultura hanno contribuito a renderlo tale.

Grazie anche ad Alle e Fra, molto più che colleghi, amici. A tutti gli aperitivi che abbiamo fatto e che dovremo ancora fare. Con te Alle, anche le giornate più grigie sono state a colori; sei il collega che in ufficio tutti dovrebbero avere e per questo mi mancherai, per il resto possiamo ancora continuare, ti voglio bene. Fra, invece a te che dire, sei stato quel fratello a cui potevo chiedere aiuto anche a notte fonda e quell'amico su cui poggiare la spalla quando una spalla non ce l'avevo. "Noi siamo soli, le nostre famiglie sono lontane, se non possiamo contare l'uno sull'altra come facciamo?" io non le dimenticherò mai queste tue parole, per me sei stato sostegno concreto, sempre sarai il mio fratello di Reggio.

Ringrazio tutti i ragazzi del Maha Fluid Power Research Lab della Purdue University. Ringrazio il professor Andrea Vacca

per avermi accolta nel suo laboratorio in piena pandemia, quando viaggiare per andare dall'altra parte del mondo non era un gioco da ragazzi. A very special thanks go to Sangbeom, Federico, Mateus, Marie, Michael and Till who will be forever in the memories of my 6 months in the States.

Non posso non citare l'anima gemella che gli Stati Uniti mi hanno regalato per la Vita, Annalisa. Mia complice, mia amica, mia sorella, il mio alter ego, il mio cattivo umore e la mia gioia di vivere, la mia pazzia e la mia esuberanza dall'altra parte del mondo. Ora che ti ho incontrata, non ti lascerò mai più andare, ti voglio bene pazza del mio cuore!La Florida sarà sempre la mia seconda casa, un porto sicuro dove poter scappare.

Ringrazio mia mamma e mio padre, ancora una volta le mie rocce. L'inizio di questo percorso ha determinato l'inizio della mia Vita da adulta ed anche per voi non è stato proprio semplice. Mi avete accompagnata per mano come due eccellenti genitori sanno fare e poi quella mano al momento giusto l'ho saputa lasciare per proseguire da sola. Se ad oggi sono soddisfatta dei sacrifici che ho fatto e degli obiettivi che ho raggiunto lo devo solo ed esclusivamente a voi. Siete voi che mi avete dato quei giusti valori che ad oggi mi hanno portata ad essere una ragazza autonoma, intraprendente, indipendente e soprattutto soddisfatta della propria Vita. Se ad oggi io sono felice, è grazie a voi, spero ne siate orgogliosi.

Ringrazio i miei fratelli, Ugo e Sabrina, siete stati sempre il sorriso nei momenti più pesanti. La vostra leggerezza e il vostro considerarmi "diversa da voi" non sono mai mancati anche questa volta. Con voi ogni parola da spendere sarebbe superflua, siete la mia Vita!

A Paolo, al mio fianco in tutti questi anni ed ancora oggi. Questa volta non è stata poi così semplice come immaginavo o come speravo, ma nonostante tutto è andata. Quell'America così

lontana è diventata poi troppo vicina, ma tuttavia necessaria ad entrambi per crescere e maturare ancora.

Un grazie va a te Amico Mio che in questo percorso rispetto a quelli precedenti ti ho vissuto un pò da lontano. Tanti sono stati i momenti in cui avrei avuto bisogno del tuo abbraccio, ma i chilometri e l'oceano, spesso, hanno avuto la meglio. Sei stato il mio supporto morale quando la vita da coinquilina di sè stessa comportava qualche difficoltà in più. Eppure, la colica renale ed il Covid li ho affrontati grazie a Te. Ci sei dall'inizio del mio percorso universitario e ci sei ancor più da vicino ora che sono alla fine, il regalo più bello che tu mi potessi fare. In fondo questo percorso è iniziato proprio "Con il Cuore a terra e gli Occhi verso il Cielo", e quel Cielo finalmente io e te l'abbiam toccato!

A tutti quelli che mi hanno sempre detto che sono un genio perché ho raggiunto ottimi risultati in tempi brevi voglio solo dire che sono una ragazza normale, che in questi anni non ho mai rinunciato alla mia vita, allo sport e agli amici, ma che ho lottato con tutte le mie forze per raggiungere il mio Sogno e questa volta, definitivamente, vi assicuro che ce l'ho fatta!

Son passati 8 lunghi anni e ad oggi non mi sento più una matricola, ma una Persona, una Donna e un Ingegnere.

"Se un giorno dovessi avere una figlia, vorrei poterle dire che può essere tutto quello che vuole".

Samanta Cristoforetti, 27 Aprile 2022